Report
R-19-11
May 2019

Modelling of concrete degradation – Hydro-chemical processes

Report for the safety evaluation SE-SFL

Andrés Idiart

Babak Shafei

SVENSK KÄRNBRÄNSLEHANTERING AB

SWEDISH NUCLEAR FUEL
AND WASTE MANAGEMENT CO

Box 3091, SE-169 03 Solna
Phone +46 8 459 84 00
skb.se

SVENSK KÄRNBRÄNSLEHANTERING

ISSN 1402-3091
SKB R-19-11
ID 1542377

May 2019

Modelling of concrete degradation – Hydro-chemical processes

Report for the safety evaluation SE-SFL

Andrés Idiart, Babak Shafei
Amphos 21 Consulting S. L.

This report concerns a study which was conducted for Svensk Kärnbränslehantering AB (SKB). The conclusions and viewpoints presented in the report are those of the authors. SKB may draw modified conclusions, based on additional literature sources and/or expert opinions.

Summary

Concrete degradation has been simulated for the BHK vault of the proposed repository concept for SFL. Reactive transport modelling has been performed using iCP, a software interface between Comsol Multiphysics (version 5) and Phreeqc (version 3). This report presents the setup of the reactive transport model and the results of two-dimensional (2D) and three-dimensional (3D) simulations.

An initial benchmark exercise has been performed where the iCP approach to modelling concrete degradation has been compared to previous simulations by Höglund (2014). Höglund (2014) modelled concrete degradation in the BMA vaults in SFR using the reactive transport code PHAST, which couples the groundwater flow simulator HST3D with Phreeqc.

A range of sensitivity cases has been run using a 2D model to evaluate the influence of various assumptions on the results. The main objectives of the sensitivity studies were to identify the most relevant processes and their governing parameters and to optimize the numerical performance for subsequent simulations in 3D models. The sensitivity cases considered the

- type of boundary conditions used for the fluid flow and solute transport,
- treatment of concrete and waste domains as homogeneous or heterogeneous porous media,
- chemical composition of inflow groundwater,
- coupling between physical and chemical processes (coupled versus non-coupled scenarios),
- initial concrete chemical setup and mineral assemblage of the domains (full and simplified chemistry cases).

The final part of the work reported here concerns the modelling of concrete degradation in 3D geometries. A model of a concrete compartment in the BHK vault has been implemented, as well as a model of the entire vault. The feasibility of running 3D reactive transport models has been explored. Furthermore, results from 2D and 3D simulations have been compared from both a qualitative and quantitative standpoint.

Sammanfattning

Betongdegradering har simulerats för förvarssalen BHK i det föreslagna förvarskonceptet för SFL. Reaktiv masstransport har modellerats med hjälp av iCP, ett mjukvaruinterface som kopplar samman Comsol Multiphysics (version 5) och Phreeqc (version 3). Denna rapport presenterar modellen för reaktiv transport och simuleringsresultat från tvådimensionella (2D) och tredimensionella (3D) geometrier.

I ett första steg jämfördes resultat från iCP med tidigare modelleringsresultat av betongdegradering genomförd av Höglund (2014). Höglund (2014) modellerade betongdegradering i BMA salarna i SFR med hjälp av beräkningsverktyget PHAST. PHAST kopplar samman flödemodellering från koden HST3D med Pheeeqc.

En serie av känslighetsfall har beräknats med en 2D-modell för att utvärdera påverkan av olika antaganden. Huvudsyftet med känslighetsfallen har varit att identifiera de huvudsakliga processerna och deras styrande parametrar samt att optimera den numeriska prestandan inför vidare simulering i 3D. Känslighetsfallen har beaktat

- randvillkor för grundvattenflöde och masstransport,
- beskrivning av betongen som homogen eller heterogent poröst medium,
- kemisk sammansättning av inkommande grundvatten,
- koppling mellan fysikaliska och kemiska processer (kopplade och okopplade fall),
- beskrivning av betongens initiala kemi och fassammansättning (fall med komplett och förenklad kemi).

Denna rapport presenterar avslutningsvis modellering av betongdegradering i 3D-geometrier. En modell omfattar ett enskilt fack i BHK och en annan modell representerar hela förvarssalens geometri. Genomförbarheten för reaktiv transportmodellering i 3D har utvärderats. Kvantitativa och kvalitativa jämförelser av resultat från 2D och 3D simulering har också genomförts.

Contents

1 Introduction

SKB plans to dispose of long-lived low and intermediate level waste in a deep geological repository called SFL. Possible repository concepts for SFL have been evaluated and Elfwing et al. (2013) proposed a repository concept to be analysed in an evaluation of post-closure safety (SE-SFL). This report focusses on the concept proposed for metallic waste which relies on extensive use of cementitious materials for constructing the engineered barrier system.

The long-lived low and intermediate level waste from the nuclear power plants consists of neutron-irradiated components and control rods. The total quantity of long-lived waste planned for SFL is estimated to approximately 16 000 m^3, of which about one third originates from the nuclear power plants. The remainder comes from AB SVAFO and Studsvik Nuclear AB, who manage the legacy waste and the waste from hospitals, industry and research.

In the proposed concept (Elfwing et al. 2013), SFL has two storage vaults:

- one vault for the metallic waste from the nuclear power plants (BHK), and
- one vault for legacy waste from AB SVAFO and Studsvik Nuclear AB (BHA).

The vault for the metallic waste (BHK) is planned to be backfilled with concrete, which acts as a barrier against groundwater flow and contributes to a low diffusion rate and high sorption of many radionuclides. The concrete also creates an alkaline environment in the repository vault, reducing the corrosion rate of the steel and limiting the release rate of radionuclides. Over time, the concrete barrier will however transform and its ability to retain radionuclides will be affected. In order to assess the potential of the repository concept it is therefore essential to be able to simulate the evolution of concrete properties, under repository conditions and considering long time scales.

Individual processes related to chemical and physical degradation of concrete have been intensively studied in concrete technology since the 1970's and are relatively well understood when studied independently from each other. Degradation processes are however interdependent and need to be considered simultaneously in order to improve the reliability of predictive simulations of concrete property evolution. This requires considerable additional efforts.

The present work aims to address concrete degradation and long-term performance of the BHK vault of the SFL repository by advanced reactive transport and multiphysics numerical models. These models include groundwater flow, chemical reactions within the concrete barriers, and physical degradation of the concrete barriers (flow and transport properties). Specifically, 3D models of the SFL near-field hydrology have been implemented in Comsol Multiphysics, including geometric representation of vault structures and barriers. The methodology followed is similar to the one used in the development and implementation of the SFR near-field hydrology model (Abarca et al. 2013). Mass transport and chemical reactions have been subsequently added in a fully coupled manner using iCP (Nardi et al. 2014). iCP interfaces the Comsol flow and transport models to PhreeqC concrete degradation chemistry models.

1.1 The BHK vault

The proposed design of the concrete vault (BHK) of the SFL repository has been described elsewhere (Grahm et al. 2013, Elfwing et al. 2013). The main components of the engineered barrier system are shown in Figure 1-1 and Figure 1-2. The waste is segmented, after which the parts are deposited in steel tanks and stabilized with grout. The steel tanks are emplaced in compartments of reinforced concrete with a thickness of ~0.5 m. The volume outside the concrete compartments will be backfilled with concrete.

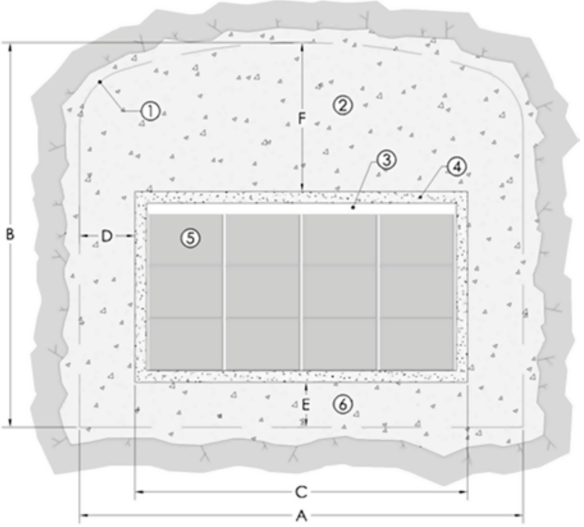

Figure 1-1. *Schematic cross-sectional layout of the BHK vault for metallic waste (from Elfwing et al. 2013). Legend: 1.) Theoretical tunnel contour. 2) Concrete backfill. 3) Grout. 4) Concrete structure. (0.5 m). 5) Steel tanks. 6) Concrete. Approximate dimensions: A = 20.6 m, B = 19.6 m, C = 15 m, D = 2.8 m, E = 2.4 m, F = 8.8 m.*

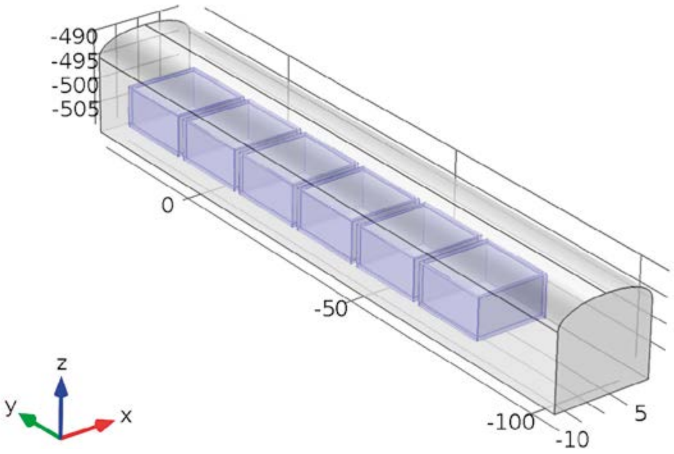

Figure 1-2. *Schematic view of the BHK vault showing the six waste compartments (in blue) and the concrete backfill (light grey). Dimensions are in metres.*

2 Objectives

The work in the present report concerns four related modelling studies:

- A benchmark of the iCP reactive transport modelling approach.
- Concrete degradation in a 2D cross-section of the BHK vault, investigating a range of sensitivity cases.
- Concrete degradation in a 3D model of a BHK compartment, comparing results with 2D models.
- Concrete degradation in a 3D model of a the full BHK vault, investigating the feasibility of running large scale reactive transport models using iCP.

The objectives of the different studies are presented below.

2.1 iCP reactive transport benchmark

The objective of this study has been to verify the numerical approach followed by iCP, an interface between Comsol and Phreeqc (Nardi et al. 2014), for the modelling of concrete degradation. A benchmark example has been set up in iCP and PHAST based on published results of the modelling of concrete degradation of the 2BMA vault of the future extension of the SFR repository (Höglund 2014). The agreement between both codes for a given conceptual model and input data (thermodynamic data, flow and transport properties as a function of time, and initial and boundary conditions) has been compared.

2.2 Concrete degradation in a 2D cross-section of the BHK vault

The objective of this study has been to implement a 2D model in iCP, to simulate the most relevant reactive transport processes responsible for concrete degradation in a cross-section of the BHK vault. Different modelling assumptions have been examined and compared to identify the optimum physical and chemical setup that properly characterizes the studied system. A range of calculation cases has been run to study the sensitivity of the model to changes in several variables, parameters, and boundary conditions. In addition, this has allowed for optimization of the numerical performance of the system, for subsequent three-dimensional reactive transport simulations.

2.3 Concrete degradation in a 3D model of a BHK compartment

The objective of this study has been to implement a 3D model in iCP, of the concrete degradation processes in a single compartment of the BHK vault. The feasibility of performing large-scale 3D reactive transport models using iCP has been investigated. Also, the results from the 3D model have been compared to results from 2D modelling, to assess qualitative and quantitative differences between the approaches.

2.4 Concrete degradation in a 3D model of a the full BHK vault

The objective of this study has been to implement a 3D model in iCP, of the concrete degradation processes in the entire BHK vault. The feasibility of performing large-scale 3D reactive transport models using iCP has been investigated.

3 Methodology

3.1 iCP reactive transport benchmark

The work concerns the implementation of an existing reactive transport model of the degradation of concrete in a model of the 2BMA vault in the software iCP (Nardi et al. 2014). This model corresponds to the case Large20 described in Höglund (2014), and represents the base case providing concrete degradation data to the safety assessment SP-PSU (SKB 2015). The goal is to compare the results of iCP with the original model in PHAST and identify possible sources of mismatch, if any. In the following, the conceptual model and its implementation in iCP are described.

The time span of the simulations presented by Höglund (2014) was 100 000 years, using a time step of 1 year for the entire period. This leads to long computational times, on the order of several weeks (as stated in Höglund 2014). It is not essential for the purpose of the present benchmark to model the entire time period in iCP, which would also take several weeks in a desktop computer. Therefore, it was decided to restrict the analysis to 30 000 years.

An additional benchmark exercise has also been simulated using PHAST and iCP. It consists of a 1D simulation of a 0.5 m concrete wall. The chemical setup used was exactly the same as that used for the concrete walls in the 2D iCP model. The setup and results of the 1D benchmark exercise are presented in Appendix D.

3.2 2D reactive transport model of BHK vault

The goal of this study is to perform a preliminary assessment of the potential degradation processes of the cement and concrete barriers. Degradation is mainly driven by the interaction of the barriers with groundwater. To this end, numerical 2D models of a BHK vault cross section have been developed. Reactive transport simulations, coupling fluid flow, solute transport, and chemical reactions have been performed using iCP (Nardi et al. 2014).

In this work, the analysis of the uncertainty has been based on the definition of a series of sensitivity cases. In total, eleven simulation cases of the cross-section of the BHK vault have been performed. Table 3-1 summarizes the main features of each simulation case. In the following paragraphs, the motivation for each of these cases is discussed.

Case I has been selected as a base case, to compare with the remaining sensitivity cases. Sensitivity cases aim to study the following aspects:

- Initial state of the concrete barriers: Most of the simulation cases have assumed a homogeneous concrete material. Two additional cases have been simulated considering different heterogeneities in the hydraulic conductivity field of the concrete.
- Description of the chemical system: Two different chemical models of concrete have been used in the simulations that differ in the level of complexity.
- Boundary conditions for solute transport: Either fixed concentration or open boundary conditions have been used in the simulations.
- Boundary conditions for groundwater flow: Either constant inlet flow or constant hydraulic head gradient have been used in the simulations.
- Groundwater type: An old meteoric groundwater composition has been used in most the simulation, except in one sensitivity case where a more diluted glacial meltwater has been employed.
- Feedback between physical and chemical processes: Uncoupled and coupled scenarios have been considered, using either the Kozeny-Carman or the modified Kozeny-Carman relations for the porosity-permeability coupling.

Table 3-1. Summary of simulation cases for the reactive transport model of the BHK vault cross-section. BC = boundary condition.

		Case I	Case II	Case III	Case IV	Case V	Case VI	Case VII	Case VIII	Case IX	Case X	Case XI
Initial State	Homogenous	■			■	■	■	■	■	■	■	■
	Heterogeneous (Gaussian Model)		■									
	Heterogeneous (SGSIM Model)			■								
Concrete Chemical Setup	Full	■	■	■	■			■	■			■
	Simplified					■	■			■	■	
Solute Transport BC	Open Boundary		■		■	■	■	■	■			■
	Fixed Concentration	■		■						■	■	
Fluid Flow BC	Hydraulic head			■					■			
	Constant inlet flow	■	■		■	■	■	■		■	■	■
Groundwater Type	Meteoric	■	■	■	■	■	■	■	■	■	■	
	Glacial											■
Physical-Chemical Feedback	Coupled: Kozeny-Carman	■	■	■	■	■			■	■		■
	Coupled: Modified Kozeny-Carman							■				
	Uncoupled						■				■	

A combination of these modelled variables leads to a total of $3 \times 2 \times 2 \times 2 \times 2 \times 3 = 144$ possible cases. The reasoning to reduce the number of simulations is as follows:

- The main focus is on the initial homogeneous state of concrete. In order to gain some insight regarding the effect of heterogeneities in the hydraulic conductivity field, only two simulations with different sources of heterogeneity have been considered. Thus, from the total of possible combinations, the number is reduced to 48 + 2 = 50.
- The old-meteoric groundwater type represents the most plausible composition and has been used in most of the simulations. An additional simulation assuming glacial groundwater has been assumed sufficient to assess the sensitivity with respect to groundwater composition. Thus, the number is reduced to 48/2 + 2 + 1 = 27.
- In the majority if the simulations the Kozeny-Carman relation has been used to described the coupling of porosity and hydraulic conductivity. In two simulations the coupling has been neglected. Since the boundary condition for transport had important implications, uncoupled simulations were done for the two different solute transport boundary conditions. One additional simulation has been used to test the sensitivity of the model to the more aggressive porosity-hydraulic conductivity relation described by the modified Kozeny-Carman relation. Thus, the number is reduced to 24/3 + 2 + 1 + 3 = 14.
- Most of the simulations have been performed considering what is referred to as the full chemical system (see Section 5.1). Still, four simulations have been set up using a simplified chemical system. These cases assume a homogeneous initial state, a constant inlet flow boundary conditions, and an old-meteoric groundwater composition. The simulation cases have been used to assess the effects not only of the chemical system definition, but also of solute transport boundary conditions and the feedback between porosity and physical properties. Thus, the number is reduced to 14/2 + 4 = 11.

3.2.1 Homogeneous vs. heterogeneous hydraulic conductivity

The BHK vault will be backfilled with concrete. The detailed installation procedures have yet to be established. One of the main concerns is how to avoid or at least control the formation and propagation of cracks in the concrete backfill and structures (Grahm et al. 2013).

In the present work, this uncertainty has been analysed by assigning spatially homogeneous and heterogeneous hydraulic conductivity fields for the concrete materials. The heterogeneity of the initial state will certainly depend on a number of factors, such as the construction method, mechanical constraints, environmental conditions (relative humidity, temperature), reinforcement corrosion, etc. The assessment and prediction of the initial state using mechanistic models is out of the scope of this study. Instead, the hydraulic conductivity field has been defined using one of the following alternatives:

- A homogenous property field described by a constant value.
- A heterogeneous property field described by a Gaussian distribution of values.
- A heterogeneous property field described by multi-step transformation of a multi-Gaussian distribution of values.

In all cases considered, the hydraulic conductivity tensor is isotropic and of the form $K_{ij} = \delta_{ij}K$, where = δ_{ij} is the Kronecker delta function. The aim of the heterogeneous cases is to study the effect of different degrees of connectivity of high hydraulic conductivity volumes on the reactive transport processes. Case II in Table 3-1 considers a Gaussian distribution, while Case III is based on a successive transformation of a multi-Gaussian field. The latter case is representative of a more connected hydraulic conductivity field, caused by local defects or fractures. Concrete degradation is expected to proceed more quickly in this case.

The remaining cases (Case I, and Cases IV to XI) consider a homogeneous hydraulic conductivity field in the concrete backfill and the waste domain.

3.2.2 Full vs. simplified chemical system

The effect of the level of sophistication of the chemical system on the degree of concrete degradation has been also studied. The goal has been to optimize the computation time without compromising the main chemical processes leading to degradation and porosity increase. An optimized chemical system is thought to be necessary in order to enable 3D reactive transport simulations of the BHK vault (Section 6).

A full chemical system and a simplified system have been considered. The full chemical system refers to the concrete degradation model proposed by Höglund (2014) for modelling the evolution of concrete in the SFR repository. The simplified chemical system refers to the model proposed by Pękala et al. (2015) for studying the evolution of the redox in the SFL repository. The differences between the complexities of each system are presented in Section 5.1.

3.2.3 Boundary conditions

3.2.3.1. Solute transport

Boundary conditions represent an important part of any reactive transport model. Time dependent changes are driven by the differences between the initial conditions and the boundary conditions. To model solute transport different choices are possible. The choice of appropriate boundary condition relates to the importance of the transport processes in the model. In cases where advection is thought to dominate solute transport over diffusion, an open boundary condition at the inlet is typically used:

$$(\boldsymbol{q} \cdot \boldsymbol{n})(\boldsymbol{c} - \boldsymbol{c}_{\boldsymbol{gw}}) = 0 \tag{3-1}$$

where $\boldsymbol{q}$ (m/s) is the Darcy flow vector, $\boldsymbol{n}$ (–) is the normal vector, $\boldsymbol{c}$ (M) is the solute concentration vector, and $\boldsymbol{c}_{gw}$ (M) is the groundwater concentration vector.

In cases where diffusive transport is clearly dominant, fixed concentration boundary conditions can be used instead. In that case, it is assumed that groundwater in contact with the concrete backfill is flushed out before out-diffusion from the latter leads to changes in groundwater composition. This type of boundary condition is considered a limiting case for diffusion-dominated problems and has been used in this report to consider an aggressive scenario.

Available predictions of the groundwater flow across the SFL repository indicate very low flow rates. Under these conditions, the selection of the boundary conditions is not evident. Two different sets of cases have therefore been simulated. In Cases I, III, IX, and X fixed concentration boundary conditions have been assumed. For the remaining of cases an open boundary condition for solute transport has been assumed. In this way, the effects of different boundary conditions for solute transport for a given groundwater flow field have been assessed.

3.2.3.2. Groundwater flow

For groundwater flow, most of the simulation cases have been performed using a constant inlet flow boundary condition on the left boundary of the rock domain (see Section 5.1 for more details). The mass flux has been derived from the work by Abarca et al. (2016). With this type of boundary condition, the maximum flow rate that can cross the barriers is limited by the mass flux.

A hydraulic head gradient condition has also been used (Cases III and VIII). The reasoning behind this selection is that when the barriers degrade and hydraulic conductivity increases, the flow may redistribute based on a pressure gradient. In this case, the maximum flow rate that can cross the barriers depends on the level of degradation and the associated hydraulic conductivity.

With both types of boundary conditions, groundwater flow across the barriers in their initial state can be similar. However, differences of flow field distribution are expected when degradation proceeds.

3.2.4 Groundwater type

In order to assess the influence on chemical degradation due to different groundwater compositions, a simulation case with an alternative groundwater composition has been proposed (Case XI). In the remaining simulation cases, an old meteoric groundwater type has been used, which is representative of present day conditions. In Case XI, a glacial groundwater type has been set, following the work by Pękala et al. (2015). This composition is significantly different to the present day conditions. It consists of diluted water, poor in calcium, sulphate, and alkalis, and with a lower pH than the meteoric water (Section 5.1).

3.2.5 Feedback between physical and chemical processes

Chemical degradation is represented as a sequence of dissolution/precipitation reactions involving mineral phases. This process has a direct consequence on the total porosity. In turn, porosity is the main parameter controlling the hydraulic and transport properties in concrete. Hydraulic conductivity and the effective diffusion coefficient depend to a large extent on porosity. Therefore, a coupled scheme between physical and chemical processes is needed to correctly capture this interdependence. Most of the simulation cases proposed here considers a coupled scheme, except Cases VI and X which do not account for this coupling (Uncoupled scenarios). The dependence of hydraulic conductivity on porosity is modelled through the well-known Kozeny-Carman relation (Carman 1937):

$$K(\varphi) = K(\varphi_0)G(\varphi) \tag{3-2}$$

$$G(\varphi) = \frac{(1-\varphi_0)^2}{\varphi_0^3}\frac{\varphi^3}{(1-\varphi)^2} \tag{3-3}$$

In these equations, $K(\varphi)$ is the hydraulic conductivity (m/s), which is a function of porosity (φ, m^3/m^3), and $K(\varphi_0)$ is the hydraulic conductivity (m/s) associated with the initial porosity (φ_0, m^3/m^3).

The effective diffusion coefficient depends on porosity as well, following the equation:

$$D_e = f(\varphi)D_{e,0} \tag{3-4}$$

$D_{e,0}$ (m^2/s) is the initial effective diffusion coefficient and $f(\varphi)$ is an empirical power law of porosity, expressed as:

$$f(\varphi) = \left(\frac{\varphi}{\varphi_0}\right)^n \tag{3-5}$$

In Equation (3-5), n is an exponent that typically ranges between 1 and 5. In this work, a value of 2.5 has been assumed. This value has been selected based on Figure 8.1 of Höglund (2014), where different diffusion-porosity relations are plotted. The initial effective diffusion coefficient value has been derived from the following equation, using the parameters given by Abarca et al. (2016) and Pękala et al. (2015):

$$D_{e,0} = \tau\varphi_0 D_0 \tag{3-6}$$

In Equation (3-6), τ (–) is the tortuosity of the porous medium. D_0 is the species diffusion coefficient in water, assumed to be 1.0×10^{-9} m^2/s (similar to Pękala et al. 2015).

Case VII has been simulated assuming a modified Kozeny-Carman relation, as described in Höglund (2014). In this case, the hydraulic conductivity of concrete ranges between the values for the initial state and for a state in which cement paste has been completely degraded. A log-linear relation has been applied to extrapolate to the totally leached concrete, yielding:

$$K = C(\vartheta_c)\frac{\varphi^3}{(1-\varphi)^2} \tag{3-7}$$

where

$$\log C(\vartheta_c) = \left(1 - \frac{\vartheta_c}{\vartheta_{c,0}}\right)\log C_{ballast} + \frac{\vartheta_c}{\vartheta_{c,0}}\log C_{conc} \tag{3-8}$$

In Equation (3-8), $\vartheta_{c,0}$ and ϑ_c are the volume fractions of the cement minerals in intact concrete and partially leached concrete, respectively. $C_{ballast}$ and C_{conc} are given by:

$$C_{ballast} = K(\varphi_{ref})\frac{\left(1-\varphi_{ref}\right)^2}{\varphi_{ref}{}^3} \tag{3-9}$$

$$C_{conc} = K(\varphi_0)\frac{(1-\varphi_0)^2}{\varphi_0{}^3} \tag{3-10}$$

In Case VII, the conductivity of the fully leached concrete has been assumed equal to 1×10^{-4} m/s, with a $\varphi_{ref} = 0.3$, similar to Höglund (2014).

The aim of cases VI, VII, and X is to study the influence of the degree of coupling on the concrete degradation results. The two uncoupled scenarios differ in the boundary condition used for solute transport (Section 3.2.3.1). An open boundary condition is used in Case VI and a fixed concentration condition in Case X.

3.3 3D reactive transport models of BHK vault

The 2D reactive transport models discussed above have been used to evaluate the chemical degradation processes affecting the concrete barriers in a cross-section of the BHK vault. A number of simulation cases with different settings and assumptions were tested to study the sensitivity with respect to the results (Section 5).

Since three-dimensional reactive transport simulations are computationally demanding, the 2D models presented in Section 5 were also used to select a representative simulation case for the 3D models. The selection criteria are not only based on the representativeness of the system setup, but also consider the numerical efficiency. From the results presented in Section 5, it may be concluded that Case IX can be used for the 3D simulations of the BHK vault. This case has a similar setup to the base case (Case I), except that in Case IX a simplified chemistry setup has been assumed.

One of the main objectives of performing 3D reactive transport simulations of the BHK vault is to test the feasibility of implementing and solving large-scale models in iCP, to gain more insight on the numerical performance of the tool. In addition, an important goal is to assess the benefits of performing a 3D simulation of the BHK vault or a single compartment as compared to the 2D model of a typical cross-section. Some important questions are:

- Are the degradation trends obtained with the different models similar?
- Does the heterogeneity of the vault in the longitudinal direction play an important role in the degradation process?
- Does the heterogeneity of the flow field at the vault-scale or compartment-scale lead to a significant level of heterogeneity in the degradation fronts?

To address these questions two different reactive transport models have been set up in 3D;

a compartment level and a model of the entire BHK vault. In both cases, the groundwater flow field calculated by Abarca et al. (2016) has been used to define the boundary conditions (Figure 6-3). This corresponds to the case in which the SFL repository is located at a depth of 500 m.

4 Benchmark modelling

4.1 Description of conceptual model

The 2BMA vault is part of SKB´s repository for short-lived low level waste, to be built using non-reinforced concrete barriers. Fourteen separate concrete compartments will hold the waste. When each compartment is full, a 0.5 m thick concrete lid will be placed on top of the waste. The concrete constructions will be supported from the inside by the waste packages and the concrete grout and on the outside by macadam (i.e. crushed rock). The concrete floor will rest on a bed of packed gravel, which is considered equivalent to the macadam used for the backfill.

Dimensions of a cross-section of the 2BMA vault are shown in Figure 4-1 (real dimensions on the top and right of the figure). Höglund (2014) describes the long term evolution of concrete in the 2BMA based on reactive transport modelling, employing a simplified geometry in 2D. The dimensions of the model were reduced while maintaining the thickness of the concrete walls, lid, and floor. In this way, it was ensured that the diffusive transport of dissolved species was estimated with reasonable accuracy. The dimensions of the modelled geometry are shown in Figure 4-1 (model dimensions on the left and bottom of the figure).

The model by Höglund (2014) also included 4 thin fractures (aperture of 0.1 mm) in the concrete structures to evaluate their impact on concrete degradation. The results showed that the overall evolution of concrete degradation was not affected by the presence of these fractures. Therefore, it has been decided to exclude them from the iCP model presented here. Nonetheless, a test has been performed in iCP considering the effect of these fractures. It was observed that their impact is localized to the fractures.

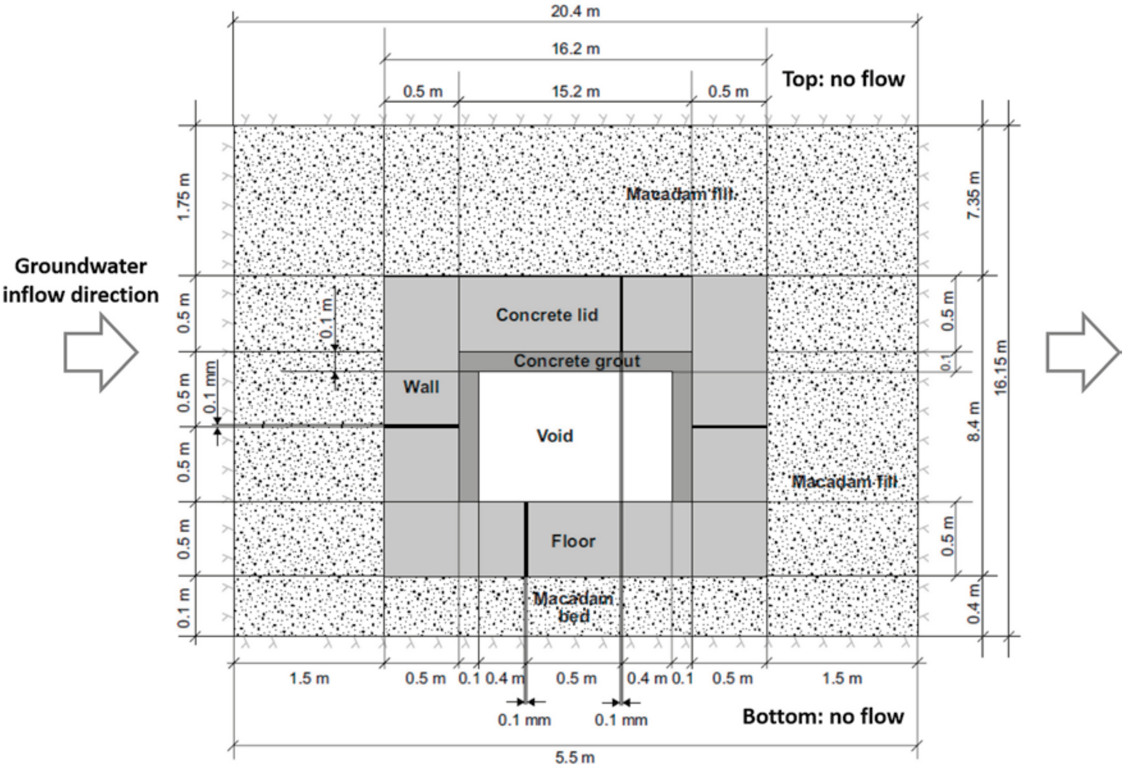

Figure 4-1. *Schematic representation of a cross-section of the 2BMA vault of SFR extension and flow boundary conditions (adapted from Höglund 2014). Dimensions (m) on the right-hand side and at the top refer to the real dimensions of the vault whereas the left-hand side and the bottom consider the dimensions used in the model.*

The model geometry considers four different domains:

- Unreinforced concrete (walls, lid, and floor).
- Cement grout surrounding the waste.
- A void space filled with cementitious water that occupies the volume of the waste.
- Macadam (crushed rock) surrounding the concrete structure.

The flow and transport properties for each domain are presented in Table 4-1 (see also Höglund 2014). The feedback between porosity changes and transport properties was not considered in the simulations, similar to Höglund (2014). These properties were assumed to increase with time in a stepwise constant manner. This variation was introduced to represent the effect of concrete degradation on flow and transport properties. These transient material properties have been defined in iCP using the same stepwise increases, but with a smoothing transition function between steps, to avoid encountering discontinuities such as step functions and associated convergence issues. The same methodology has been applied for time-dependent flow boundary conditions (Table 4-2). The temporal transition zone between the two values of a step was implemented using two different time intervals. To this end, two different time lengths of the transition zones were used: 0.1 and 0.008. These correspond to what is subsequently referred to as smooth and less smooth scenarios, respectively.

A horizontal inflow of groundwater has been assumed as boundary condition on the left boundary, referred to as constant inlet flow. The top and bottom boundaries have been set as no flow boundaries. A constant hydraulic head has been imposed on the right boundary. An inflow that increases over time in a stepwise manner is considered on the left boundary (Table 4-2). For these flow conditions, the dimensionless Péclet number (*Pe*) of each modelled domain has been calculated as a function of time using the following equation:

$$Pe = \frac{qL_c}{\varphi D_e} \qquad (4\text{-}1)$$

Above, L_c (m) is a characteristic length, φ is porosity, and D_e (m^2/s) the effective diffusion coefficient (dispersion is negligible in the modelled system). Values much lower or much higher than 1 indicate diffusion-dominated or advection-dominated conditions, respectively. The characteristic length is related in this work with the finite element size, *h* (m), which is calculated internally in Comsol. This assumption has the benefit of enabling Péclet number calculation over the entire domain, depending on the refinement of the mesh. However, it is acknowledged that the choice of using the element size as characteristic length in not based on physical reasons. Selecting a physically reasonable characteristic length for the entire domain (concrete backfill and waste domain) is not an easy task. Grain size such as the maximum aggregate size (in the order of few cm) is sometimes used, which would lead to very small Péclet numbers. Another possibility is to select a representative length, for example the thickness of the concrete walls. In the latter case, typical values would be in the range 1 to 3 m approximately. Therefore, the choice of using the finite element size, typically in the range 0.03 to 0.6 m in the models presented in this report, appears as a reasonable compromise.

In this benchmark exercise, as the simulation time increases, both the Darcy velocity and the diffusion coefficient are modified leading to different Péclet numbers in time and space. Average Péclet numbers for each domain and for different times are shown in Table 4-3. Initially, the entire system is diffusion-dominated due to the very low water fluxes. As the groundwater flow magnitude increases with time, and the transport properties change, the Péclet number increases substantially. However, only the macadam domain shows values slightly larger than 1.

All the calculations have been performed assuming thermodynamic equilibrium for chemical reactions. No reaction kinetics has been considered. The thermodynamic database used in the simulations is the MintqCem-2001. More details about this database may be found in Höglund (2014) and references therein. The groundwater composition used in the simulation is shown in Table 4-4 (see Appendix A for saturation indices). The initial porewater composition in equilibrium with the mineral phases is shown in Table 4-5 for each modelled domain. The mineralogical phase assemblage for concrete and cement grout is presented in Table 4-6. In the model by Höglund (2014), leaching of alkali hydroxides (K^+, Na^+) is represented by an ion exchange model, where alkalis can be exchanged by Ca^{2+}. That ion exchange model was calibrated against experimental data by Lagerblad and Trägårdh (1994) and has the effect of prolonging the period during which the pH is higher than would be expected from equilibrium with portlandite. The initial composition of the exchanger is given in Table 4-6. No reactive minerals where considered initially present in the macadam or the void space. Table 4-7 presents the secondary minerals allowed to precipitate in each domain in case supersaturation of the solution is reached.

Table 4-1. Material properties and their variation over time for different model components in concrete barriers in 2BMA (from Höglund 2014). The effective diffusion coefficient is calculated according to the following equation: $D_e = \varphi \cdot \tau \cdot D_0$, where D_0 is the diffusion coefficient in free solution (assumed 1×10^{-9} m^2/s) and φ and τ are the values of porosity and tortuosity specified in the table, respectively. These values change as a function of time, but do not change as a result of mineralogical changes. Longitudinal and transversal dispersivity values are equal to 1.0×10^{-11} m for all modelled domains (Höglund 2014).

		Time period (years)			
		0–100	100–10 000	10 000–20 000	20 000–100 000
Concrete	Porosity	0.11			
	Tortuosity	0.032	0.045	0.091	1.818
	D_e (m^2/s)	3.50E–12	5.00E–12	1.00E–11	2.00E–10
	K (m/s)	8.30E–10	8.00E–08	1.00E–06	1.00E–05
Grout	Porosity	0.30			
	Tortuosity	0.167	0.267	0.33	0.5
	D_e (m^2/s)	5.00E–11	8.00E–11	1.00E–10	1.50E–10
	K (m/s)	8.30E–09	8.00E–07	3.00E–05	8.00E–05
Macadam*	Porosity	0.3			
	Tortuosity	0.5			
	D_e (m^2/s)	1.5E–10			
	K (m/s)	1.00E–03			
Void space	Porosity	1.0			
	Tortuosity	1.0			
	D_e (m^2/s)	1.00E–09			
	K (m/s)	0.1			

* The macadam below the concrete floor has slightly reduced transport properties during the period 100–100 000 years: $\tau = 0.33$; D_e (m^2/s) = 1.0×10^{-10}; K (m/s) = 1.0×10^{-4}.

Table 4-2. Assumed groundwater flow into the 2BMA vault at different time periods, used as boundary conditions for the reactive transport calculation (from Höglund 2014).

Time period (years)	Groundwater inflow (m^3/m^2/year)
0–1 000	6.50×10^{-5}
1 000–3 000	5.30×10^{-3}
3 000–100 000	6.70×10^{-3}

Table 4-3. Average values of the Péclet number of different domains at different times according to Equation (4-1).

Time (years)	Péclet number, *Pe*			
	Concrete	Grout	Void	Macadam
0	2.0×10^{-6}	3.0×10^{-8}	1.2×10^{-9}	0.016
5 000	0.012	1.7×10^{-4}	1.0×10^{-5}	1.470
30 000	0.046	0.013	0.0015	1.738

Table 4-4. Groundwater composition for the freshwater period assumed in the simulations (from Höglund 2014). Groundwater in equilibrium with calcite (SI = 0.02) and undersaturated with respect to all other minerals presented in Table 4-7. S(6) stands for SO_4^{-2}.

Groundwater composition	
pH	7.50
pe	–0.40
Temperature (°C)	25
Species (totals)	**Concentration (mol/kg water)**
Al	1.00E–10
C	4.96E–03
Ca	8.80E–04
Cl	1.27E–03
K	1.03E–04
Mg	3.73E–04
Na	4.39E–03
S(6)	5.25E–04
Si	9.50E–05

Table 4-5. Porewater composition in equilibrium with the mineral phases considered (primary and secondary minerals in Table 4-7) for the concrete, cement grout, void, and macadam modelled domain. S(6) stands for SO_4^{-2}.

Porewaters	**Concrete**	**Grout**	**Void**	**Macadam**
pH	12.96	12.96	12.92	7.30
Temperature (°C)	25			
Ionic strength (mol/kg w)	0.13	0.13	0.114	0.175
Species (totals)	**Concentration (mol/kg water)**			
Al	1.66E–05	1.65E–05	4.02E–05	1.00E–10
C	1.63E–05	1.61E–05	1.00E–10	1.56E–03
Ca	5.21E–03	5.27E–03	9.22E–04	1.08E–02
Cl	5.12E–05	5.12E–05	5.12E–05	1.42E–01
K	9.09E–02	8.98E–02	8.33E–02	5.16E–04
Mg	1.59E–08	1.60E–08	1.00E–10	1.12E–02
Na	2.67E–02	2.64E–02	2.81E–02	1.10E–01
S(6)	2.29E–04	2.24E–04	4.02E–05	5.25E–03
Si	1.76E–04	1.72E–04	8.03E–04	9.50E–05

Table 4-6. Calculated composition of concrete and cement grout used in the 2BMA (Höglund 2014). The chemical composition of the minerals and their equilibrium constants are presented in Appendix A.

	Concentration in concrete		**Concentration in grout**	
Primary mineral	(mol/liter medium)	(mol/kg water)	(mol/liter medium)	(mol/kg water)
CH (portlandite)	1.1825	10.750	1.0293	3.431
$CSH_{1.8}$	1.3629	12.390	1.1202	3.734
Ettringite	0.0356	0.324	0.0293	0.098
$C_3FH_6(C)$ [#]	0.1122	1.020	0.0922	0.307
Monocarboaluminate	0.0728	0.661	0.0219	0.073
Calcite	0.0434	0.394	0.0356	0.119
Brucite	0.0676	0.615	0.0556	0.185
Exchanger composition*	(mol/liter medium)	(mol/kg water)	(mol/liter medium)	(mol/kg water)
CaX_2	0.00046	0.00420	0.00048	0.00437
KX	0.05332	0.48470	0.05330	0.48450
NaX	0.00795	0.07229	0.00794	0.07222

[#] $C_3FH_6(C)$ was considered in the simulations in PHAST, but has been eliminated from the iCP simulation due to numerical convergence issues with the Phreeqc solver.

* The selectivity coefficients (log K) for cation exchange are, assuming Ca as a reference: 0.3 for K and 0.6 for Na.

Table 4-7. Secondary minerals allowed to precipitate in all model domains (from Höglund 2014). The chemical composition of the minerals and their equilibrium constants are presented in Appendix A.

Secondary minerals allowed to precipitate*	
$CSH_{0.8}$	Friedelsalt
$CSH_{1.1}$	Hemicarboaluminate
$SiO_2gel(am)$	Syngenite
$C_3AH_6(C)$	AFm
$Fried_{0.86}Al_{5.14}OH$	Gypsum
$Fried_{0.88}Al_{5.12}OH$	Thaumasite
$Fried_{1.04}Al_{4.96}OH$	$(CaO)_3CaCl_2$:15H2O
$Fried_{1.34}Al_{4.66}OH$	
$Fried_{1.42}Al_{4.58}OH$	
$Fried_{1.96}Al_{4.04}OH$	

* In the macadam and void domains, no primary reactive minerals are considered. Secondary minerals allowed to precipitate in those domains include all the primary minerals of Table 4-6 and secondary minerals of the cementitious domains.

In the iCP model, the calculation of porosity has been performed by initially deriving the inert mineral volume fraction from the initial porosity:

$$V_{inert} = 1 - \varphi_0 - \varphi_0 \sum_{i=1}^{M} C_{0,i} V_{m,i} \qquad (4\text{-}2)$$

In Equation (4-2), φ_0 (m^3/m^3) is the initial porosity (0.11 for concrete), V_{inert} (m^3/m^3) is the volume fraction of chemically unreactive material, $C_{0,i}$ is the i-th mineral concentration in mol/m^3 of water, and $V_{m,i}$ is the molar volume of i-th mineral (m^3/mol). Substituting initial mineral concentrations in Equation (4-2), the value of V_{inert} is 0.693 (m^3/m^3). The inert volume fraction corresponds to the aggregate volume fraction of the concrete mix of SFR. The latter has been calculated from the mixing proportions of construction concrete (Höglund 2014, Table 2-4) assuming a ballast density of 2 650 kg/m^3. It is noted that the porous media composed of cement hydrates occupies a volume fraction of 0.307. The inert volume is assumed to have a negligible porosity.

The porosity values at each time step, n, can be calculated as follows:

$$\varphi^n = \varphi_0 + \varphi_0 \cdot \left(\sum_{i=1}^{M} C_{0,i} V_{m,i} - \sum_{i=1}^{M} C_i^n V_{m,i} \right) \qquad (4\text{-}3)$$

In Equation (4-3), φ^n is the porosity at time t^n, which depends on the current concentrations of all the solid minerals, denoted as C_i^n. Equation (4-3) is equivalent to the porosity calculation performed by Höglund (2014). It assumes that there is no coupling between chemical reactions and porosity changes. This is actually the case in the present benchmark, since PHAST does not currently allow this coupling. Using this expression, porosity can be calculated as a post-processing step to the reactive transport simulation.

If the coupling between chemical reactions and porosity would be explicitly considered, the update of porosity would need to be calculated using a different expression. This expression results from affecting the term $C_i^n V_{m,i}$ in Equation (4-3) by the updated porosity instead of the initial porosity, leading to:

$$\varphi^n = \frac{1 - V_{inert}}{1 + \sum_{i=1}^{M} C_i^n V_{m,i}} \qquad (4\text{-}4)$$

4.2 Numerical model setup

The conceptual model described in the previous section has been implemented in iCP (Nardi et al. 2014). In this section presents the details of the numerical implementation.

Three iCP simulations of the conceptual model described above have been performed using different time-stepping schemes (the differences are explained in Section 4.2.2 and Table 4-9).

4.2.1 Finite element mesh

Preliminary tests of the model implementation resulted in an optimized spatial discretization, time discretization, and chemical setup. The iCP model considers a total of 4212 linear triangular finite elements (FE) distributed in concrete (1.754 FE), grout (781 FE), macadam (827 FE), and void (816 FE). The minimum and maximum FE sizes in each domain are presented in Table 4-8. The finite element mesh used in the simulation is presented in Figure 4-2.

Table 4-8. Minimum and maximum size of finite elements used in each domain.

	Concrete	Grout	Void	Macadam
Minimum size (m)	0.032	0.030	0.034	0.050
Maximum size (m)	0.170	0.034	0.170	0.320

4.2.2 Temporal discretization

iCP uses the sequential non-iterative approach (SNIA) to solve the reactive transport problem. Communication times between the multiphysics solver (Comsol) and the geochemical solver (Phreeqc) need to be defined by the user. These communication times define the size of time steps of the SNIA. Within each time step, the Comsol and Phreeqc models may divide the time into substeps to reach convergence of the multiphysics and chemical parts, respectively. Note that Phreeqc only subdivides the time step in case that reaction kinetics is considered. In this work, the entire reaction network is assumed to be at chemical equilibrium. More details about the management of time steps in the different solvers can be found in Nardi et al. (2014).

A transition zone size (TZS) of either 0.008 or 0.1 for the smoothing functions has been used. These are referred to as TZS-0.1 and TZS-0.008, respectively.

Two different communication times were considered for the simulations, as shown in Table 4-9. The main purpose has been to study the effect of time discretization on the results obtained by iCP. In addition, the simulation with a coarse time stepping scheme was repeated using a less smooth function for the transient properties (see Section 4.1).

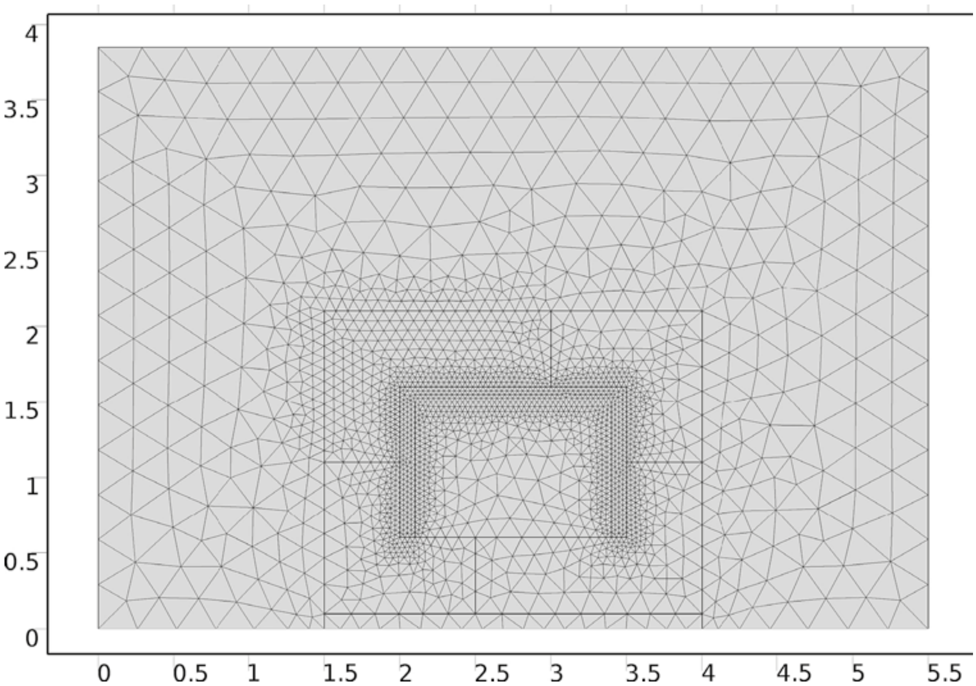

Figure 4-2. Finite element mesh used in the iCP simulation. Dimensions are in metres (m).

Table 4-9. Communication times considered in iCP for the sequential non-iterative approach. CTS and FTS refer to coarse and fine time-stepping schemes, respectively. Cases CTS-TZS-0.1 and FTS-TZS-0.1 use smoothing functions containing transition zone relative size (TZS) of 0.1. CTS-TZS-0.008 uses similar time discretization intervals as PHAST-CTS (Section 4.2.5) and uses smoothed functions of relative size 0.008.

Time period (years)	Time step size (years)		
	CTS-TZS-0.1	FTS-TZS-0.1	CTS-TZS-0.008
0–0.1	0.1	0.1	1
0.1–1	0.1	0.9	1
1–10	0.5	2.5	1
10–100	2.5	7.5	2
100–1 000	12.5	7.5	2.5
1 000–2 000	10	8	5
2 000–10 000	10	5	5
10 000–20 000	10	5	8
20 000–25 000	40	4	8
25 000–30 000	40	5	8

In order to set up the communication time step size for the given finite element mesh, groundwater flow conditions, and the effective diffusion coefficient and dispersivity, two criteria have been applied. The first is the Von Neumann criterion for preventing numerical oscillations, which states:

$$\Delta t \leq \frac{\Delta x^2}{2D_L} \tag{4-5}$$

where Δt (s) is the time step size, Δx (m) is the finite element size, and D_L (m^2/s) is the dispersion-diffusion tensor. For a given FE mesh and material properties, the theoretically maximum time step can be calculated. In the present benchmark, these properties evolve with time (Table 4-1). For the mesh used in the iCP simulations (Section 4.2.1), the maximum time step size has been calculated using Equation (4-5) for different times. This is shown in Table 4-10. Note that the diffusion coefficient in the void and macadam domains remains constant in time (Table 4-1) and therefore the maximum time step range is equal for all the time periods. In the concrete and grout domains, the maximum theoretical time step size decreases over time. This is due to the increase over time of the respective diffusion coefficients (Table 4-1).

Table 4-10. Maximum theoretical time-step (in years) according to Von Neumann criterion for each modelled domain and time period with constant transport properties.

Range of maximum time step (years) in each domain according to Equation (4-5)				
Time period (years)	Concrete (years)	Grout (years)	Void (years)	Macadam (years)
0–100	8–60	0.36	~0.1	1.8–9.5
100–10 000	5–45	0.24	~0.1	1.8–9.5
10 000–20 000	2–22.5	0.19	~0.1	1.8–9.5
20 000–100 000	0.1–1.0	0.12	~0.1	1.8–9.5

The second criterion is given by the Courant number (C_r). This criterion states that the time step size must be smaller than the time for water to travel to adjacent grid points. If v_i (m/s) is the component of interstitial velocity in the i-th direction, the Courant condition is simply:

$$C_r = \frac{v_i \Delta t}{\Delta x_i} < 1 \qquad \text{or} \qquad \Delta t < \frac{\Delta x_i}{v_i} \tag{4-6}$$

The theoretically maximum time step can be calculated using Equation (4-5) as a function of the mesh refinement and groundwater velocities. In the present benchmark, the velocities evolve with time due to the increase of (1) the groundwater flow boundary condition and (2) the hydraulic conductivity. The resulting maximum time step size for each domain is shown in Table 4-11 and graphically in Figure 4-3. This figure shows the most restrictive value of the maximum time step size, for each domain (concrete, grout, void, and macadam).

Table 4-11. Maximum theoretical time-step according to the Courant criterion for each modelled domain, for the most restrictive period (higher velocities), i.e. from 20 000 to 100 000 years.

Most restrictive value of maximum time step (years)				
Time period (years)	**Concrete**	**Grout**	**Void**	**Macadam**
20 000–100 000	4.31	4.74	14.08	0.84

It may be observed that the Courant criterion is not very restrictive for the present model setup. Only the macadam domain shows a maximum time step size of 0.83 years at an advanced stage of concrete degradation. For the rest of the domains, the time step size is always higher than 4 years. Therefore, it may be concluded that the Courant criterion is fulfilled in the iCP simulations that use a fine time discretization (FTS).

It is noted that the dimensions of the SFR vault simulated in Höglund (2014) were smaller than the real geometry, except for the thickness of the concrete walls. If one would use a similar finite element mesh to represent the actual dimensions of the vault, the finite element size would be larger. In this case, the maximum time steps would also increase: they depend linearly (Courant number) or on the square of the mesh size (Von Neumann criterion).

4.2.3 Initial and boundary conditions

Boundary conditions for groundwater flow described in Section 4.1 have been imposed (constant inlet flow) on the left boundary and a zero hydraulic head along the right boundary. In addition, no flow boundary conditions have been set at the upper and lower boundaries. As initial condition, a zero hydraulic head has been set.

For solute transport, boundary conditions are set to no flow at the upper and lower boundaries, and open boundary condition (see Equation 3-1) along the left boundary. Along the right boundary, an outflow condition applies as follows:

$$-\boldsymbol{n} \cdot (\boldsymbol{D}\nabla \boldsymbol{c}) = 0 \tag{4-7}$$

Above, $\boldsymbol{D}$ (m^2/s) is the dispersion-diffusion isotropic tensor, $\boldsymbol{n}$ (–) is the normal vector, and $\boldsymbol{c}$ (M) is the solute concentration vector.

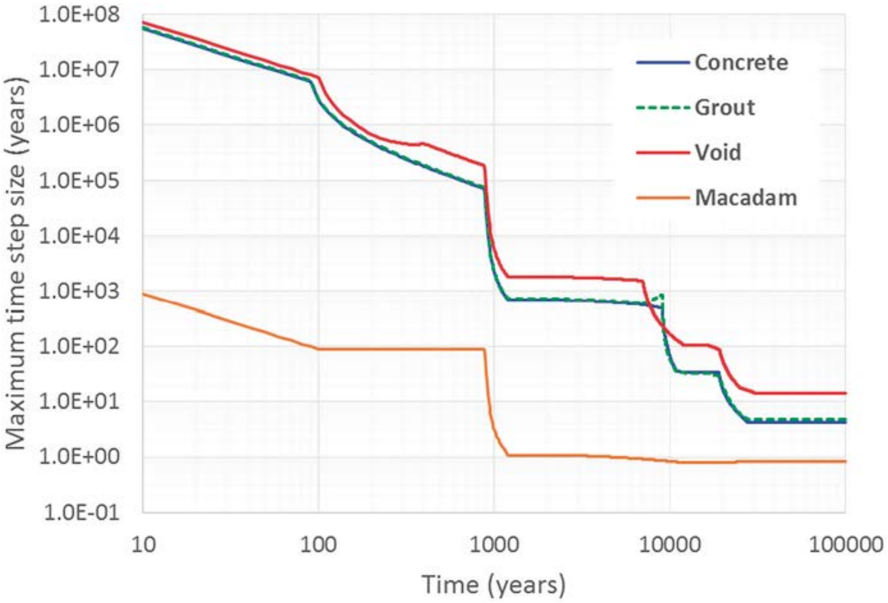

Figure 4-3. *Maximum time step size according to Courant criterion for each model domain.*

4.2.4 Implementation of a modified chemical setup

The chemical setup presented in Section 4.1 represents the final system used in iCP for the benchmark. The chemical system presented in Höglund (2014) differs slightly. However, the implementation of the initial chemical system of Höglund (2014) pointed to the identification of convergence issues. These issues were present both in iCP and PHAST (version 2.48). However, a different version of PHAST, named PHAST for Windows, was capable of running the simulation with this system. An exhaustive analysis of the different domains in batch mode using 0D simulations in Phreeqc were carried out to find a solution. The convergence issue was caused by the iron, present in the system as aqueous Fe and the cement hydrate $C_3FH_6(C)$. The issues were solved by removing iron from the system. This mineral phase is not essential for the purpose of the benchmark, given the low iron concentration in the porewater and the small amount of mineral phases with iron initially present.

In order to perform a better comparison between the reactive transport simulation in iCP and PHAST, the PHAST simulation has been repeated with the modified chemical system. To this end, PHAST version 2.48 (Parkhurst et al. 2010) has been used. The same chemical setup as used in iCP has been implemented in PHAST (see Section 4.1). Therefore, the new PHAST simulations allow a more accurate comparison between PHAST and iCP models.

The model of the PHAST simulation has been implemented using exactly the same setup of Höglund (2014), except for the modified chemical reactions. More details about the implementation of the PHAST model can be found in Höglund (2014).

The time-stepping scheme used by Höglund (2014) for the PHAST simulations considered one-year time steps over the whole period analysed. The behaviour of the PHAST model subjected to time steps greater than one year has been investigated here using two PHAST simulations with different time-stepping schemes. The time step size for each simulation is shown in Table 4-12. They consist of a (1) coarse and a (2) fine (i.e. one year) time stepping scheme. The main purpose has been to study the effect of time discretization on the results. The coarse time-stepping scheme coincides with the scheme used in the iCP simulation CTS-TZS-0.008 (see above).

Table 4-12. Time stepping schemes used in the new PHAST simulations using the same chemical system as implemented in iCP.

Time period (years)	Coarse Time Step (CTS) size (years)	Fine Time Step (FTS) size (years)
0–10	1.0	1.0
10–100	2.0	1.0
100–1 000	2.5	1.0
1 000–10 000	5.0	1.0
10 000–30 000	8.0	1.0

4.3 Results and comparison

For comparison of the results, an observation point in the concrete structure has been defined. Its location is given by the intersection between the mid planes of the left concrete wall and the top concrete lid (x = 1.75 m; y = 1.85 m). This observation point is referred to point GH in Höglund (2014). The same nomenclature is used here.

First, the results presented in Höglund (2014) are compared to the new PHAST simulations performed in this work. Thereafter, the iCP model results are presented and compared to the new PHAST simulations.

4.3.1 Comparison of PHAST results

This section presents the results of the comparison between the different PHAST simulations:

1. The case Large20 presented in Höglund (2014).
2. The case with fine time-stepping (FTS) scheme performed in this work.
3. The case with coarse time-stepping (CTS) scheme performed in this work.

Figure 4-4 presents the results of the new PHAST simulations in terms of mineralogical phase assemblage. It depicts the temporal evolution of calcite, portlandite, ettringite, and C-S-H gels at point GH corresponding to the coarse and fine time-stepping schemes. The results clearly show the impact of using a coarse time discretization, delaying the leaching of portlandite and CSH_1.8. As a result, the onset of precipitation of CSH_1.1 is also delayed. Leaching of Ca from C-S-H has not reached the point of dissolution of CSH_1.1 and formation of CSH_0.8 after 30 000 years. Ettringite precipitation is on the other hand not very much affected by a coarser time discretization. Results of the fine time discretization (FTS) in Figure 4-4 can be qualitatively compared with the results of Höglund (2014), which are presented in Figure C-1 of Appendix C. A similar degradation process may be observed between the FTS case of Figure 4-4 and Figure C-1 in Appendix C: exhaustion of portlandite after ~15 000 years and degradation of CSH_1.8 to CSH_1.1 thereafter.

The quantitative comparison of different PHAST results has also been made in terms of temporal evolution of porosity (Figure 4-5) and pH (Figure 4-6) over 30 000 years. The results are compared with digitized values from the report by Höglund (2014). The details of the procedure to calculate porosity are discussed in Section 4.1.

It may be observed that the new PHAST simulation with FTS agrees relatively well with the porosity evolution reported in Höglund (2014). The effect of a coarser time discretization is clearly observed. Compared to the FTS case, the increase in porosity with time is significantly slower in the case of adopting coarse time steps. Small discrepancies between the new PHAST simulation (FTS) and the results by Höglund (2014) are still observed. These are apparently not related to the removal of C_3FH_6 mineral phase from the chemically reactive system, since this mineral does not react for at least the first 30 000 years in Höglund (2014) results.

As stated above, the hardened cement paste is the only porous material of concrete, assuming no porosity in the aggregates. Therefore, an initial porosity of concrete of 0.11 corresponds to a porosity of the cement paste of 0.358. After ~17 000 years, the porosity of concrete has increased to a value of ~0.165. The corresponding porosity in the degraded cement paste is 0.537.

Another quantitative indicator which is important for direct comparison of the results is pH, which is shown in Figure 4-6. It may be observed that the FTS case leads to a pH evolution similar to the results in Höglund (2014). On the other hand, the CTS case shows a deviation of pH between 17 000 and 24 000 years. This is related to the evolution of the mineralogical phase assemblage, as shown in Figure 4-4.

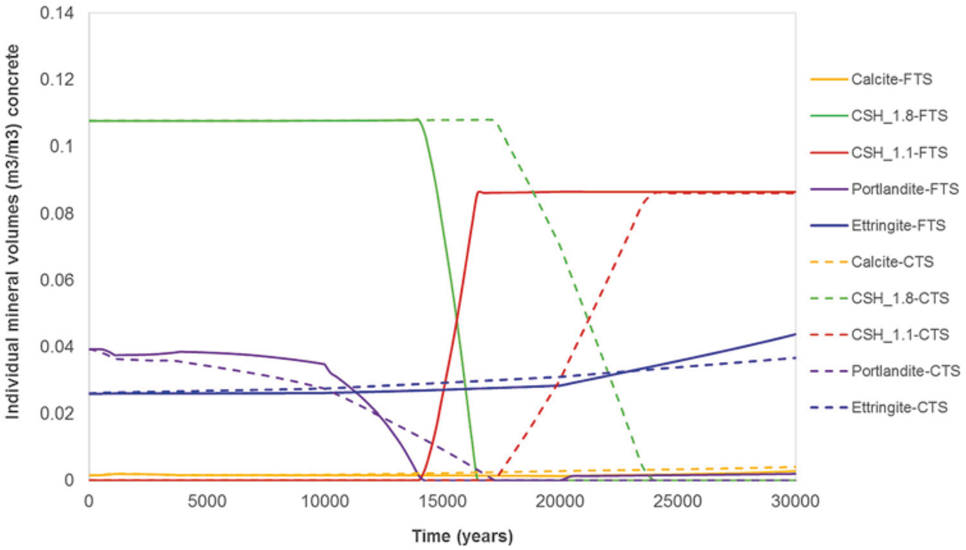

Figure 4-4. *Temporal evolution of cement hydrates at observation point GH using the code PHAST (new simulation results): coarse vs. fine time-stepping schemes.*

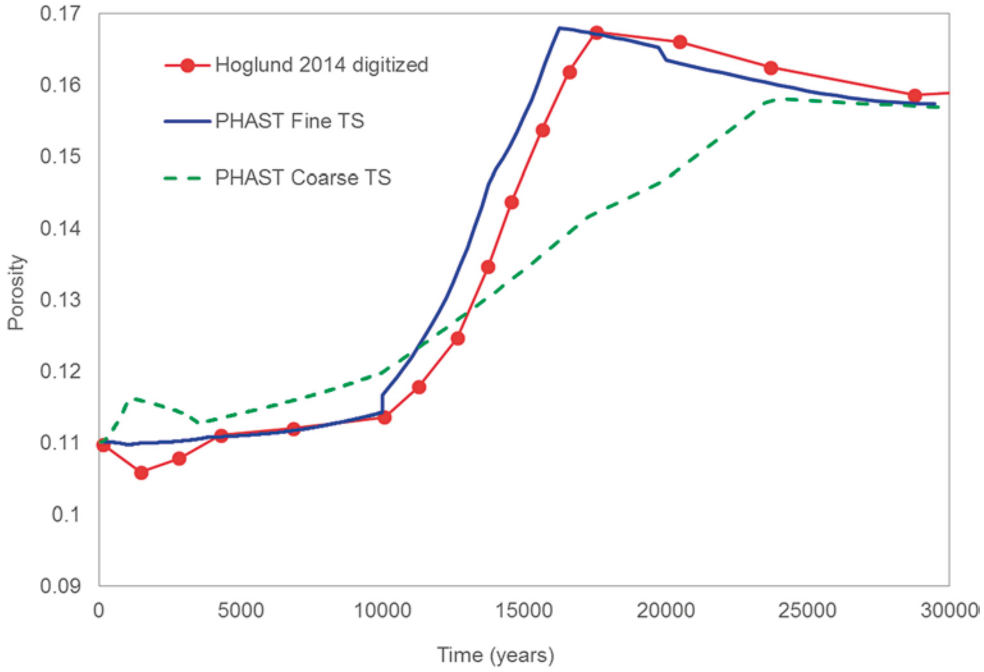

Figure 4-5. Comparison of temporal evolution of concrete porosity at point GH: new PHAST simulations with coarse and fine time-stepping scheme and results digitized from Höglund (2014).

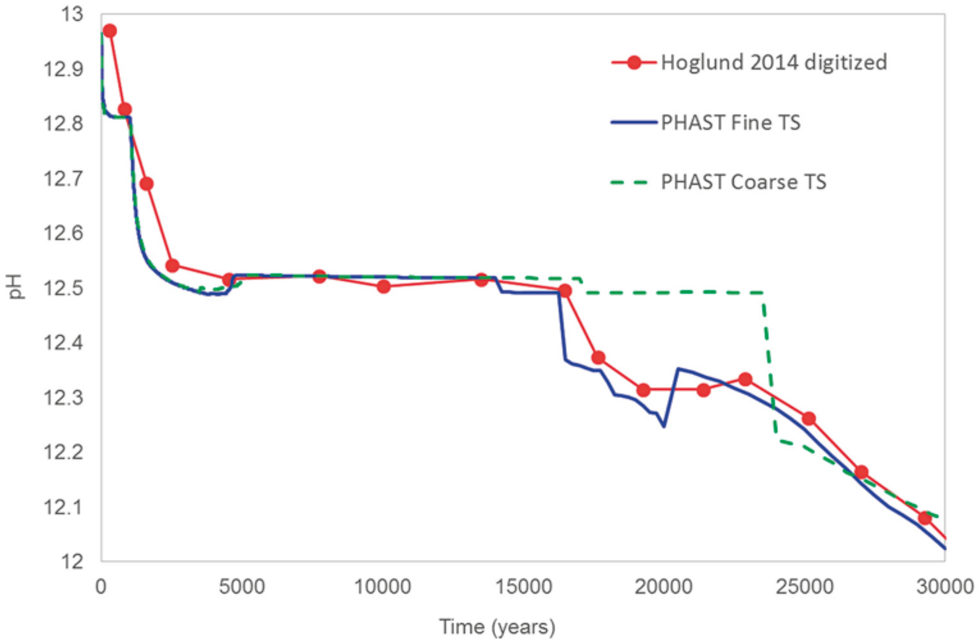

Figure 4-6. Temporal evolution of pH at point GH: new PHAST simulations with coarse and fine time-stepping schemes and results digitized from Höglund (2014).

From these comparisons, it may be concluded that the new PHAST simulation with a fine time discretization (FTS) is representative of the case Large20 present in Höglund (2014). Therefore, this case may be considered suitable for comparison with the iCP model.

4.3.2 Comparison of iCP and PHAST: groundwater flow

The magnitude of the inflow on the left boundary increases with time at 1 000 and 3 000 years, as shown in Table 4-2. In turn, the hydraulic conductivity increases at 100, 10 000, and 20 000 years, as shown in Table 4-1. These time-dependent properties of the system lead to an increasing flow across the barriers. This is shown in Figure 4-7, which presents the distribution of the Darcy velocity in the horizontal direction. It may be observed how the flow is also redistributed through the barriers.

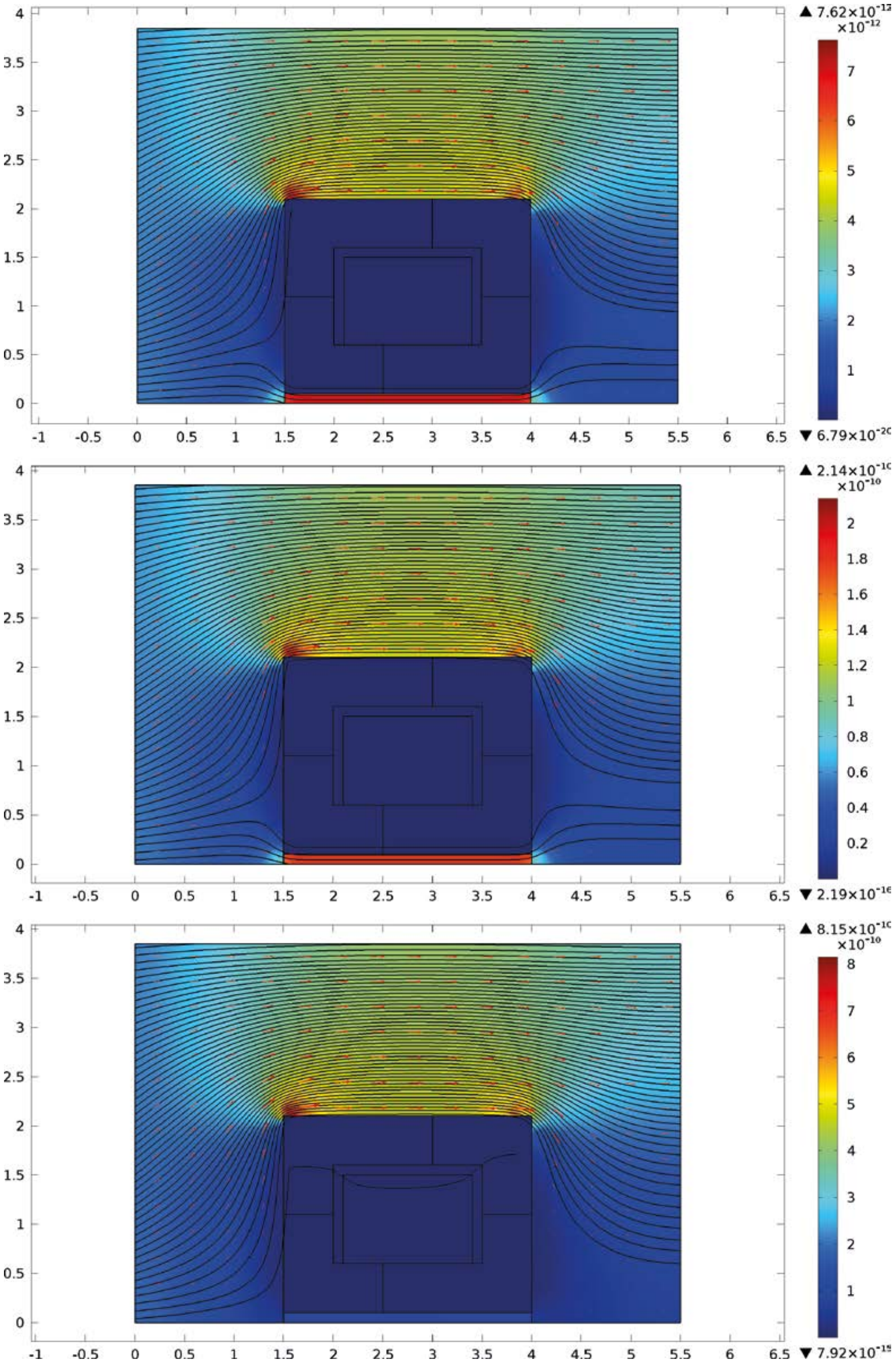

Figure 4-7. *Darcy velocity in the horizontal direction (m/s), streamlines, and arrow fluxes for the modelled domain at 100 (top), 1 000 (middle), and 10 000 (bottom) years. Note the different scales in each figure.*

The Darcy velocities of iCP and PHAST simulations at the observation point GH are compared in Table 4-13 and graphically in Figure 4-8. Note that the simulation in PHAST presents step (abrupt) changes in the velocity field due to the time-dependent setup of the system. In iCP, it has been decided to introduce smooth transitions of the time-dependent properties. This difference, observed in Figure 4-8, may lead to a slightly slower degradation of concrete in iCP simulations.

Table 4-13. Comparison of the Darcy velocity in x (v_x) and y (v_y) directions at observation point GH: results of iCP (TZS 0.1) and PHAST at 4 different times.

Time (years)	v_x iCP (m/s)	v_x PHAST (m/s)	v_y iCP (m/s)	v_y PHAST (m/s)	Difference in x	Difference in y
10	2.760E–10	2.246E–10	2.878E–11	6.786E–11	22.88 %	–57.59 %
2000	2.202E–06	2.209E–06	2.364E–07	3.184E–07	–0.35 %	–25.76 %
15000	3.798E–05	3.578E–05	4.104E–06	2.900E–06	6.15 %	41.56 %
50000	3.510E–04	3.364E–04	4.400E–05	2.846E–05	4.29 %	54.72 %

Table 4-13 shows larger velocity differences in the y-direction, perpendicular to the imposed groundwater flow. These deviations are more important when a large transition zone size (TZS) is imposed in the smoothing process in the Comsol model. iCP values converge to the results in PHAST when the smoothing size is minimized (Figure 4-8). The use of a smoothing function for the imposed transient groundwater flow is needed to avoid reaching a singularity in the Darcy's law solver.

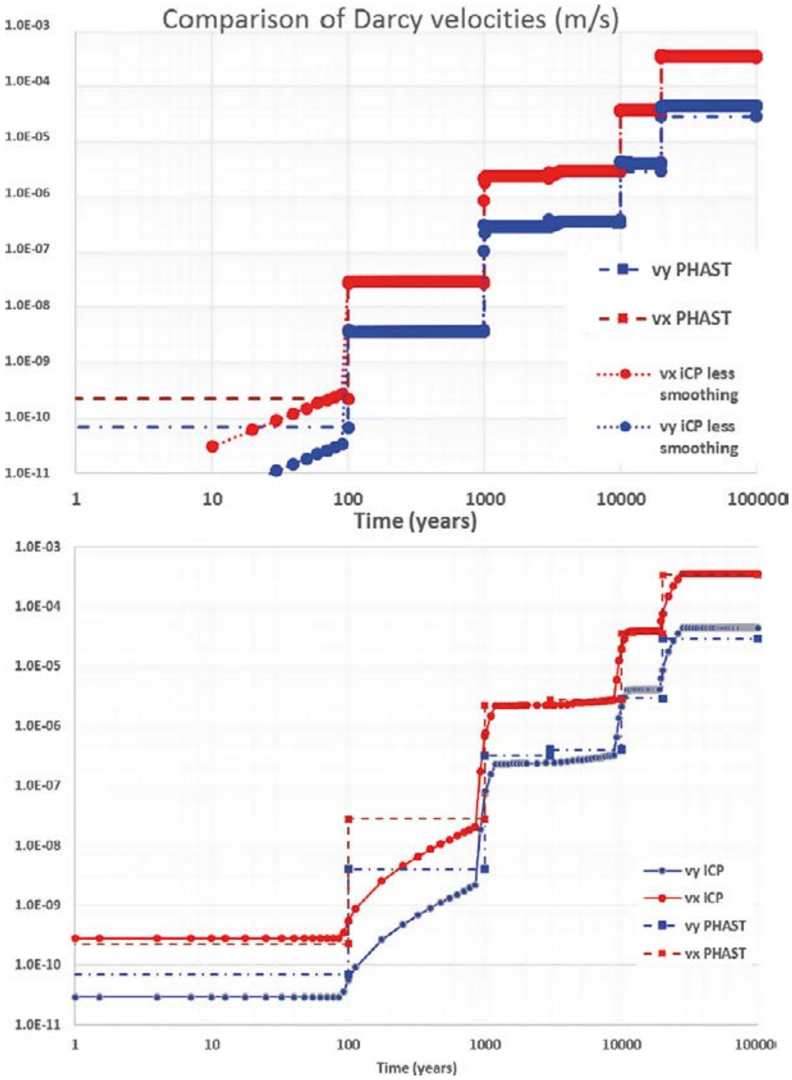

Figure 4-8. *Time evolution of Darcy velocity in x and y directions at observation point GH: comparison of PHAST and iCP results: (bottom) using TZS 0.1, and (top) using TZS 0.008.*

Another source of differences in the Darcy velocities is related to the underlying numerical algorithms used in PHAST and iCP. PHAST is based on the finite difference method. iCP uses Comsol to solve flow and solute transport, which uses the finite element method. Comparison of finite difference and finite element methods have been extensively discussed in the literature (e.g. van Genuchten 1982, Simpson and Clement 2003). In fact, the comparison of finite element and finite difference solutions in two-dimensional flow equations has pointed to some fundamental differences. These are related to the way in which variable material properties are spatially averaged, and to how the Neumann boundary condition is treated. The difference becomes negligible if a high resolution discretization is used in one-dimensional problems. However, in two dimensions the finite difference solution for a given spatial discretization can still introduce numerical errors. In the current model, a Neumann type boundary condition is imposed along the left boundary. Therefore, small discrepancies between iCP and PHAST can in part be due to the different numerical methods. A short discussion on the way Neumann boundary conditions are treated in finite element and finite difference methods is presented in Appendix B.

4.3.3 Comparison of iCP and PHAST: chemical evolution

The concrete degradation processes and gradual leaching of cement hydrates over a period of 30 000 years are shown in Figure 4-9 through Figure 4-13. The evolution of pH is presented in Figure 4-14. These results correspond to the iCP simulation Case 3 denoted as FTS-TZS-0.1, see Section 4.2. Calcium leaching and calcite formation are the main processes at play. The figures illustrate how portlandite and CSH-1.8 are gradually depleted from the system after 30 000 years. This depletion results in the precipitation of secondary minerals, such as CSH-1.1. The onset of calcite precipitation is also observed, which remains in the system for the remaining simulated time. Calcite precipitates primarily in the macadam fill near the inlet side and in the outermost part of the concrete wall, especially at the left side (Figure 4-10). The location of the zones where calcite forms in the macadam fill are governed on one hand by the groundwater flow field: the streamlines show the hydraulic cage effect of the macadam, which leads to a distribution of the streamlines with a significant vertical component. On the other hand, the mixing between the inflowing groundwater, with a relatively high aqueous carbonate concentration, and the high calcium and pH plume from concrete degradation establishes a relatively narrow mixing zone in the macadam where calcite precipitation is favoured.

These figures can be qualitatively compared with the results of Höglund (2014). Some of these results have been included in Appendix C (Figure C-2 and Figure C-3) for comparison. Note that different scales have been used in Appendix C.

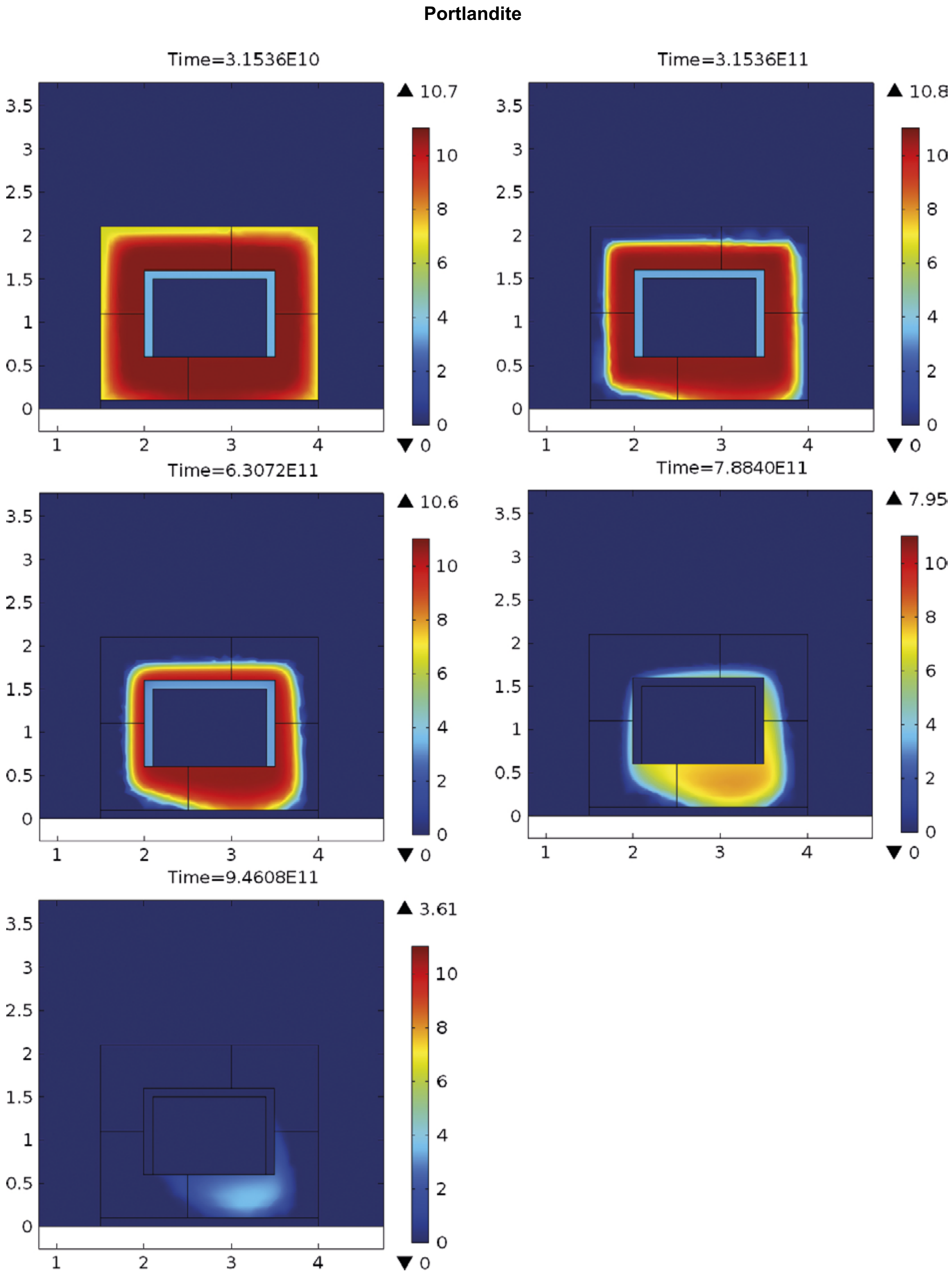

Figure 4-9. *iCP results (fine time discretization): Illustration of temporal evolution of portlandite (mol/kgw) after 1 000, 10 000, 20 000, 25 000, and 30 000 years.*

Calcite

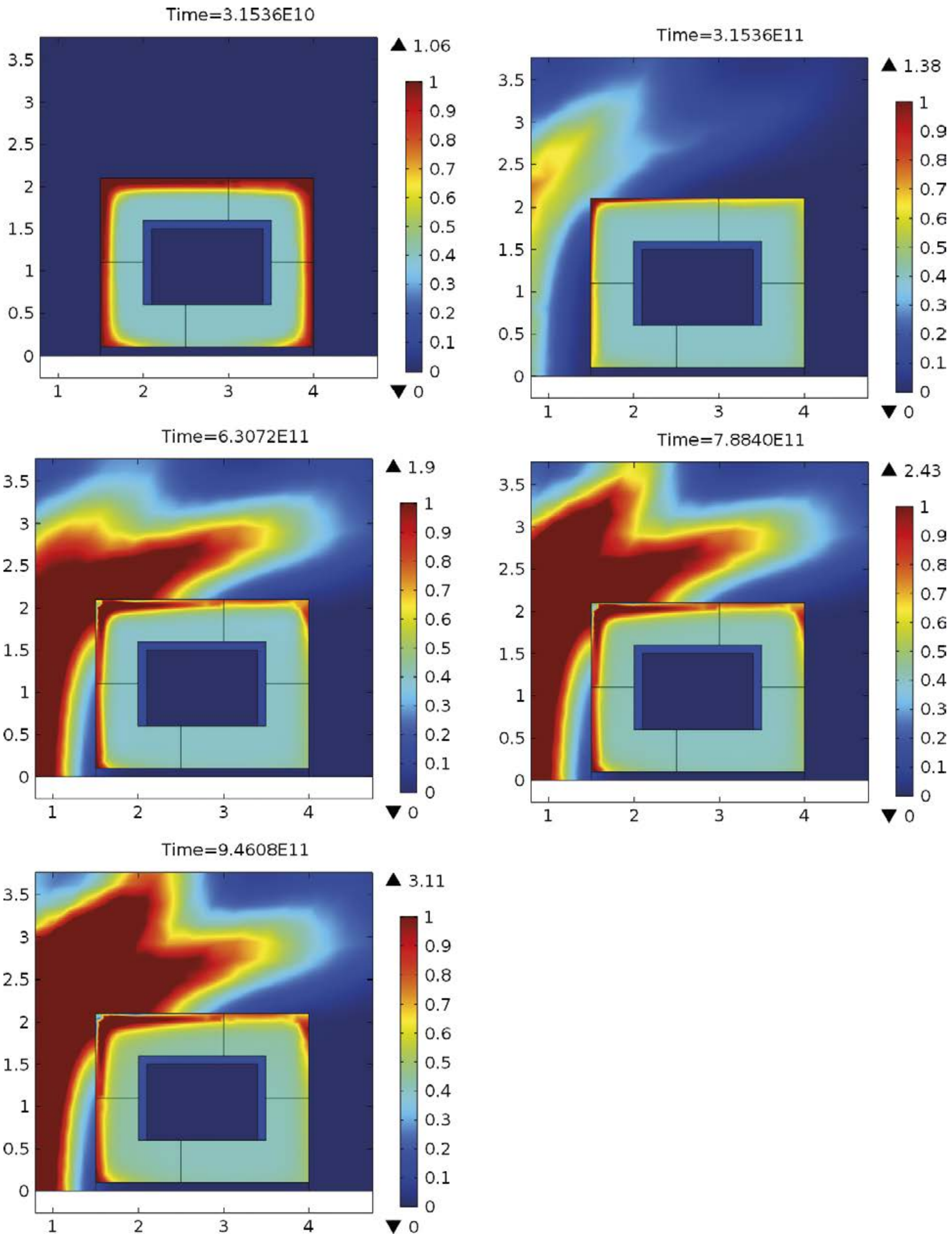
Time=3.1536E10

Time=3.1536E11

Time=6.3072E11

Time=7.8840E11

Time=9.4608E11

Figure 4-10. *iCP results (fine time discretization): Illustration of temporal evolution of calcite (mol/kgw) after 1 000, 10 000, 20 000, 25 000, and 30 000 years.*

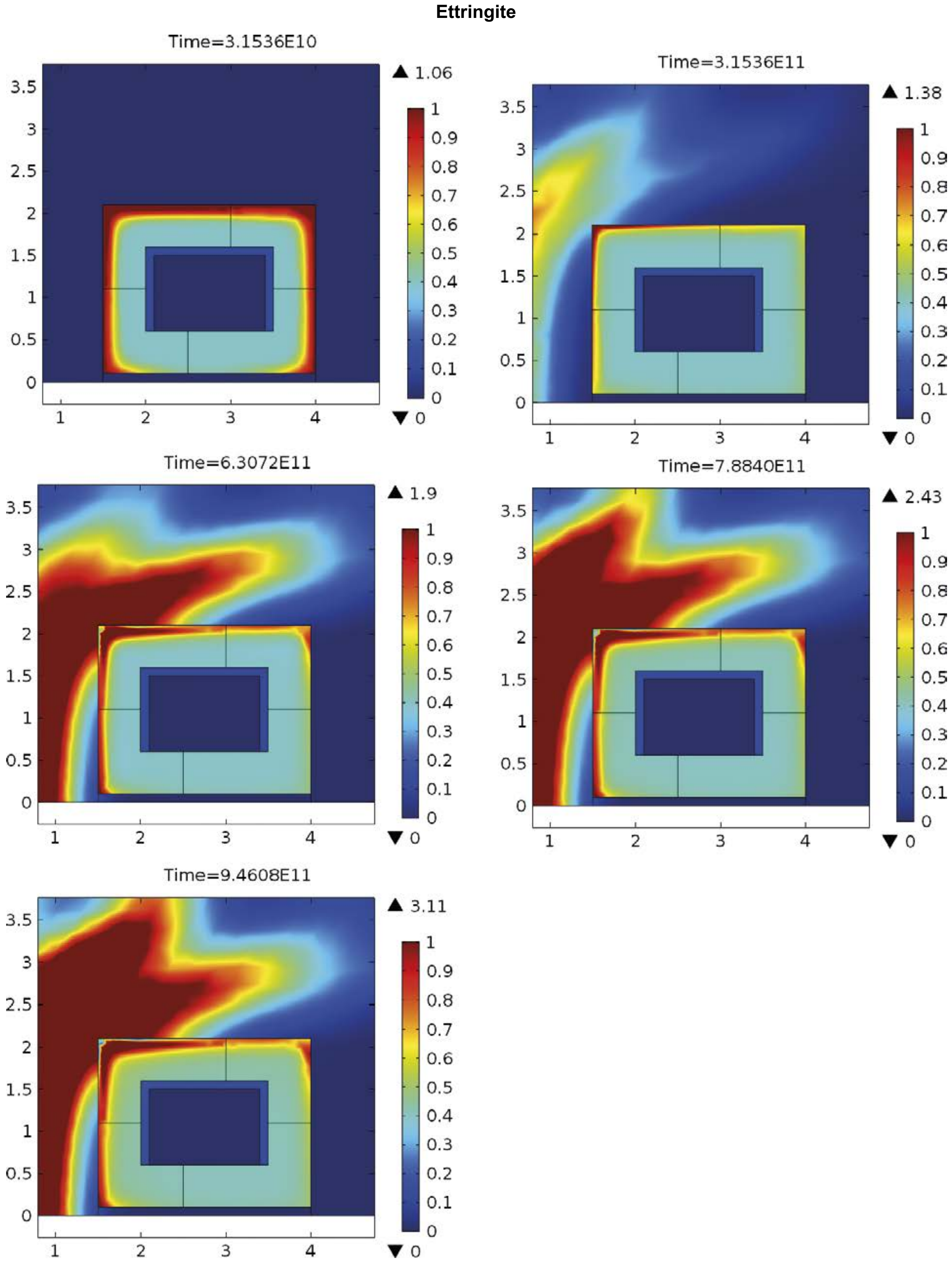

Figure 4-11. *iCP results (fine time discretization): Illustration of temporal evolution of ettringite (mol/kgw) after 1 000, 10 000, 20 000, 25 000, and 30 000 years.*

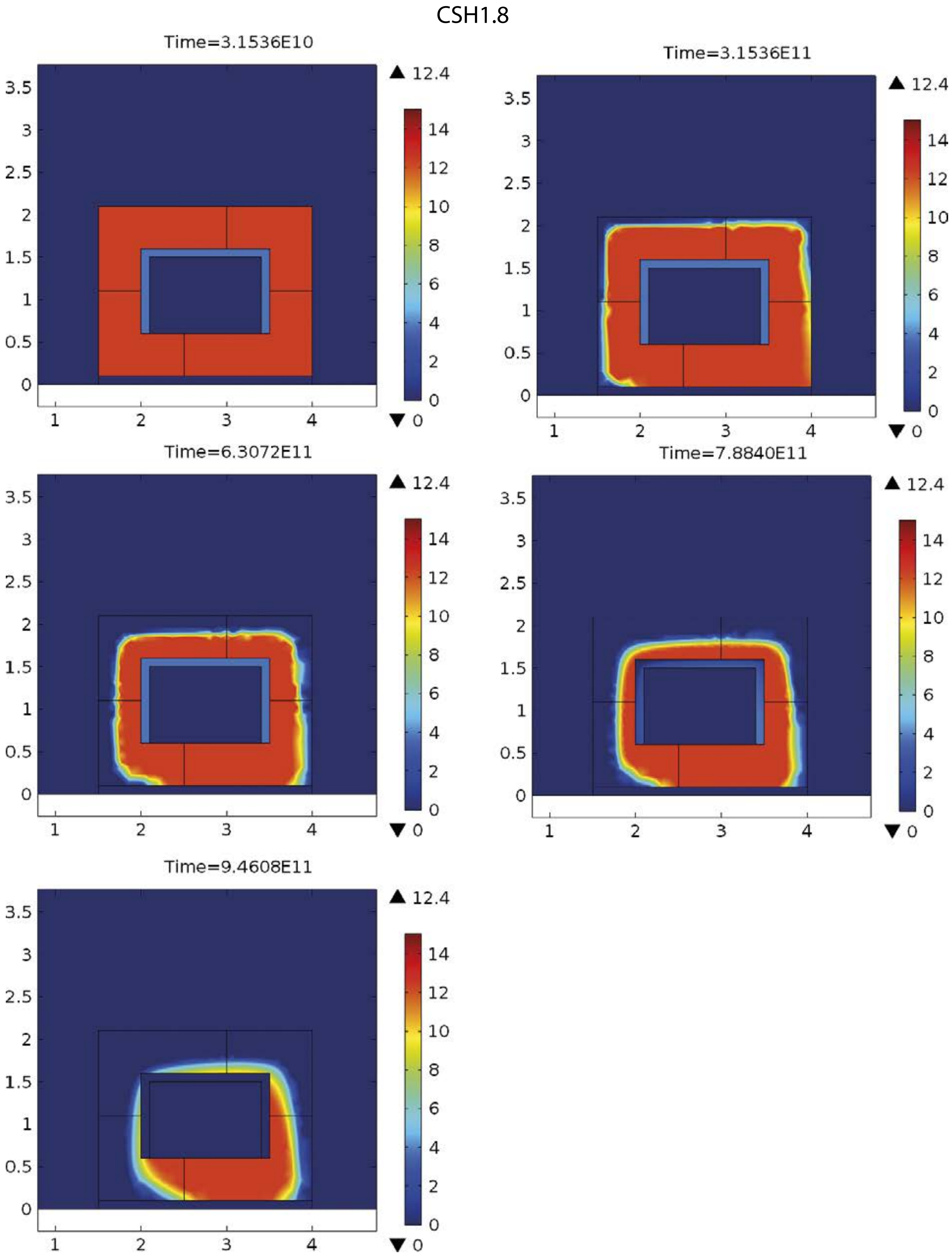

Figure 4-12. iCP results (fine time discretization): Illustration of temporal evolution of CSH-1.8 (mol/kgw) after 1 000, 10 000, 20 000, 25 000, and 30 000 years.

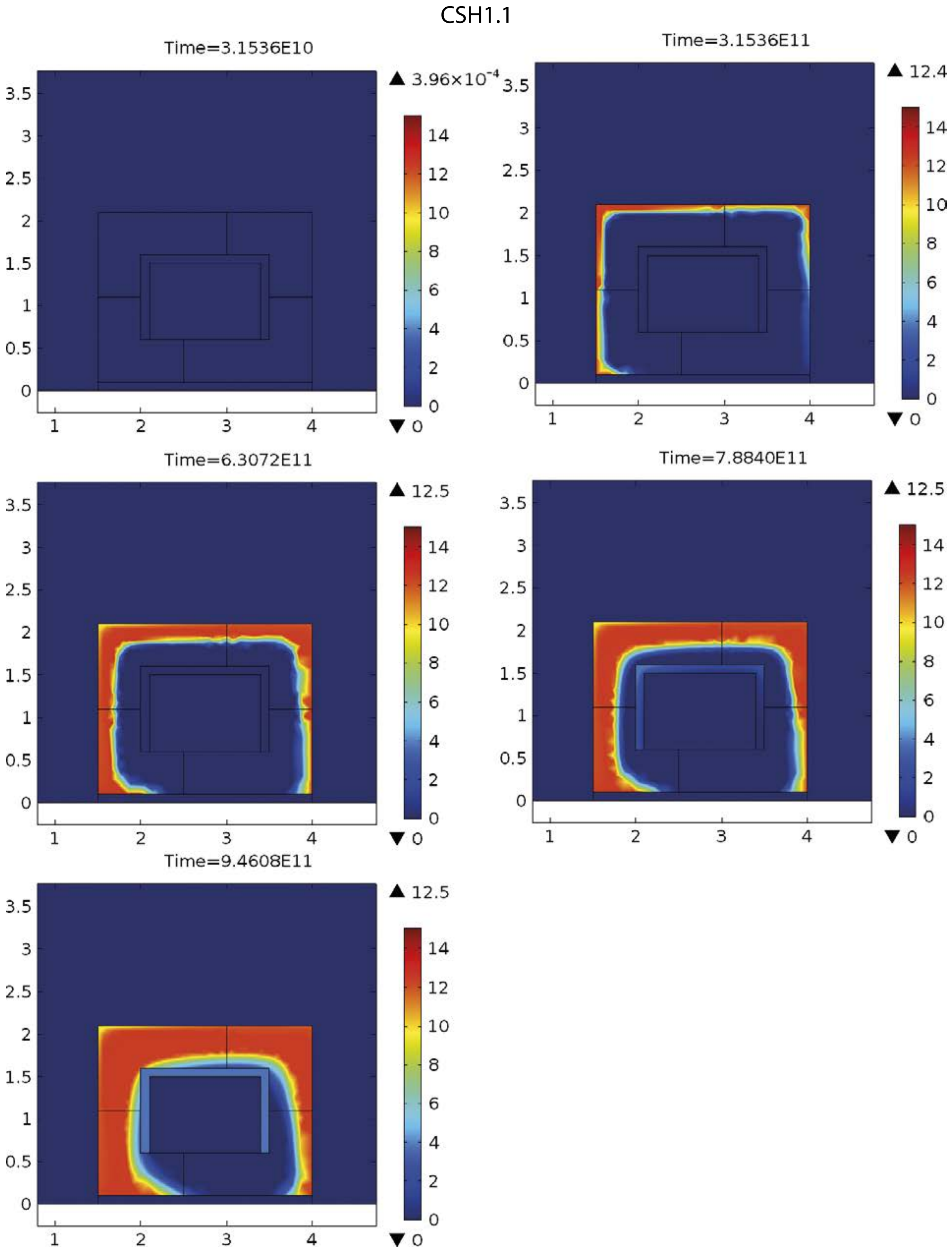

Figure 4-13. iCP results (fine time discretization): Illustration of temporal evolution of CSH-1.1 (mol/kgw) after 1 000, 10 000, 20 000, 25 000, and 30 000 years.

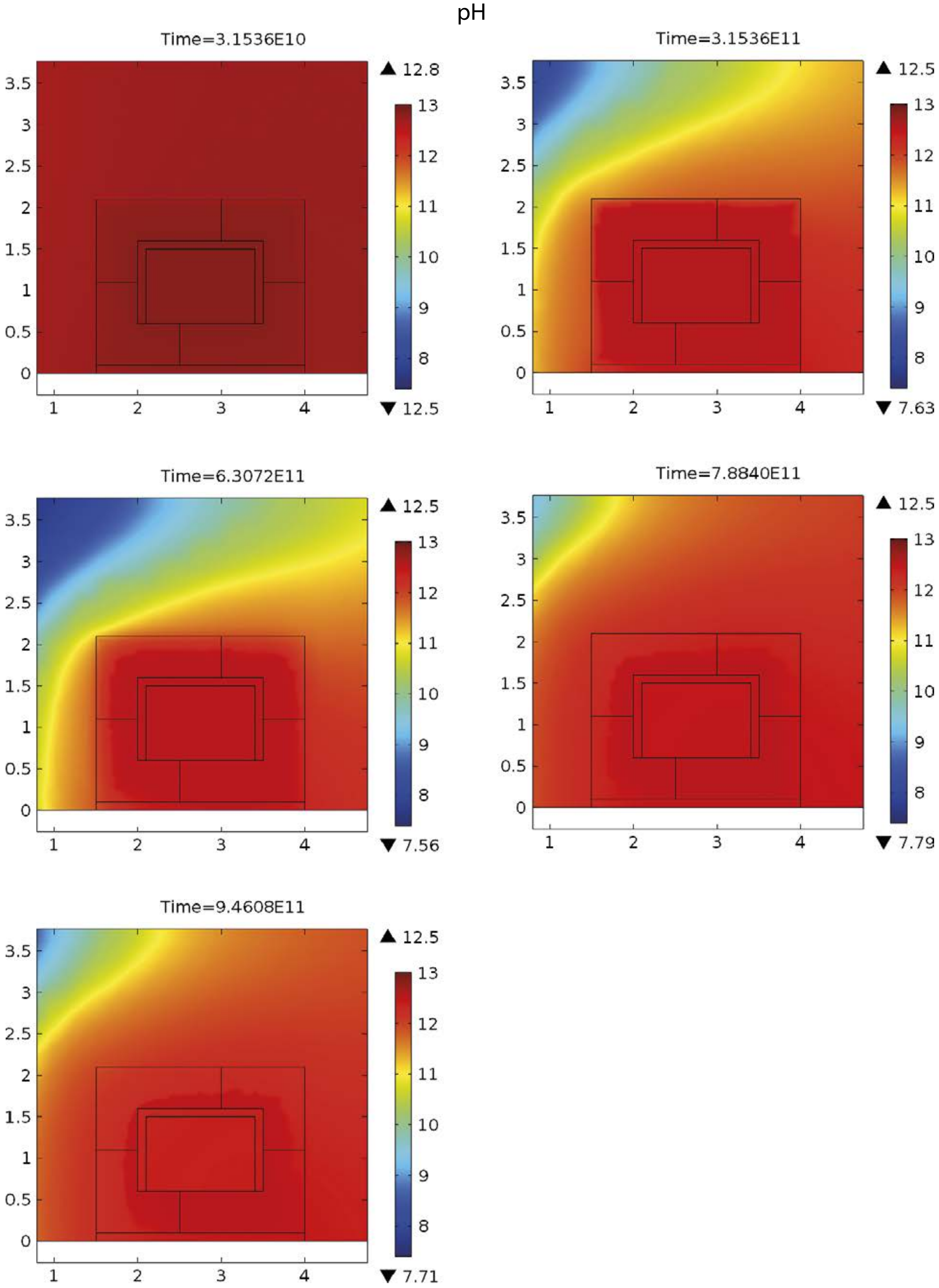

Figure 4-14. *iCP results (fine time discretization): Illustration of temporal evolution of pH after 1 000, 10 000, 20 000, 25 000, and 30 000 years.*

The evolution of the volume fraction of selected minerals at observation point GH is presented in Figure 4-15 and Figure 4-16 over a period of 30 000 years. In Figure 4-15, the results of iCP, Case 3 (FTS-TZS-0.1), are compared to those from the FTS PHAST simulation. In turn, Figure 4-16 shows the results of iCP corresponding to Case 1 (CTS-TZS-0.1).

A relatively good agreement between PHAST and iCP FTS cases is observed in Figure 4-15 with respect to cement hydrates evolution. The C-S-H gels are degraded more slowly in the iCP simulation. This may be due to the influence on the dissolution rate of the larger time step size used in iCP.

The effect of different time discretization schemes in iCP can be observed when comparing Figure 4-15 and Figure 4-16. Similar to the PHAST results presented in Section 4.3.1, a coarser discretization in iCP causes an underestimation of the concrete degradation rate after 30 000 years.

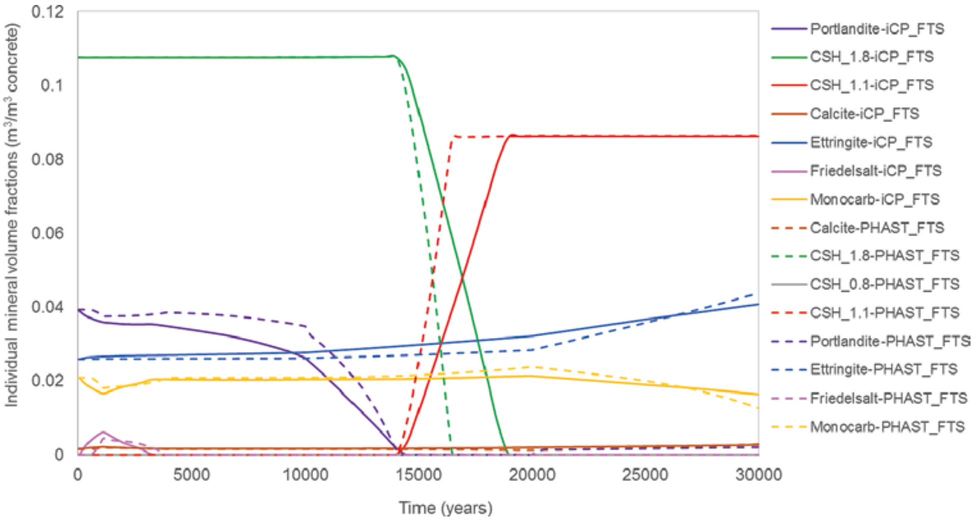

Figure 4-15. *Comparison of iCP and PHAST (new simulations) results: Temporal evolution of individual mineral volume fractions at observation point GH. iCP results correspond to the case with fine time discretization (FTS) using a transition zone relative size of 0.1. PHAST results correspond to the case with fine time discretization.*

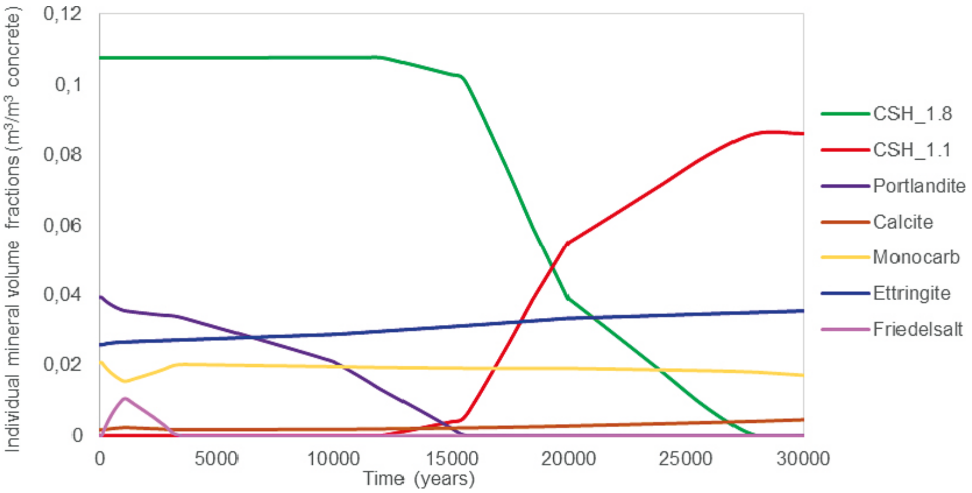

Figure 4-16. *iCP results: Temporal evolution of individual mineral volume fractions at observation point GH for the case with coarse time discretization (CTS), using a transition zone relative size of 0.1.*

The pH and porosity values from iCP simulations are compared with the new PHAST results in Figure 4-17 and Figure 4-18, respectively. These figures present the time evolution at observation point GH. The results show how the coarse time discretization deviates from the fine time descretization, especially in iCP. It may also be observed that the pH and porosity evolution of the iCP FTS-TZS-0.1 case agree relatively well with the PHAST case FTS over a period of 30 000 years.

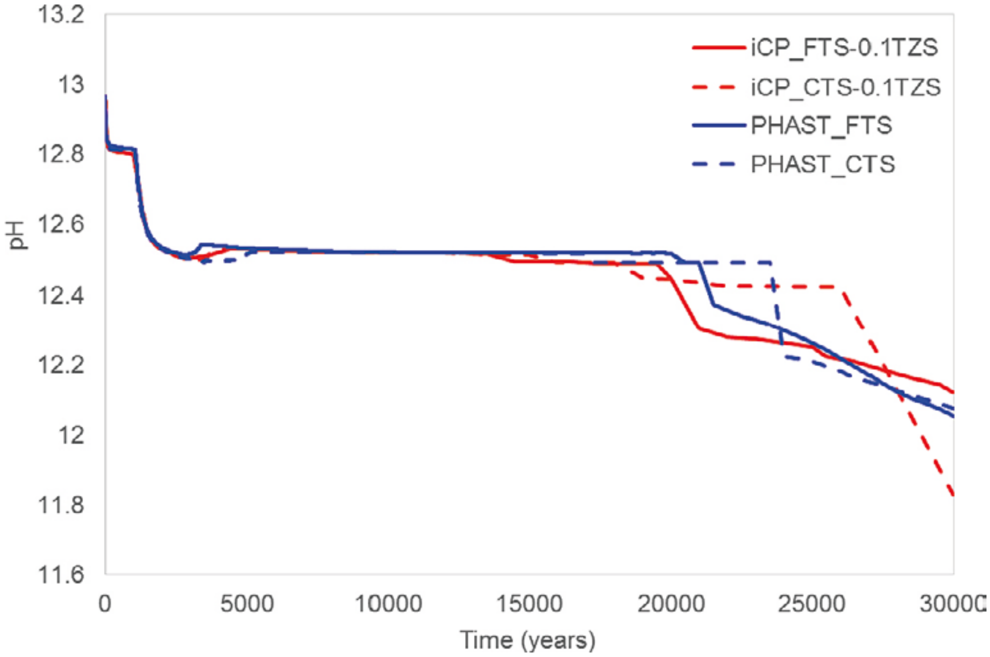

Figure 4-17. *iCP vs. PHAST results: Temporal evolution of pH values obtained from iCP simulations compared with PHAST (CTS and FTS correspond to coarse and fine time discretization, respectively).*

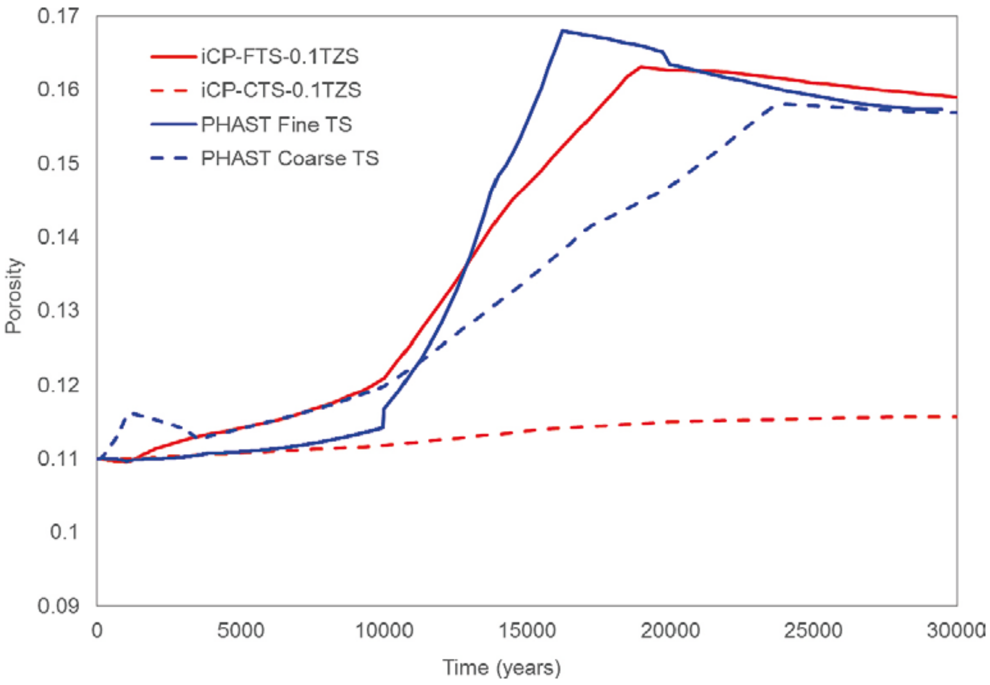

Figure 4-18. *iCP vs. PHAST results: Temporal evolution of porosity values obtained from iCP simulations compared with PHAST (CTS and FTS correspond to coarse and fine time discretization, respectively).*

Table 4-14 and Table 4-15 present a comparison between different simulations of pH values and CSH_1.1 concentrations (mol/kgw), respectively. The results are presented for two different times, i.e. 25 000 and 30 000 years. It may be observed that the iCP Case 2 CTS-TZS-0.008 compares well with the results of the CTS case in PHAST. These two cases have the same time discretization. In contrast, the iCP simulation Case 1 CTS-TZS-0.1 deviates significantly from these results. This is mainly due to the coarser time discretization used in this case (see Table 4-9), as well as a larger transition zone relative size.

Table 4-14. Comparison of pH values between the results of iCP and PHAST at 2 different times (25 000 and 30 000 years). FTS: fine time discretization; CTS: coarse time discretization; TZS transition zone (relative) size.

pH	iCP_CTS-0.1TZS	iCP_CTS-TZS-0.008	PHAST-CTS
25 000	12.42	12.19	12.21
30 000	12.12	12.10	12.07

Table 4-15. Comparison of CSH_1.1 (mol/kgw) values between the results of iCP and PHAST at 2 different times. FTS: fine time discretization; CTS: coarse time discretization; TZS transition zone (relative) size.

CSH_1.1	iCP_CTS-0.1TZS	iCP_CTS-TZS-0.008	PHAST-CTS
25 000	12.06	12.46	12.45
30 000	13.68	12.45	12.44

4.4 Concluding remarks

This section summarizes the main conclusions from the benchmarking studies between iCP (Nardi et al. 2014) and PHAST (Parkhurst et al. 2010). The study has been conducted to verify the modelling tools used to simulate concrete degradation. The 2D reactive transport model of the 2BMA vault in SFR extension has been used for the benchmark (case Large20 in Höglund 2014). In addition, a 1D setup of the concrete wall of the 2BMA vault has also been implemented (Appendix D).

The chemical system used in Höglund (2014) has convergence issues. An exhaustive analysis of the different chemical domains in batch mode (0D simulations in Phreeqc) has led to the identification of the problem origin of the initial system. As a result, a slightly different system has been used to overcome these difficulties in the iCP model. The only difference between the two systems is the removal of iron in the latter. New PHAST simulations with the modified chemical system have also been performed for a more precise comparison with the iCP model. For a time period of 30 000 years, the results of the new PHAST simulations agree relatively well with those of Höglund (2014). The comparison improves when using a similar time discretization.

Different time-stepping schemes have been used in PHAST and iCP to assess the sensitivity of the results to a fine and a coarse time discretization. These results indicate that the new PHAST simulations are suitable for a more rigorous comparison with the iCP model.

Regarding the iCP model, it is noted that Darcy velocities from iCP simulations give slightly lower values compared to values derived from the PHAST model. This discrepancy is mainly due to the smoothing approach that is used in the Comsol flow model, but also to intrinsic differences between finite elements (iCP) and finite differences (PHAST) in 2D simulations (see Appendix B). Applying smoothing to stepwise transitions in the inlet flow is necessary as the solution reaches singularity without it. iCP simulations were performed using two different transition zone relative sizes (0.1 and 0.008). As expected, by minimizing the transition zone size the estimated Darcy velocities approximately converge to the values obtained in PHAST.

The temporal evolution over 30 000 years of individual mineral volume fractions and their effect on porosity and pH has been assessed with iCP. No feedback of porosity has been considered, similar to the PHAST simulations. The quantitative comparison with PHAST results at an observation point in the concrete structure is relatively good. The degradation sequence of cement hydrates follows the same pattern. The temporal evolution of porosity and pH of the pore solution is very similar when using iCP or PHAST. The best comparison between iCP and PHAST calculations is achieved when using the fine time discretization in both codes.

From the benchmark study, it may be concluded that the iCP model predicts a concrete degradation sequence that matches the results of the PHAST model. However, some minor discrepancies are still observed, which could be related to the different methods used by both codes (see Appendix B) and to a different temporal and spatial discretization (triangular elements have been used in iCP).

5 BHK cross-section reactive transport model

5.1 Description of conceptual model

The geometry of the 2D model implemented in this study corresponds to a typical cross-section of the BHK concrete vault of the SFL repository. It has been extracted from the 3D groundwater flow model developed by Abarca et al. (2016). It consists of three different domains: the host rock, the concrete backfill, and a waste domain (Figure 5-1). The volume of the backfill has been conceptualized as a monolith made of concrete. The same concrete composition as that used in the SFR repository has been assumed (Höglund 2014). The radioactive waste is stored in steel tanks. The steel tanks are in turn emplaced in concrete compartments that are that are subsequently grouted (Elfwing et al. 2013). All these components are simplified in the model as one homogeneous waste domain. The only chemically reactive material that has been considered in this work is concrete. The volume of the waste domain is only partly occupied by concrete. Its volume fraction has been calculated by Pękala et al. (2015) based on the current BHK vault design. The same concrete composition as that of the concrete backfill has been assumed. The host rock has only been considered for groundwater flow. Although the geochemical interaction between concrete and rock may play an important role, it has been decided to not include this process in the present study. The reason behind this simplification is to reduce the complexity of the model and the sources of uncertainty. It is expected that as a result of calcium leaching from concrete and the high pH plume generated will lead to precipitation of calcite in the bedrock. This precipitation will in turn induce a reduction in porosity, which could have consequences for the kinetics of the degradation process. A reduced porosity could positively impact the long-term performance of concrete by decreasing the mass transfer of solutes by advection and diffusion from the rock to the concrete structure. Thus, neglecting these processes in this study is considered to be a conservative assumption.

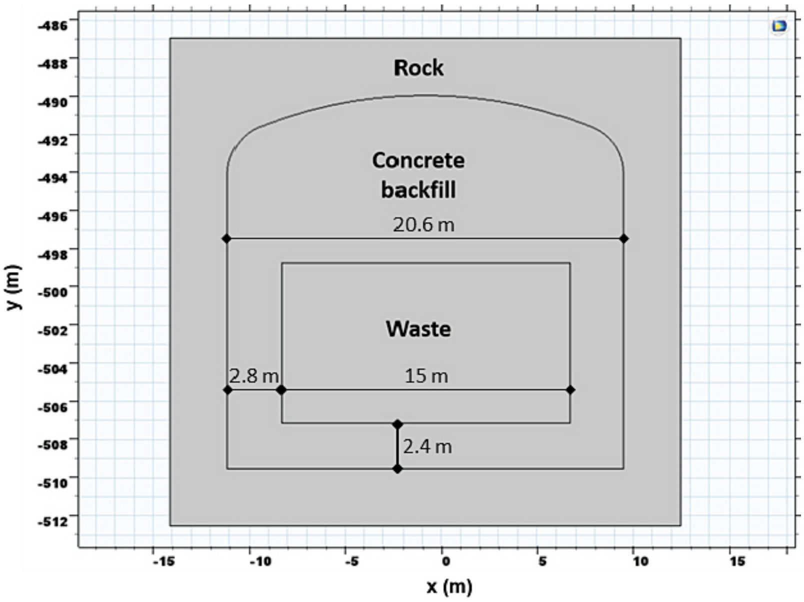

Figure 5-1. 2D cross-section of BHK vault and dimension in metres (m), including three domains: host rock, concrete backfill and waste.

Material properties for flow and transport of each domain are presented in Table 5-1. These properties may evolve with time in the *coupled* modelling scenarios. The coupling between concrete degradation and material properties that has been considered here is based on variations in porosity. Chemical reactions leading to mineral dissolution and precipitation induce these porosity changes. The affected flow and transport parameters are hydraulic conductivity, K (m/s), and effective diffusion coefficient, D_e (m^2/s).

The chemical setup is based on the use of the thermodynamic database CEMDATA07 (e.g. Lothenbach et al. 2008). This database has been rewritten in Phreeqc format by Jacques (2009). Two different sets of initial chemical composition of concrete have been assumed:

- Simplified system: the composition is similar to the work by Pękala et al. (2015), using the thermodynamic database CEMDATA07 (Lothenbach et al. 2008) and excluding redox reactions and iron in the system.
- Full system: the composition is similar to the system defined in Höglund (2014).

The following groundwater flow boundary conditions have been assumed:

- Constant inlet flow along the left boundary (horizontal flow).
- No flow boundary conditions on the top and bottom boundaries.

Two sensitivity cases consider a constant hydraulic head horizontal gradient boundary condition instead of the constant inlet (Table 3-1). The groundwater composition used in the simulations is shown in Table 5-2 (see Appendix A for saturation indices). Similar to Pękala et al. (2015), glacial melting water has been tentatively used as alternative boundary water. Its chemical composition is summarized in Table 5-3.

All chemical reactions have been calculated assuming thermodynamic equilibrium. The initial concrete porewater composition that has been considered in the full and simplified chemistry simulations is presented in Table 5-4 and Table 5-5 for each modelled domain. The porewater composition is in equilibrium with the mineral phases. The mineralogical phase assemblages and exchanger composition to represent alkali uptake of the concrete and waste domains are presented in Table 5-6 and Table 5-7. Table 5-6 corresponds to the full chemistry setup, while Table 5-7 presents the simplified chemistry setup. The full chemical composition is based on the work by Höglund (2014). Here, the calculated the mineral assemblage of SFR construction concrete based on the cement mix and a previously developed hydration model. The simplified chemical phase assemblage is based on the work by Pękala et al. (2015). Table 5-8 presents the secondary minerals that have been allowed to precipitate in case supersaturation of the solution is reached for the full and simplified chemistry scenarios.

In the simplified chemistry setup, C-S-H jennite-like and C-S-H tobermorite-like are the only C-S-H gels that can precipitate or dissolve following portlandite dissolution. Calcite, ettringite, and gypsum are the other secondary minerals that are considered in the simplified chemical domain compositions.

The motivation to study two different levels of complexity of the mineral phase assemblage is that the calculation time depends on the size of the chemical system. This is an important issue, especially for the much more computationally demanding 3D simulations presented in Section 6. The goal is to establish whether the simplified chemistry can represent the main degradation processes observed with the full chemical system.

Table 5-1. Physical properties of the domains: values of concrete and waste from Pękala et al. (2015); values for concrete are consistent with Höglund (2014). Relations between porosity and physical properties are described in Section 3.2.5. The value of tortuosity for the waste is valid as long as the effective diffusion coefficient is equal or lower than the diffusion in free solution, which is the case in all simulated cases (a porosity of the waste of 0.458 would need to be attained).

Domain	Porosity, φ_0	Tortuosity, τ	D_e (m^2/s)	K_0 (m/s)
Concrete	0.11	0.0318	3.50×10^{-12}	8.30×10^{-10}
Waste	0.3	1.1600	3.50×10^{-10}	1.00×10^{-7}
Rock*	-	-	-	5.00×10^{-9}

* Hydraulic conductivity of the rock is set to obtain groundwater flow velocities in the BHK vault as close to the average value from Abarca et al. (2016) as possible.

Table 5-2. Granitic groundwater composition, old meteoric end member (see Pękala et al. 2015).

Groundwater composition	
pH	8.64
Temperature (°C)	25
Species (totals)	**Concentration (mol/kg water)**
Al	1.21E–06
C	6.91E–04
Ca	5.26E–04
Cl	4.53E–03
K	7.60E–05
Mg	1.48E–04
Na	4.79E–03
S(6)	3.73E–04
Si	1.42E–04

Table 5-3. Glacial groundwater composition. See Pękala et al. (2015) and Gimeno et al. (2010) for details.

Groundwater composition	
pH	5.8
Temperature (°C)	25
Species (totals)	**Concentration (mol/kg water)**
Al	0.0
C	2.0E–06
Ca	4.5E–06
Cl	2.5E–05
K	1.0E–05
Mg	4.1E–06
Na	7.4E–06
S(6)	5.2E–06
Si	0.0

Table 5-4. Porewater composition in equilibrium with the mineral phases considered in the full chemistry simulations for the modelled domains: concrete and waste.

Porewaters	Concrete	Waste
pH	12.975	12.961
Temperature (°C)	25	25
Ionic strength (mol/kg water)	0.128	0.127
Species (totals, mol/kg water)		
Al	5.542E–07	5.542E–07
C	1.001E–05	1.001E–05
Ca	3.684E–03	3.684E–03
Cl	5.550E–05	5.550E–05
K	8.837E–02	8.837E–02
Mg	2.526E–08	2.526E–08
Na	2.698E–02	2.698E–02
S(6)	3.289E–03	3.289E–03
Si	4.522E–05	4.522E–05

Table 5-5. Porewater composition in equilibrium with the mineral phases considered in the simplified chemistry simulations for the modelled domains: concrete and waste. S(6) stands for SO4–2.

Porewater	Concrete	Waste
pH	12.951	12.951
Temperature (°C)	25	25
Ionic strength (mol/kg water)	0.128	0.127
Species (totals, mol/kg water)		
Al	4.099E–05	4.099E–05
C	1.827E–05	1.827E–05
Ca	3.826E–03	3.826E–03
Cl	5.124E–05	5.124E–05
K	8.747E–02	8.747E–02
Na	2.667E–02	2.667E–02
S(6)	4.099E–05	4.099E–05
Si	4.449E–05	4.449E–05

Table 5-6. Mineral assemblage of concrete and waste domains in the full chemistry simulations. The chemical composition of the minerals and their equilibrium constants are presented in Appendix A.

	Concrete			Waste		
Primary mineral	Concentration (mol/liter$_{medium}$)	Concentration (mol/kg$_{water}$)	Volume fraction (–)	Concentration (mol/liter$_{medium}$)	Concentration (mol/kg$_{water}$)	Volume fraction (–)
CH (portlandite)	1.60160	14.56	0.053	0.83623	2.787	0.053
CSH$_{jen}$	1.20890	10.99	0.094	0.63119	2.104	0.094
Ettringite	0.01219	0.111	0.009	0.00636	0.0212	0.009
Hydrogarnet Si	0.10450	0.95	0.015	0.05456	0.1819	0.015
Thaumasite	0.03498	0.318	0.012	0.01826	0.0609	0.012
Hydrotalcite OH	0.01694	0.154	0.004	0.00884	0.0295	0.004
Porosity	-	-	0.110	-	-	0.300
Inert fraction	-	-	0.704	-	-	0.603
Total	-	-	1.000	-	-	1.000
Exchanger composition	(mol/liter$_{medium}$)	(mol/kg$_{water}$)		(mol/liter$_{medium}$)	(mol/kg$_{water}$)	
CaX$_2$	0.000374	0.0034		0.07617	0.2539	
KX	0.053537	0.4867		0.01124	0.0375	
NaX	0.007910	0.0719		0.00059	0.0020	

Table 5-7. Mineral assemblage of concrete and waste domains in the simplified chemistry simulations. The chemical composition of the minerals and their equilibrium constants are presented in Appendix A.

	Concrete			Waste		
Primary mineral	Concentration (mol/liter$_{medium}$)	Concentration (mol/kg$_{water}$)	Volume fraction (–)	Concentration (mol/liter$_{medium}$)	Concentration (mol/kg$_{water}$)	Volume fraction (–)
CH (portlandite)	1.03598	9.418	0.034	0.5409	1.803	0.018
CSH$_{jen}$	1.2254	11.14	0.096	0.6396	2.132	0.050
Calcite	0.06292	0.571	0.002	0.033	0.11	0.001
Porosity	-	-	0.110	-	-	0.300
Inert fraction	-	-	0.758	-	-	0.631
Total	-	-	1.000	-	-	1.000
Exchanger composition	(mol/liter$_{medium}$)	(mol/kg$_{water}$)		(mol/liter$_{medium}$)	(mol/kg$_{water}$)	
CaX$_2$	0.000374	0.0034		0.07617	0.2539	
KX	0.053537	0.4867		0.01124	0.0375	
NaX	0.007910	0.0719		0.00059	0.0020	

Table 5-8. Secondary minerals allowed precipitating in all modelled domains in the full chemistry simulations. The chemical composition of the minerals and their equilibrium constants are presented in Appendix A.

Full chemistry	Simplified chemistry
CSH_{tob2}	CSH_{tob2}
Monocarboaluminate	Ettringite
hydrogarnetOH	Gypsum
monosulfoaluminate	
Calcite	
Brucite	
hemicarboaluminate	
Gypsum	
hydrotalciteC	
SiO_2(am)	

5.2 Numerical model setup

The conceptual model described in the previous section has been implemented in iCP (Nardi et al. 2014). This section presents the details of the numerical implementation.

5.2.1 Finite element mesh

The computational domain has been discretized using triangular elements, as shown in Figure 5-2. The maximum element size is 0.6 m and the total number of finite element is 5 168 of which 2 891 compose the reactive domains (concrete and waste). The remaining elements discretize the chemically inert rock domain.

5.2.2 Temporal discretization

For the given finite element mesh and groundwater flow field, the application of the Courant stability criterion (Section 4.2.2) indicates a maximum time step size of 190 years. The Von Neumann stability criterion depends on the effective diffusion coefficient and the dispersion (Section 4.2.2). This criterion yields a maximum time step of 11.8 years in the waste domain (see Figure 5-3). Based on this analysis, time steps ranging between 2 and 9 years have selected for the communication times between the multiphysics (Comsol) and chemical (Phreeqc) solvers.

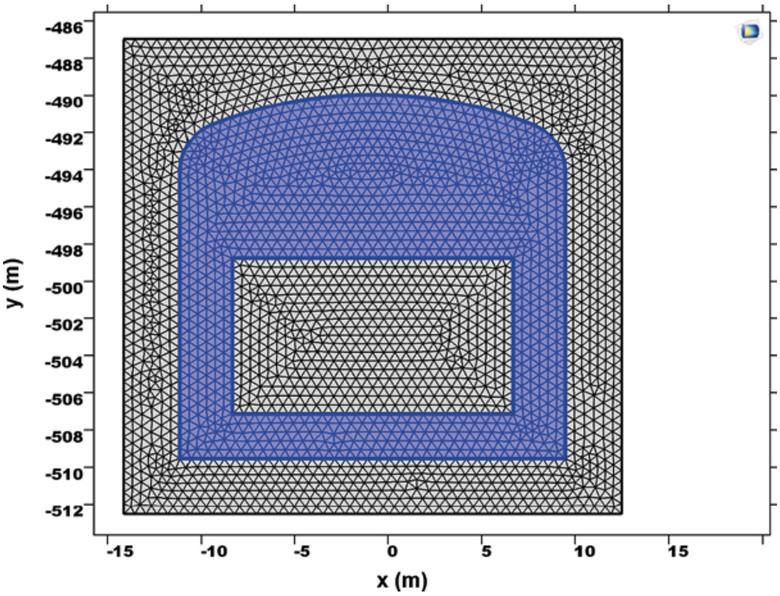

__Figure 5-2.__ Finite element mesh used in the iCP simulations. Dimensions are expressed in metres (m).

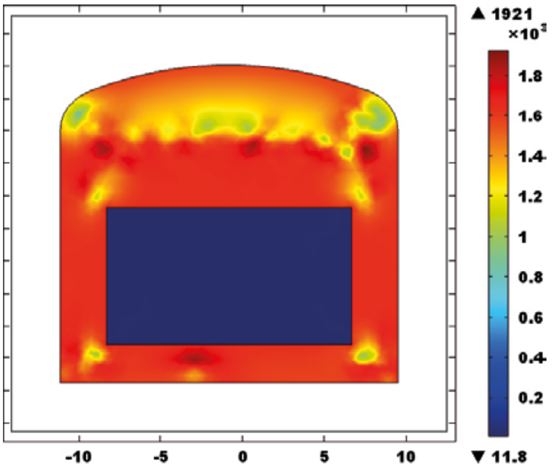

Figure 5-3. *Maximum time steps based on Von Neumann stability criterion (time scale in years).*

5.2.3 Initial and boundary conditions

5.2.3.1. Groundwater flow

As discussed in Section 3.2, two different boundary conditions are applied to simulate groundwater flow. In the first set of simulations, a *constant inlet flow* boundary condition is imposed along the left boundary of the rock domain (Figure 5-4 top). This is given by:

$$-n\rho . u = \rho U_0 \tag{5-1}$$

In Equation (5-1), U_0 is the normal inflow velocity equal to 1.03×10^{-11} m/s, n is the normal vector to the boundary surface, ρ (kg/m^3) is the fluid density, and u (m/s) is the velocity at the boundary. The inflow velocity value corresponds to an average flow from the results obtained by Abarca et al. (2016). It corresponds to the case in which the SFL repository is located at 500 m depth. The hydraulic conductivity of the surrounding rock has been set to 6×10^{-10} m/s so that the flow in the concrete backfill is mainly given by the boundary condition. Thus, the hydraulic conductivity of the surrounding rock is not necessarily representative of the actual rock.

In the second set of simulations, the boundary conditions are switched to a horizontal hydraulic gradient, as shown in Figure 5-4 (bottom). The values of the hydraulic head have been set based on the results presented by Abarca et al. (2016): H ≈ 6 m along the left boundary and H ≈ 5.8 m along the right boundary. The initial Darcy velocities obtained using the *constant inlet flow* or the *hydraulic head* boundary conditions are similar (Figure 5-5).

5.2.3.2. Solute transport

Reactive transport is only solved for in the concrete and waste domains. The rock domain is only used for calculating the groundwater flow field. Therefore, the boundary conditions for solute transport are imposed along the rock-concrete interface. Two types of boundary condition have been tested in this study, as discussed in Section 3.2:

- Fixed concentration (Cases I, III, IX, and X).
- Open boundary (remaining cases).

The assumption of fixed concentration corresponds to a system where reactive transport processes in the repository are mainly driven by diffusion. Out-diffusion from the backfill does not affect the composition of groundwater. Conversely, the case considering open boundary conditions for solute transport coupled to groundwater flow is more representative of a case dominated by advection and dispersion.

The initial Péclet number is shown in Figure 5-6 for the entire domain, based on Equation (4-1). The concrete backfill on both sides of the waste domain, subject to higher velocities, show higher Péclet numbers (Pe > 1). However, diffusion dominates solute transport in most of the modelled domain.

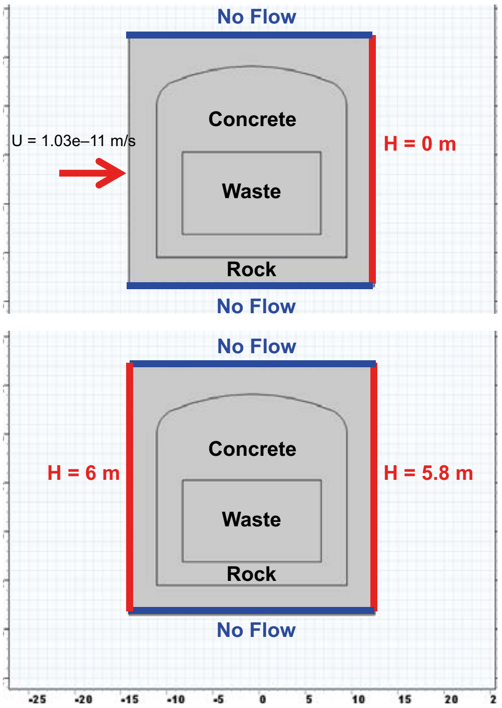

Figure 5-4. *Imposed fluid flow boundary conditions. Top: constant inlet flow (m/s); bottom: hydraulic head gradient (H, m). Hydraulic head gradient boundary conditions have been used in Cases III and VIII (Section 3.2).*

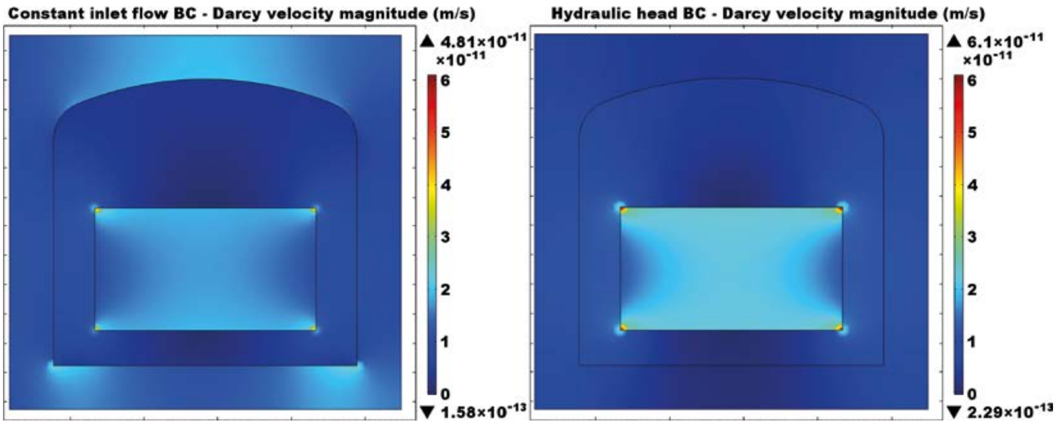

Figure 5-5. *Darcy velocity field (m/s) under constant inlet flow (left) and hydraulic head (right) boundary conditions.*

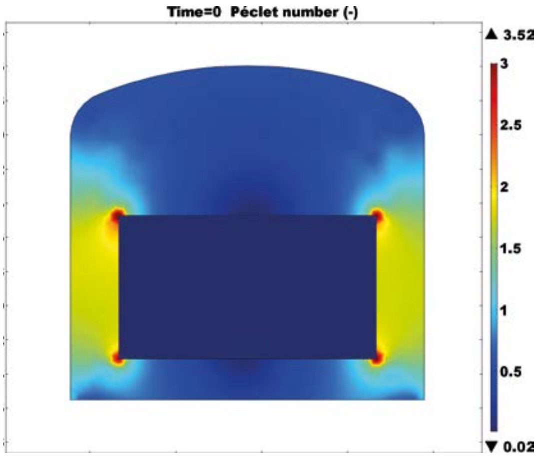

Figure 5-6. *Initial distribution of Péclet number (–).*

5.3 Results

The results are illustrated either as 2D distribution plots at given times or 1D profiles. These profiles have been defined along a horizontal flow path crossing through the centre of the waste domain, as shown in Figure 5-7. A summary and motivation for the different iCP simulation cases are presented in Section 3.2.

5.3.1 Base case (Case I): homogeneous

The base case scenario refers to the model described as Case I in Table 3-1. It consists of a homogeneous description of concrete and waste domains, with a uniformly-distributed hydraulic conductivity field. The physical properties are shown in Table 5-1. A constant inlet flow boundary condition is imposed on the left boundary and solute transport is modelled under fixed concentration boundary conditions along the entire rock-concrete backfill interface. The full chemistry setup is used to characterize the mineral assemblage and initial porewater chemistry. The groundwater composition is given by the old meteoric end-member in Table 5-2.

The results of the Base case simulation are presented in Figure 5-8 to Figure 5-13. Overall, the results obtained indicate that the concrete barriers are not significantly degraded even after 100 000 years of interaction with groundwater and the system is chemically stable. The reasons behind the predicted long-term performance explained by

- Groundwater flow into the BHK vault is very limited (Section 5.2.3, Abarca et al. 2016). Darcy velocities in the concrete backfill are $\sim 1 \times 10^{-11}$ m/s, with fluid velocities slightly lower than 3 mm/yr. This gives advective travel times through the cross-section of the vault larger than 5 000 years.
- The initial effective diffusion coefficient of the concrete backfill is very low (Table 5-1), limiting the extent of groundwater-concrete diffusive interaction.
- Related to the previous statements, the volume of concrete in the BHK vault is very large compared to the amount of water entering the vault. A substantial amount of aggressive species is needed in the model in order to degrade the structure to a significant extent. Given the large advective travel times and the low diffusion coefficients, the chemical interaction is limited, even after 100 000 years.

Figure 5-8 presents the pH of the pore solution and the porosity distribution after 100 000 years. The extent of the chemical degradation is limited in space to approximately half of the thickness of the wall of the concrete backfill (1.00 – 1.25 m). In the affected region, porosity gradually increases from 0.11 in the intact concrete to 0.25 near the rock-concrete interface (Figure 5-13). This increase is driven by the dissolution of the main cement hydrates. The concrete mix used in this study contains an aggregate volume fraction of ~0.70. Therefore, a porosity of 0.25 in the concrete backfill corresponds to a hardened cement paste with a porosity of ~0.83. In this state, it could be expected that mechanical integrity is severely compromised near the concrete-rock interface.

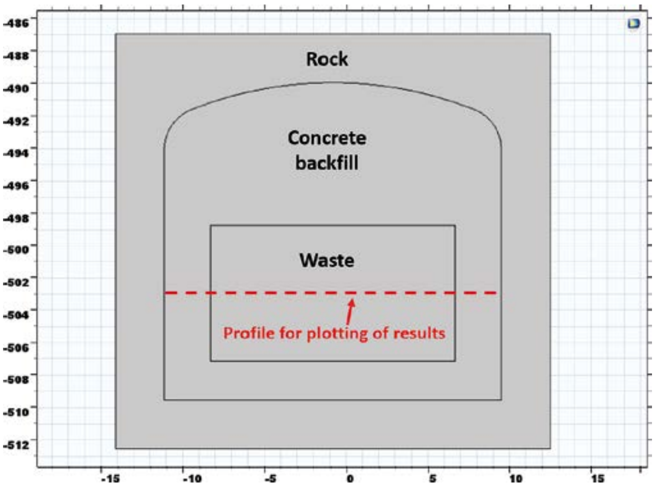

Figure 5-7. *Profile for 1D representation of reactive transport simulation results.*

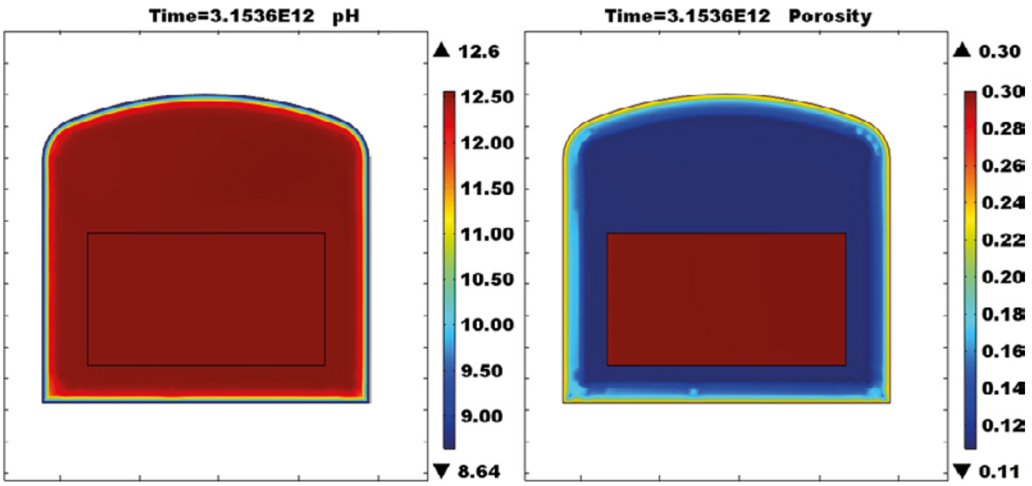

Figure 5-8. *Case I results: 2D spatial distribution of pH (left) and porosity (right) after 100 000 years.*

Results show that a majority of the secondary minerals considered in the simulation do not precipitate during 100 000 years. This is the case for brucite, hydrogarnetOH, monocarboaluminate, monosulfoaluminate, gypsum, hemicarboaluminate, and SiO_2(am) (not shown). $CSHt_{ob2}$, hydrotalciteC, and calcite are the only secondary minerals that precipitate (Figure 5-9 and Figure 5-10).

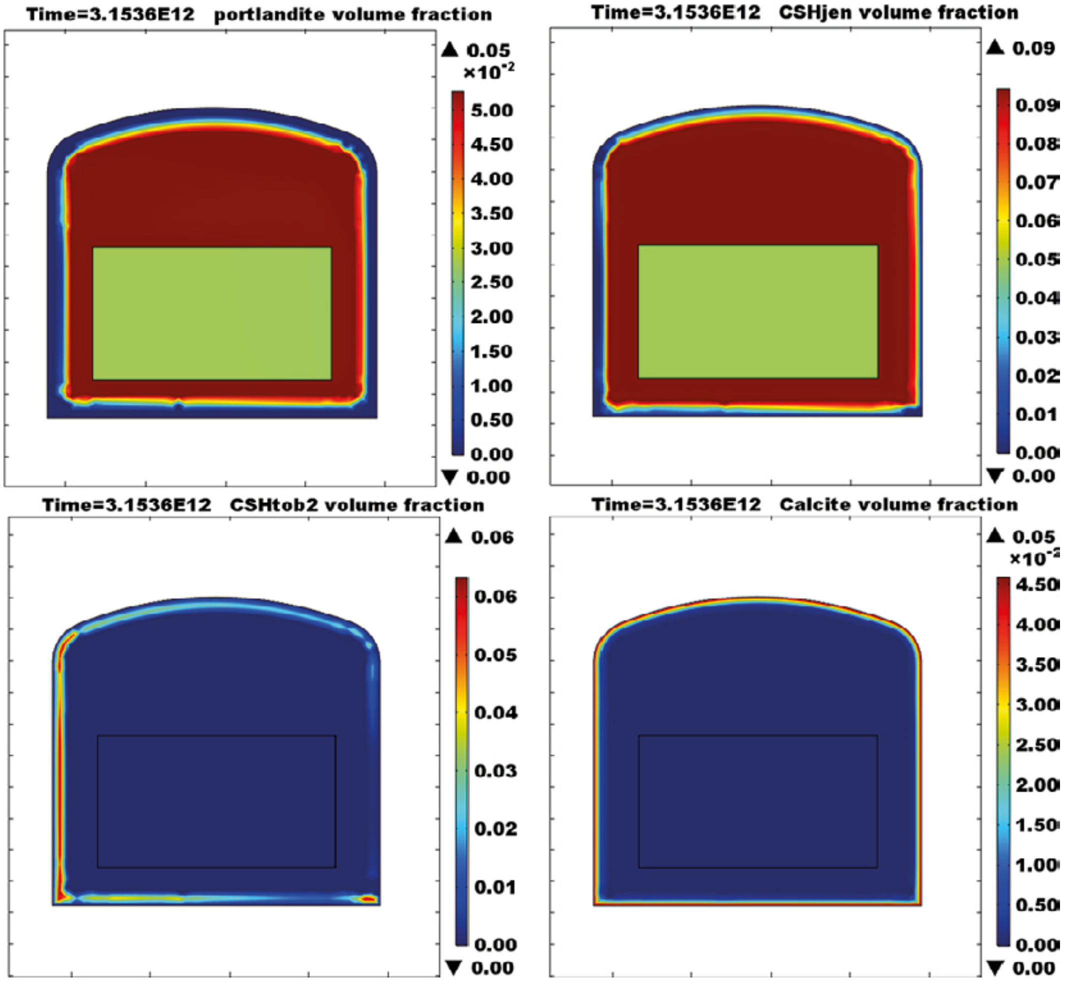

Figure 5-9. *Case I results: 2D spatial distribution of portlandite, C-S-H phases, and calcite after 100 000 years, expressed in volume fraction (–).*

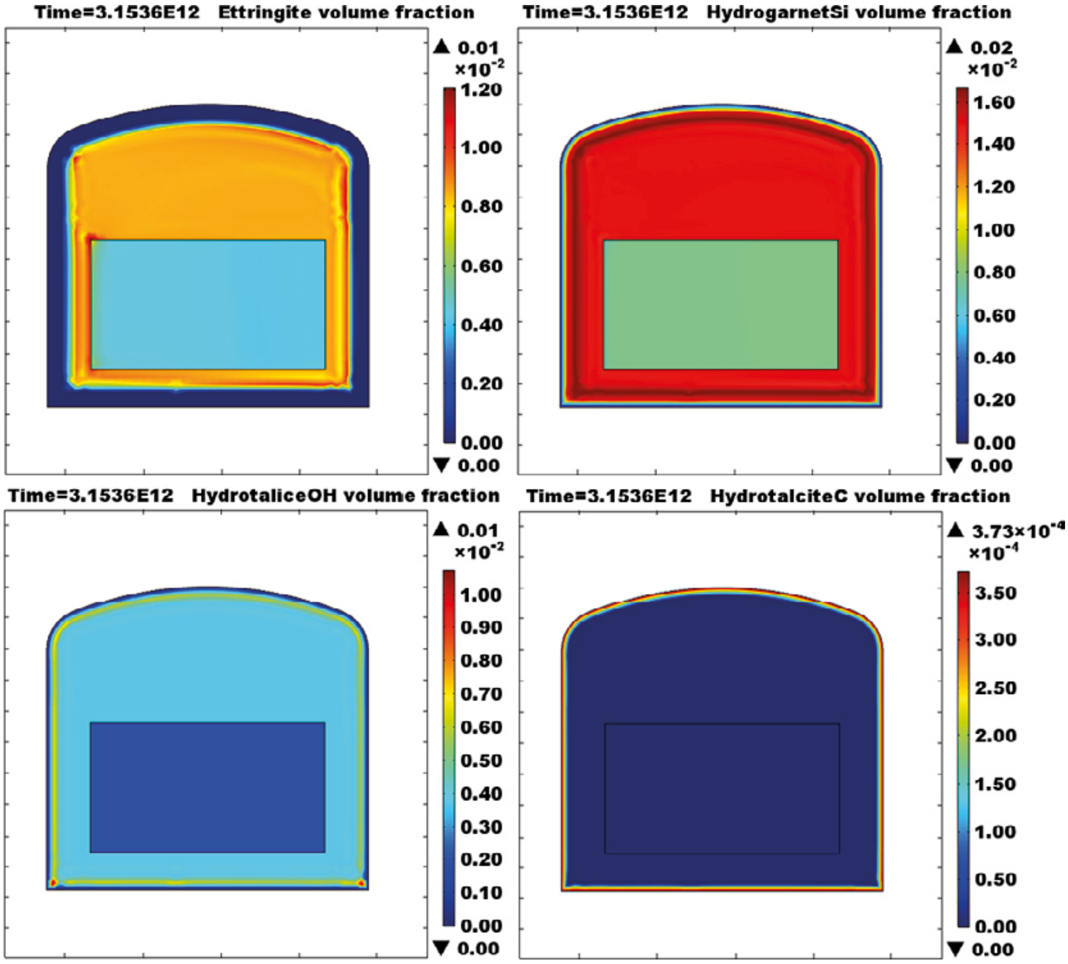

Figure 5-10. *Case I results: 2D spatial distribution of ettringite, hydrotalcite (C and OH forms), and hydrogarnet after 100 000 years, expressed in volume fraction (–).*

A 1D profile of the porosity at different times is shown in Figure 5-13 and a zoom in Figure 5-14. It suggests an asymmetric reactive transport front where the depth of degradation near the left boundary is greater than near the right boundary (Figure 5-9 to Figure 5-11). This is due to the constant inlet groundwater flow considered on the left boundary. On the other hand, degradation is driven by diffusion on the right boundary. The increase in porosity is due to a complete dissolution of portlandite and partial degradation of C-S-H phases in the outer layers (Figure 5-14). Other hydrates such as ettringite and hydrogarnet are also completely dissolved. Complete dissolution of all the cement hydrates in Case I would lead to a porosity value of ~0.3, in which case only the chemically inert aggregate volume fraction would be left (~0.7). However, in the simulation precipitation of calcite (0.046 volume fraction) and to a much lesser extent of hydrotalciteC limits the increase of porosity to a value of 0.25 at the concrete-rock interface.

The impact of the increase of porosity on the physical transport properties is also depicted in Figure 5-14, which shows the hydraulic conductivity and effective diffusivity at 3 different times for the same 1D profile. Hydraulic conductivity maximum increase is 16 times the initial value, while the diffusion coefficient increases by up to 8 times.

The alkalis uptaken in the solid matrix of concrete are gradually released due to the interaction with groundwater. After 100 000 years the exchanger composition, used to represent this alkali uptake, shows that the Na and K have been exchanged by Ca (Figure 5-11). There remains a relatively small zone of the concrete backfill dome where Na and K concentrations in the pore water have still not been leached out (Figure 5-12). This is due to the low groundwater flow value in this region and the relatively large distance to the higher flow regions. As a result, Na and K in the exchanger in equilibrium with aqueous concentrations are higher than in the rest of the structure (Figure 5-11).

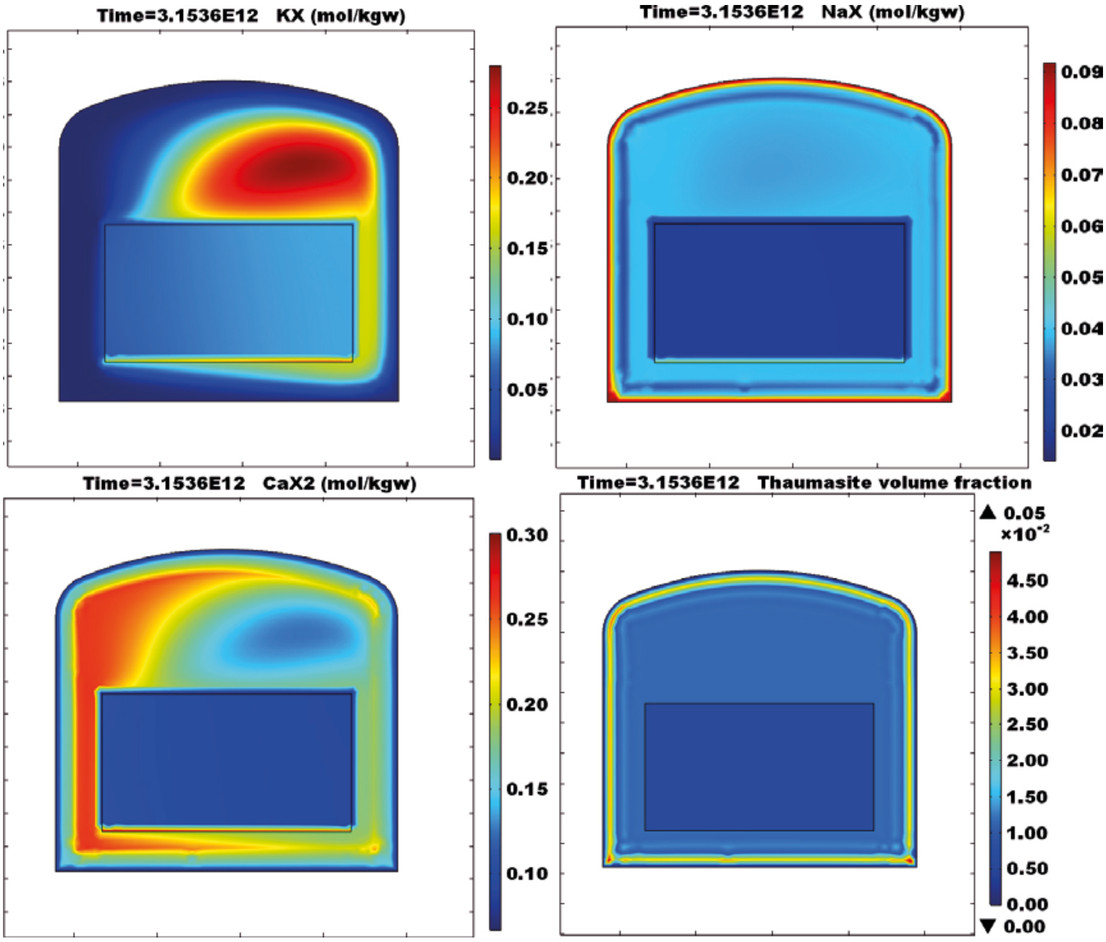

Figure 5-11. *Case I results: 2D spatial distribution of K, Na, and Ca in the cation exchanger (mol/kg$_{water}$) representing the uptake of alkalis into the C-S-H structure (see Höglund 2014 for details), and thaumasite volume fraction (–), after 100 000 years.*

These Na and K concentrations are not sufficiently high to maintain the pH significantly above the value corresponding to equilibrium with portlandite (Figure 5-8). Initial sulphate concentrations in the pore water (3.289×10^{-3} M) are gradually leached out due to interaction with groundwater (with a concentration of 5.25×10^{-4} M). Relatively higher concentrations remain in the same region as for alkalis due to the same reasons.

Regarding the evolution of the waste domain, the degradation of the cementitious materials is negligible even after 100 000 years. Almost no porosity changes or pH decrease of the pore solution are observed. This is due to the buffering effect of the concrete backfill, a massive concrete structure that protects the waste domain from hydrological and chemical perturbations.

Figure 5-12 shows the concentration in the pore solution of Ca, Cl, Si, and S. Chloride may be regarded as a conservative tracer, since in the present simulation this element is not involved in the precipitation or dissolution of any mineral. The asymmetric behaviour of the system between the left and right boundaries caused by the water inlet flow is clearly observed. Higher chloride concentrations in the waste domain as compared to the upper part of the concrete backfill are due to higher hydraulic conductivity and diffusivity in the former.

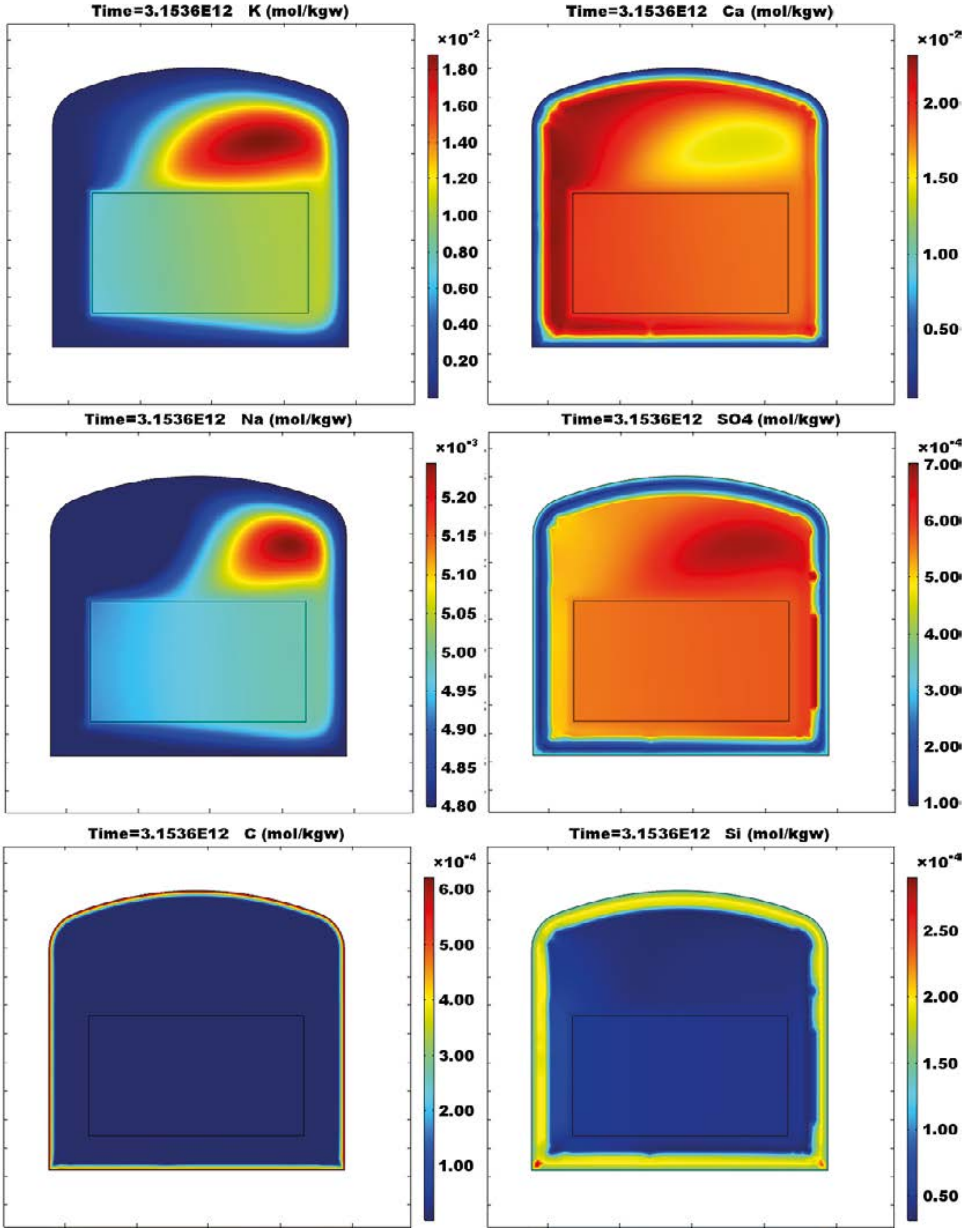

Figure 5-12. *Case I results: 2D spatial distribution of dissolved species (K, Na, Ca, S, C, and Si) after 100 000 years, expressed in mol/kg*$_{water}$.

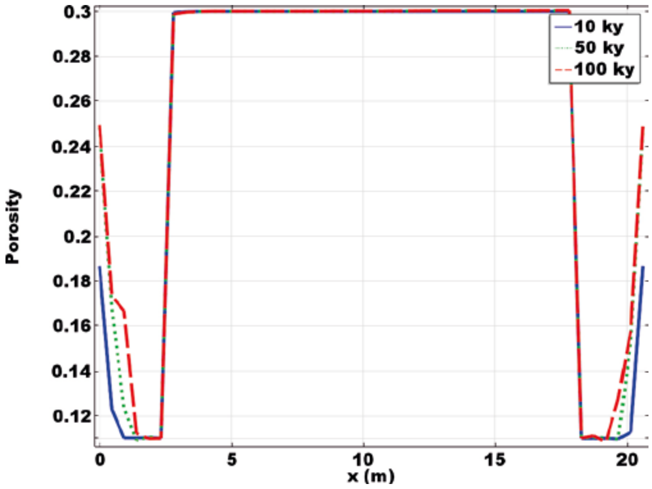

Figure 5-13. 1D porosity profiles for Case I along the central flow path crossing the concrete backfill (left and right of the plot) and the waste domain (central part of the plot) after 10 000, 50 000, and 100 000 years.

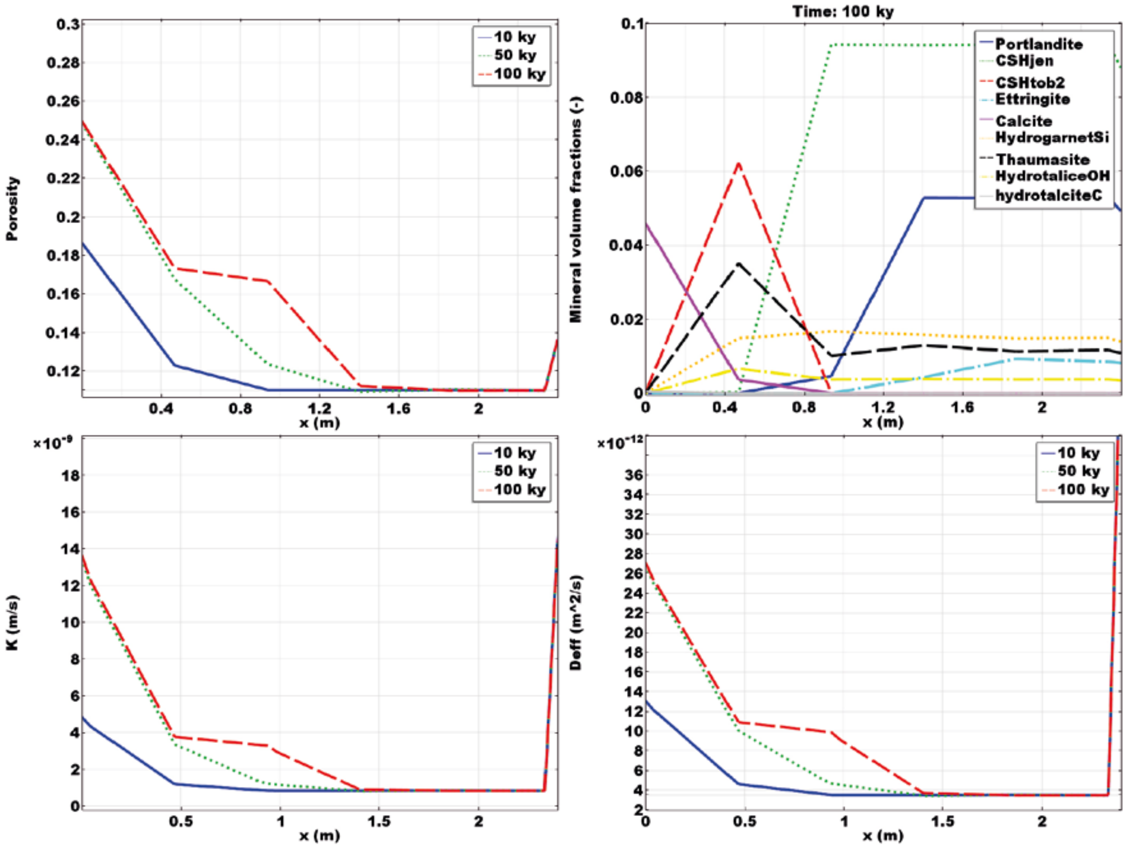

Figure 5-14. Zoom of 1D profile between x = 0 and 2.4 m: porosity, effective diffusion coefficient (m^2/s) and hydraulic conductivity (m/s) at different times and mineral volume (unity) fractions after 100 000 years. The thickness of the concrete backfill is 2.8 m.

5.3.2 Sensitivity cases

5.3.2.1. Full chemistry (Case I and IV) vs. simplified (Case V and IX)

This section studies the effect of the level of sophistication of the chemical setup on the results and on the computation time. The goal is to optimize the computation time without losing the main chemical processes leading to degradation and porosity increase. Simulations Cases IV and V consider open boundary conditions for solute transport while in Cases I and IX, fixed concentrations are prescribed. In all cases, prescribed inflow velocity for fluid flow is considered.

Table 5-9 shows the time spent calculating the transport step in Comsol and chemistry step in Phreeqc. It is observed that the full chemistry system results in a significantly longer simulation time, especially for the transport step. At the same time, the calculation time for chemistry step is similar in both cases. The reason is the additional degrees of freedom that are introduced in the full chemistry system. Comsol run time is more sensitive to the number of variables than Phreeqc. Furthermore, a majority of the secondary minerals defined in the full chemistry setup do not precipitate over the time span simulated.

Table 5-9. Average simulation times (in seconds) for full (Case IV) and simplified (Case V) chemistry setups.

	Full chemistry	**Simplified chemistry**
Average per time step	(seconds)	(seconds)
Transport step	9.3	5.3
Chemistry step	3.8	3.3
Total per step	16.3	10.1

Figure 5-15 compares the porosity profiles along the entire length of concrete and waste domains after 50 000 and 100 000 years obtained from Cases IV and V. It is seen that the full chemistry setup leads to slightly larger porosity values near the rock-concrete interface. This can be explained by the fact that the initial amount of reactive minerals available for dissolution is larger in the full chemistry setup (0.186 vs. 0.132 of the simplified chemistry setup, see Table 5-6 and Table 5-7). As a result, the full chemistry setup Case IV is slightly more prone to changes in porosity due to dissolution processes. This is shown more clearly in Figure 5-16 and Figure 5-17 which present the comparison between Case I and Case IX of porosity and mineral volume fractions profiles, respectively.

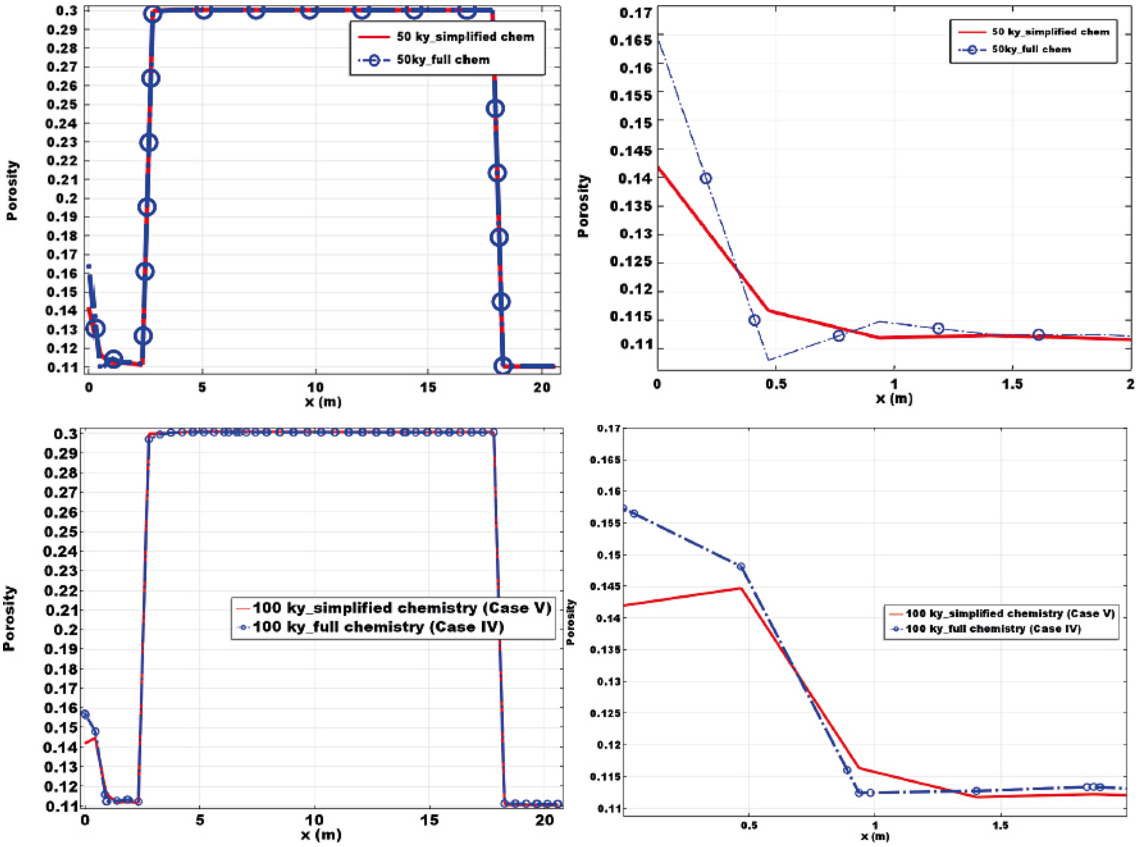

__Figure 5-15.__ Comparison of 1D profiles of porosity: simplified (Case IV) and full chemistry (Case V) simulations with open boundary conditions: after (top) 50 000 and (bottom) 100 000 years. A zoom of the first 2 metres of the left concrete backfill wall is shown on the right.

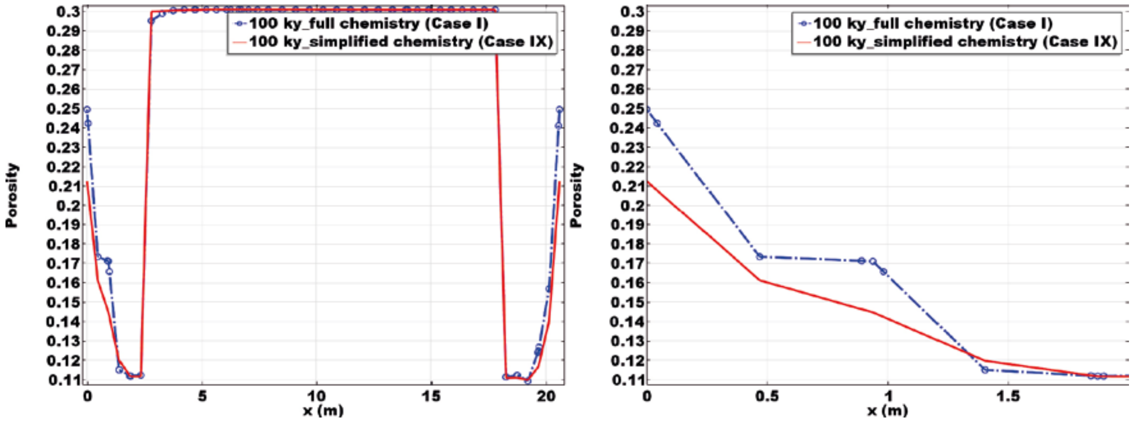

Figure 5-16. *Comparison of 1D profiles of porosity: simplified (Case IX) and full chemistry (Case I) simulations with fixed concentration boundary condition after 100 000 years. A zoom of the first 2 metres of the left concrete backfill wall is shown on the right.*

Porosity after 100 000 years is larger in the full chemistry case (Case I), reaching a value of 0.25, while in Case IX the maximum porosity value is 0.21. In both cases, the value of porosity at the boundary is a result of a complete dissolution of cement hydrates and precipitation of calcite (and hydrotalciteC in Case I). This can be observed in Figure 5-17, which shows the volume fraction of all minerals present in the system after 100 000 years. Since the full chemistry has initially a larger volume fraction of cement hydrates than Case IX, a complete dissolution of these lead to a larger porosity.

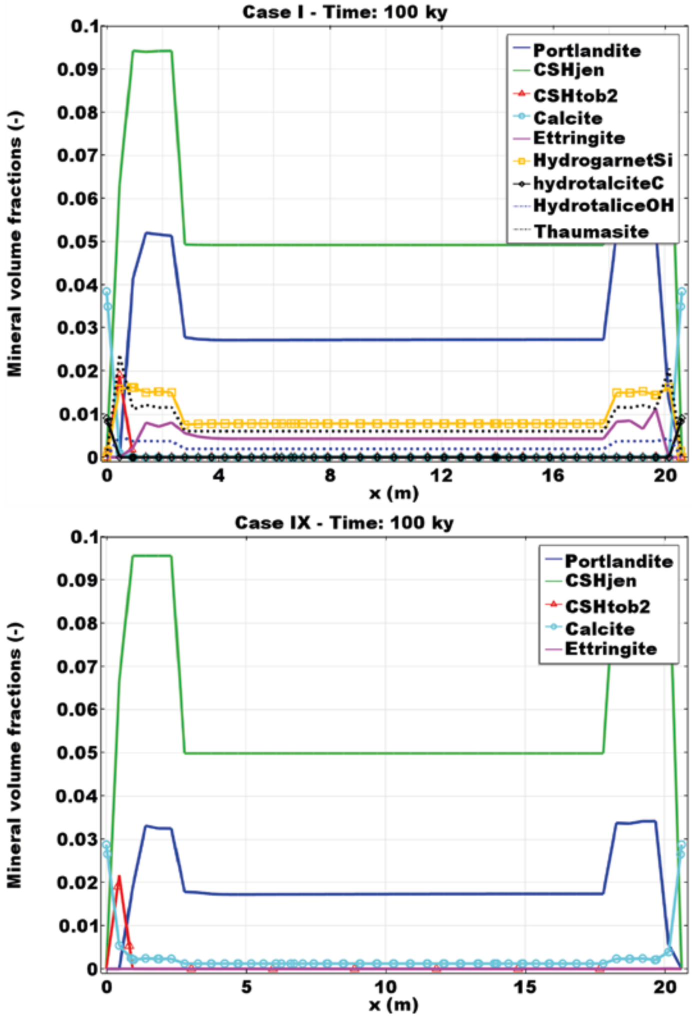

Figure 5-17. *Comparison of 1D profiles of mineral volume fractions (–): simplified (Case IX, bottom) and full chemistry (Case I, top) simulations with fixed concentration boundary condition after 100 000 years.*

The pH for the simplified and full chemistry systems after 50 000 and 100 000 years is shown in Figure 5-18 for the cases with open boundary conditions (Case IV and Case V, respectively) and Figure 5-22 for the cases with fixed concentration boundary conditions (Case IX and Case I, respectively). Only slight deviations between the two cases can be observed, with very small differences along the entire profile, except at the boundary in Figure 5-18. Based on these results, the comparison of full and simplified chemistry scenarios suggests that a simplified chemistry setup could be a valid simplification for the 3D simulations presented in Section 6.

Figure 5-20 presents the time evolution of the physical properties of concrete for Case IX (simplified chemistry) and Case I (full chemistry) at a point of the concrete backfill close to the concrete-rock interface (x = 2.10 m; y = 17.60 m). It may be observed that the hydraulic conductivity increases from its initial value of 8.3×10^{-10} m/s to ~3.3×10^{-9} m/s after 100 000 years as a result of the increase in porosity for Case I. Porosity increases from the initial value of 0.11 to 0.165. At the same time, the effective diffusivity increases up to 1.0×10^{-11} m^2/s.

The comparison between the evolution of the same physical properties in Case IX and Case I (full chemistry) shows a similar trend, as shown in Figure 5-20. However, in Case IX the increase in porosity is not as significant as in Case I (see discussion above). As expected, the transport properties follow the same trend.

These results suggest that the simplified chemical setup can be selected as a representative chemical composition of waste and concrete domains for the 3D simulations.

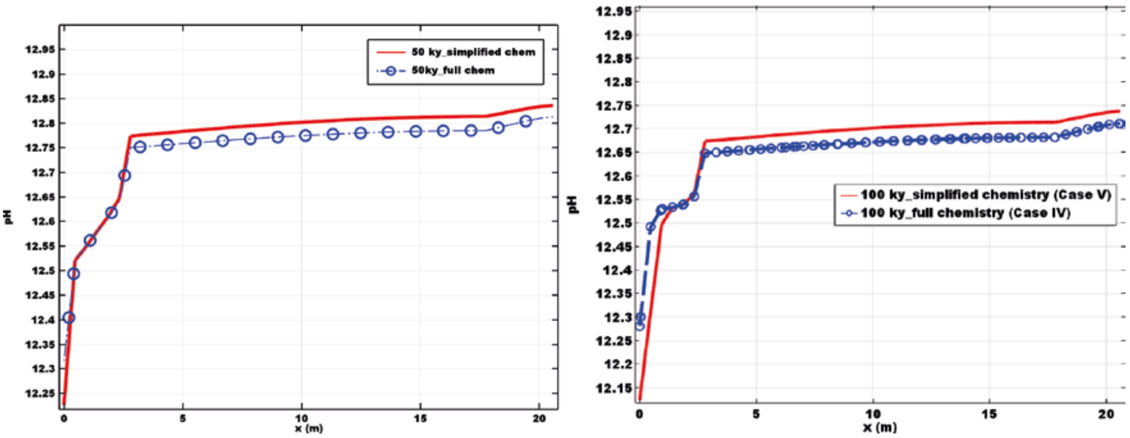

Figure 5-18. Comparison of 1D profiles along the concrete and waste domains of pH results: simplified (Case IV) and full (Case V) chemistry simulations with open boundary conditions after (left) 50 000 and (right) 100 000 years.

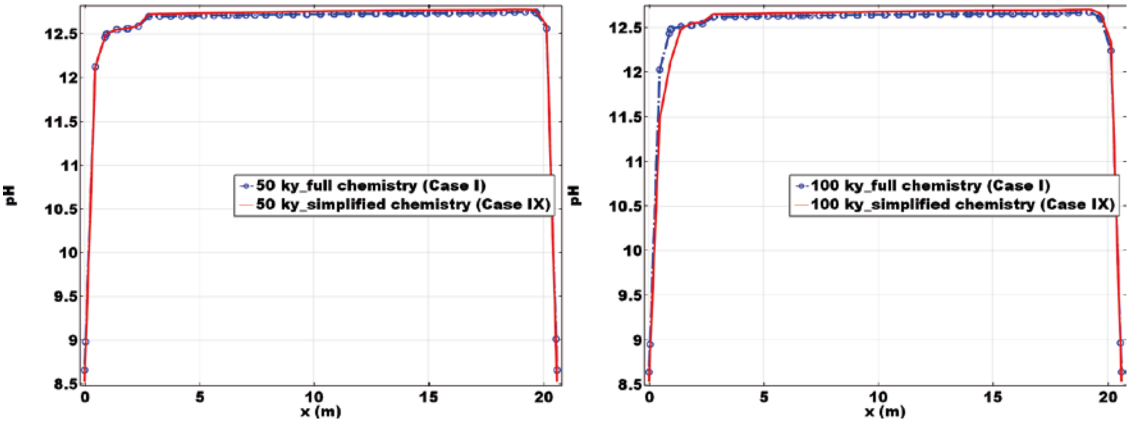

Figure 5-19. Comparison of 1D profiles along the concrete and waste domains of pH results: simplified (Case IX) and full (Case I) chemistry simulations with fixed concentration boundary conditions after (left) 50 000 and (right) 100 000 years.

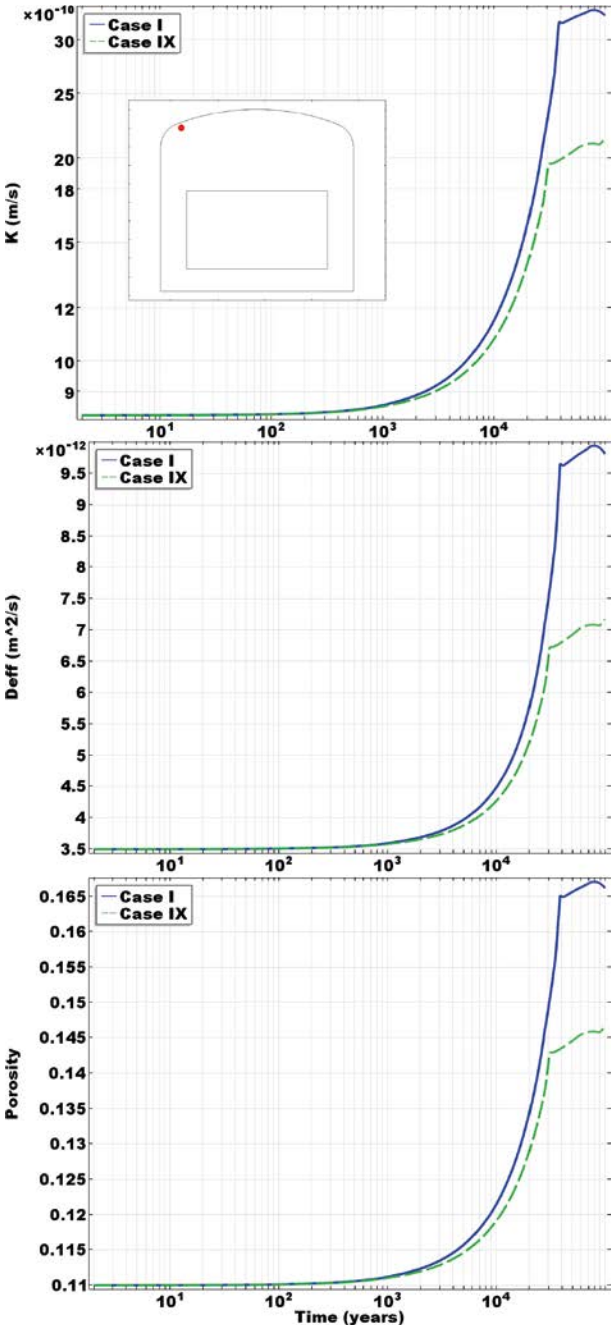

Figure 5-20. *Temporal evolution of the main physical properties of the concrete backfill i.e. hydraulic conductivity (m/s), effective diffusion coefficient (m^2/s), and porosity for Case I and Case IX at point 1: x = 2.10 m; y = 17.60 m (with respect to the bottom-left corner of the concrete domain).*

5.3.2.2. Coupling of physical and chemical processes

In this section, the influence of coupling physical and chemical processes is assessed. The results of Case V (coupled: Kozeny-Carman) have been compared with those of Case VI (uncoupled). These two cases consider a simplified chemistry setup. The results of coupled Cases IV and VII, considering a full chemistry setup, have also been compared. The difference between Case IV and Case VII is the use of a Kozeny-Carman (Case IV) or a modified Kozeny-Carman (Case VII) relation for hydraulic conductivity coupling with porosity.

Considering the feedback between physical and chemical processes leads to changes in the hydraulic conductivity and diffusivity of the concrete barriers. This feedback is driven by changes in porosity due to precipitation-dissolution reactions. More details about the calculation of porosity can be found in Section 4.1. In the coupled simulation cases, porosity has been calculated using Equation (4-3).

The feedback of porosity on the hydraulic conductivity has been formulated using the well-known Kozeny-Carman relation, as described in Section 3. Case VII has been simulated assuming a modified Kozeny-Carman relation, as described in in Section 4 (see also Höglund 2014). A full chemistry system has been assumed. The boundary conditions have been set assuming constant inlet flow of groundwater and open boundaries for solute transport.

The results of Case V are presented first. Figure 5-21 and Figure 5-22 show 1D profiles at different times of porosity and portlandite concentration, respectively. Figure 5-23 compares the hydraulic conductivity and effective diffusivity values of Case V (coupled) and Case VI (uncoupled). It may be observed that coupling leads to a non-negligible increase of the hydraulic conductivity and effective diffusion coefficient. The effect of using fixed concentration boundary condition, instead of open boundary, is also illustrated in the figure. The results of Case IX coupled scenario are also included.

Applying modified Kozeny-Carman formulation does not lead to significantly different porosities compared to the Kozeny-Carman relation, as illustrated in Figure 5-24. The flow, transport and chemical assumptions for this scenario are summarized under Case VII in Section 3.2.

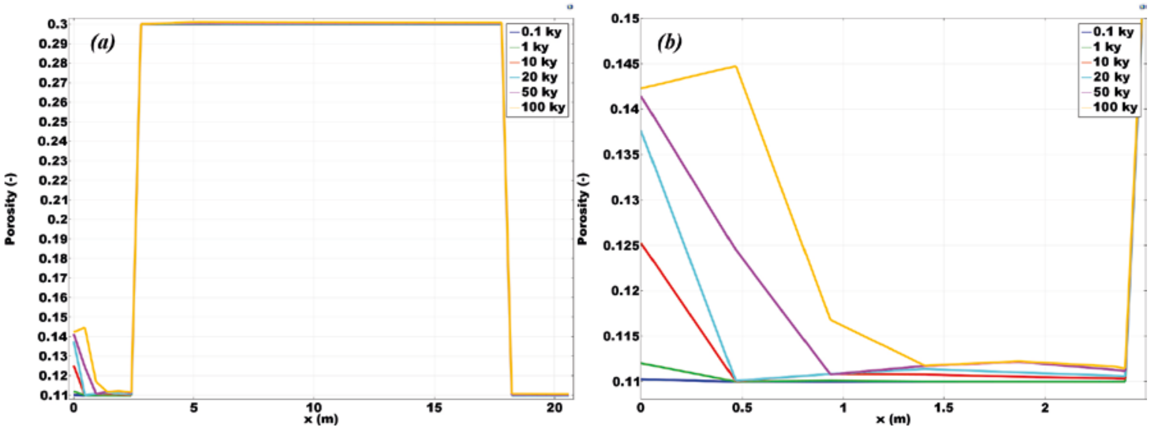

Figure 5-21. *1D profiles of porosity for Case V (coupled) after 100, 10 000, 20 000, 50 000, and 100 000 years: (a) full profile; (b) zoom of the left concrete backfill on both sides of the waste domain (0 < x < 2.5m).*

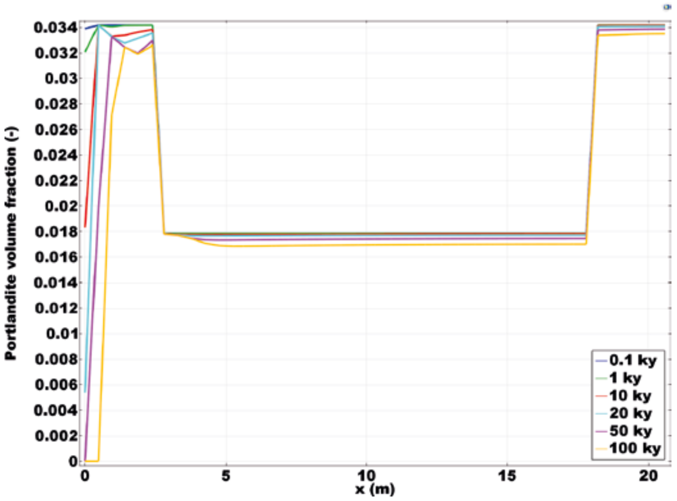

Figure 5-22. *1D profiles of portlandite volume fraction (–) for Case V (coupled) after 100, 10 000, 20 000, 50 000 years, and 100 000 years.*

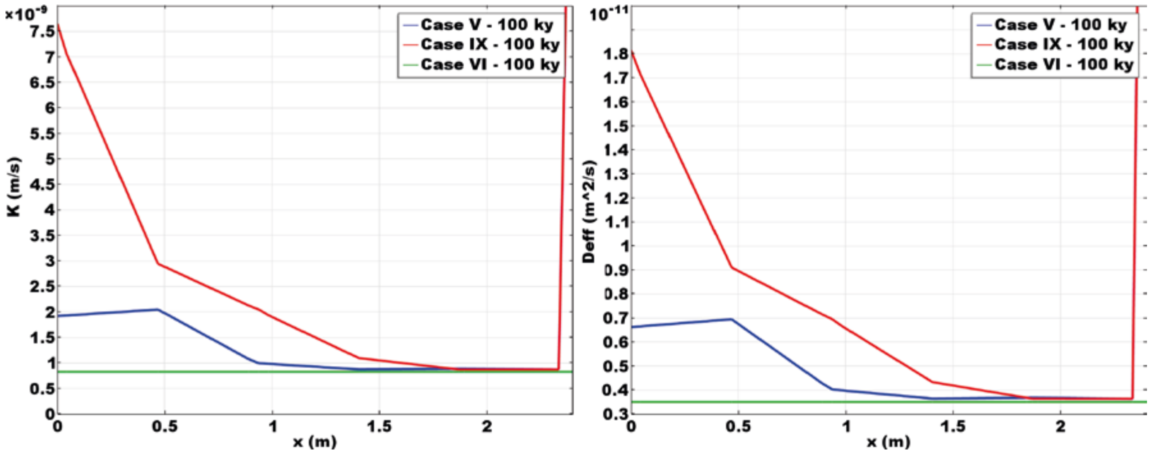

Figure 5-23. *Comparison of hydraulic conductivity (left) and effective diffusion coefficient (right) 1D profiles after 100 000 years: coupled (Case V and Case IX, with open boundary and fixed concentration boundary condition, respectively) vs. uncoupled (Case VI) scenarios.*

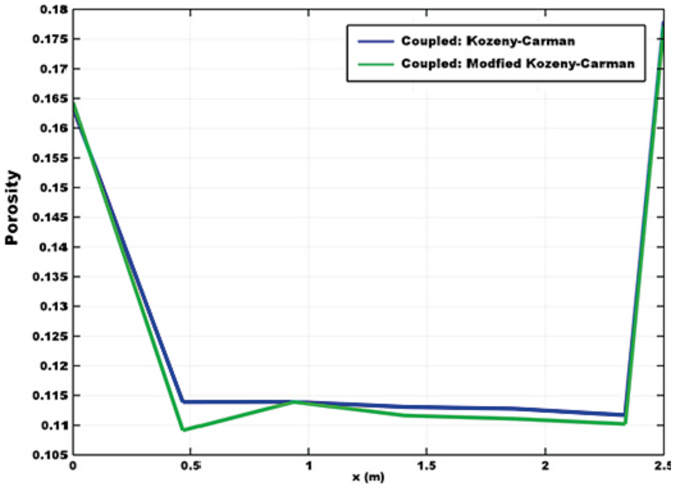

Figure 5-24. *Comparison of porosity profiles in the left concrete backfill wall after 50 000 years: Kozeny-Carman (Case IV) vs. modified Kozeny-Carman (Case VII) formulations for porosity – hydraulic conductivity relation.*

5.3.2.3. Flow boundary condition: constant inlet flow vs. hydraulic head gradient

The effect of different boundary conditions for groundwater flow in the case of considering the physical-chemical coupling has been assessed with two simulations. Case IV considers a constant inlet flow boundary condition. Case VIII is based on an identical model setup, except that fluid flow is modelled using constant hydraulic head gradient along the rock boundaries. The initial Darcy velocity fields of the two cases are comparable, as shown in Section 5.2.3.1. However, in the latter case, an increase in the hydraulic conductivity as a result of concrete degradation may lead to higher groundwater fluxes than in Case IV.

The values of porosity and pH are compared after 50 000 years in Figure 5-25 and Figure 5-26, respectively. The effect of the different fluid flow boundary conditions on pH and porosity distribution is observed to be negligible.

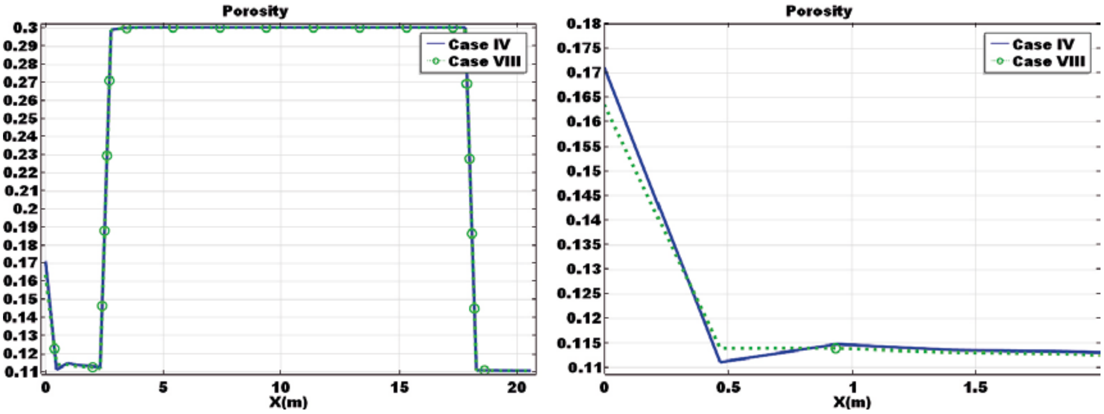

Figure 5-25. Comparison of 1D profiles of porosity after 50 000 years: constant inlet flow (Case IV) and hydraulic head gradient (Case VIII).

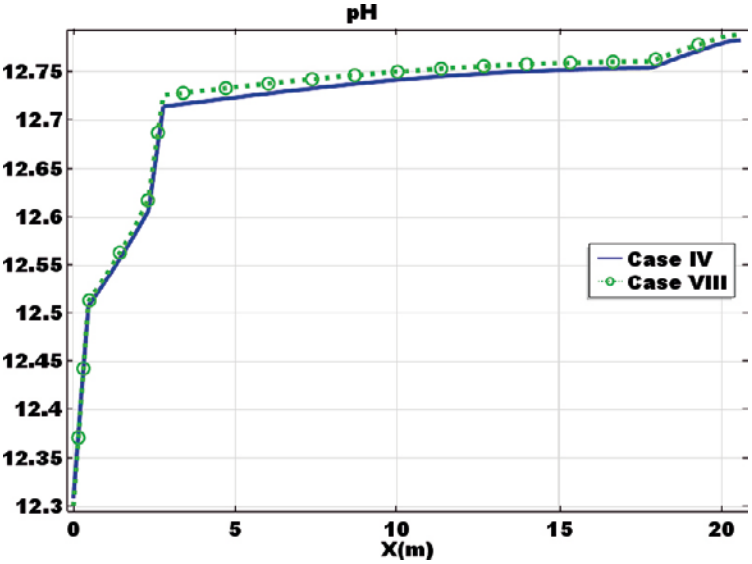

Figure 5-26. Comparison of 1D profiles of pH after 50 000 years: constant inlet flow (Case IV) and hydraulic head gradient (Case VIII).

5.3.2.4. Solute transport boundary conditions: coupled vs. uncoupled cases

In this section, the effects of the boundary conditions used for solute transport are investigated. Two sets of simulations have been performed: two cases assuming the coupling between porosity and physical properties (Cases V and IX), and two cases assuming an uncoupled scenario (Cases VI and X). Open boundary and fixed concentration boundary conditions have been explored for both sets. These simulation cases are described in Section 3.2 as Cases V and VI for open boundary conditions, and Cases IX and X for fixed concentration boundary conditions. All the simulations have been performed using the simplified chemical system and a constant inlet flow.

The results are compared in terms of pH and porosity profiles in Figure 5-27 and Figure 5-28, respectively. The results indicate that imposing fixed concentration boundary conditions leads to a significantly more aggressive scenario compared to imposing open boundary conditions. This effect is even more pronounced in the cases where coupling between porosity and physical properties is considered.

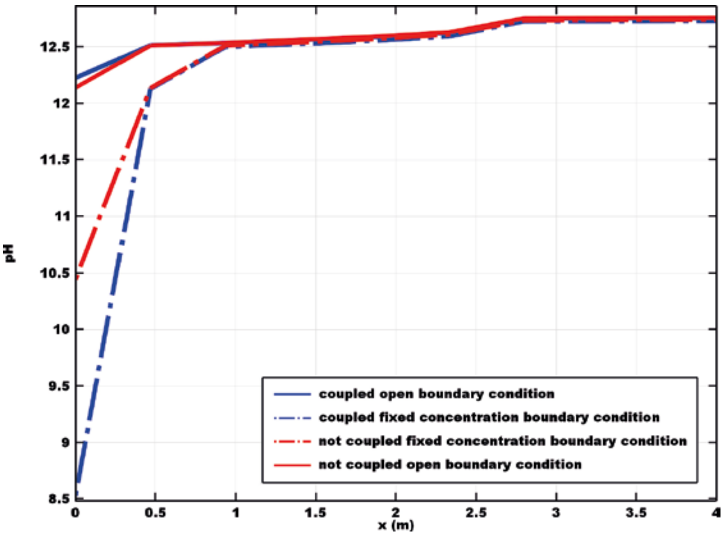

Figure 5-27. *Comparison of 1D profiles (first 4 m, as defined in Figure 5-7) of pH after 50 000 years: coupled and uncoupled cases assuming open boundary (Cases V and VI, respectively) and fixed concentration (Cases IX and X) boundary conditions for solute transport.*

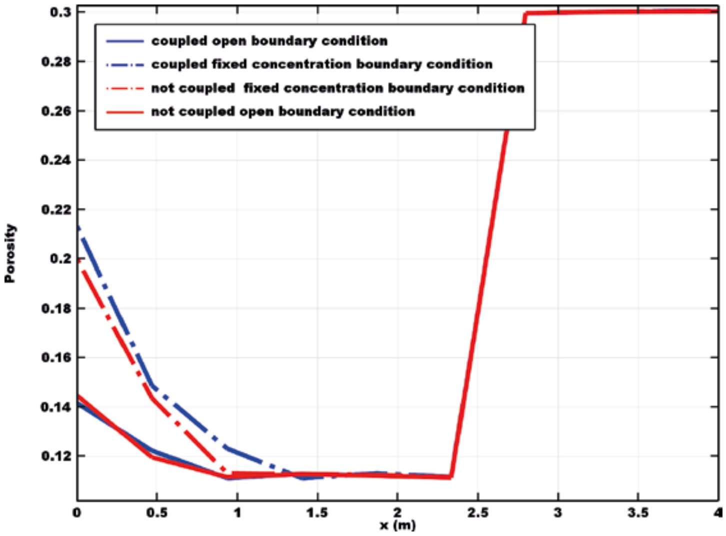

Figure 5-28. *Comparison of 1D profiles (first 4 m, as defined in Figure 5-7) of pH after 50 000 years: coupled and uncoupled cases assuming open boundary (Cases V and VI, respectively) and fixed concentration (Cases IX and X, respectively) boundary conditions for solute transport.*

Another important aspect of the effect of solute transport boundary conditions is related to the extent of degradation along the concrete-rock interface. The cases where open boundary conditions are used show systematically that degradation is limited to the inflow side of the concrete structure. On the other hand, imposing fixed concentrations at the boundary leads to a much more symmetric degradation, i.e. degradation is almost independent of the groundwater flow field. This is shown in Figure 5-29 for Cases V and IX. It is clearly seen that portlandite volume fraction and pH of the pore solution are asymmetrical in Case V and much more symmetric for Case IX.

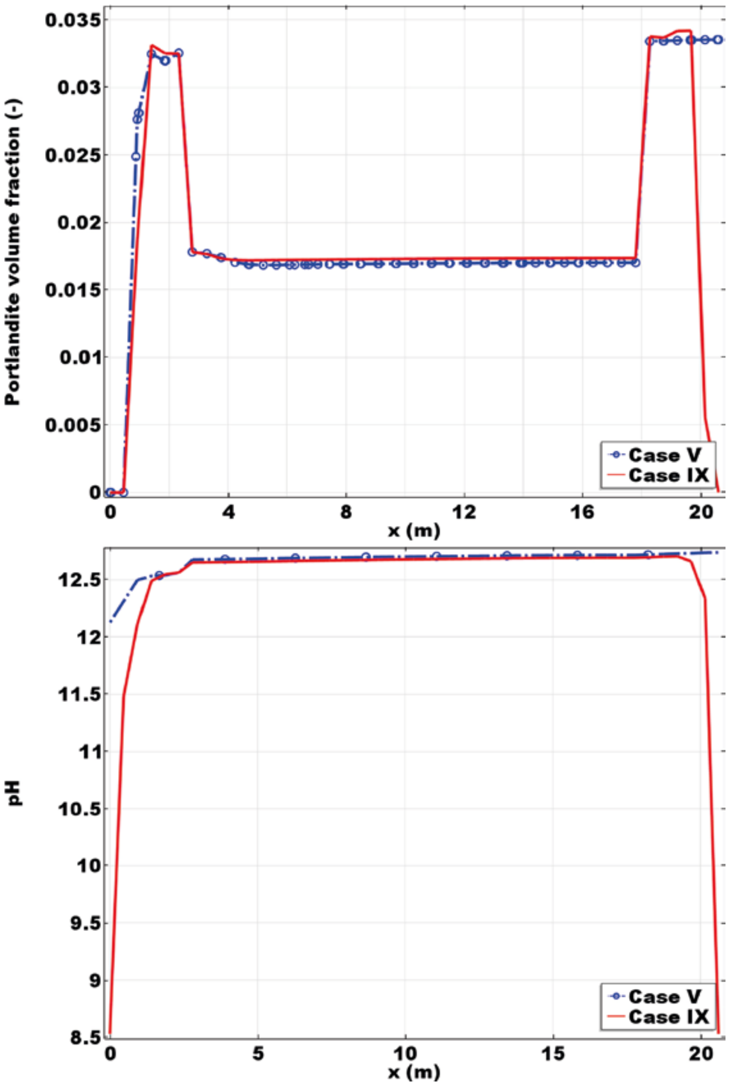

Figure 5-29. *Comparison between Case V and Case IX of 1D profiles (as defined in Figure 5-7) of portlandite volume fraction and pH after 100 000 years: open boundary vs. fixed concentration boundary conditions for solute transport.*

5.3.2.5. Groundwater composition: old-meteoric vs. glacial

Simulations with two different groundwater compositions have been performed with a full chemistry system, open boundary condition for solute transport and constant inlet fluid flow. An old-meteoric groundwater (Table 5-2, Case IV) and a glacial groundwater (Table 5-3, Case XI) have been used. These two cases only differ in the groundwater composition that enters into the system. Figure 5-30 and Figure 5-31 present the results in terms of pH and porosity 1D profiles, respectively. As can be seen, very small differences exist between the two cases, even though the glacial groundwater is much more dilute.

5.3.3 Heterogeneous cases

The results of the Base case (Case I), corresponding to initially homogeneous hydraulic properties, have shown that chemical alterations are limited in space. One of the reasons is that the initial state of the barriers considered in Case I is homogeneous and corresponds to a limited concrete degradation state. More details of the reasoning behind the initial value of hydraulic conductivtiy can be found in Höglund (2014).

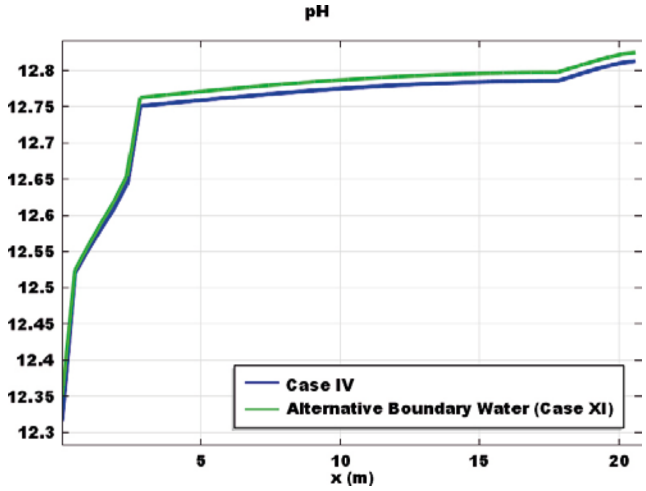

Figure 5-30. *Comparison of 1D profiles of pH after 50 000 years: effect of meteoric (Case IV) vs. glacial (Case XI) boundary water chemistry.*

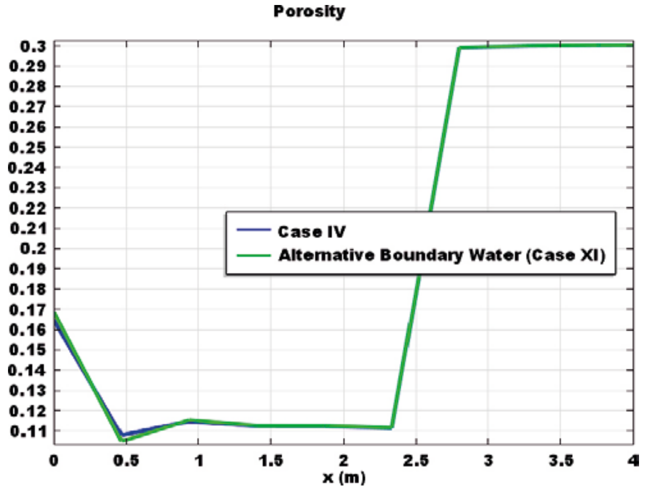

Figure 5-31. *Comparison of 1D profiles of porosity after 50 000 years: effect of meteoric (Case IV) vs. glacial (Case XI) boundary water chemistry.*

In this section, the results of two additional simulations (Cases II and III) are presented. The objective of these simulations is to study the effect of an initial heterogeneous hydraulic conductivity field on flow and transport and ultimately on concrete degradation.

The main goal of this study is to generate connected high hydraulic conductivity (K) paths, leading to chanelling and preferential flow. These preferential pathways can reduce travel times and accelerate concrete degradation processes.

It is noted that heterogeneity of the bedrock is not considered in these simulations. All of the 2D reactive transport models considered in this work assume averaged values of inlet velocities and pressure differences (see Section 5.2.3.1). However, the effect of heterogeneity of the rock on the groundwater flow field in the BHK vault is explored in the 3D simulations presented in Section 6.

5.3.3.1. Multivariate Gaussian model (Case II)

A first heterogeneous hydraulic conductivity field has been generated using a multivariate Gaussian model. In this model, the histogram of the logarithm values follows a Gaussian (normal) distribution. Two paramters are required to fully characterize the multi-Gaussian log-conductivity field: mean (μ) and standard deviation (σ) values. Once the minimum (K_{min}) and maximum (K_{max}) values of the hydraulic conductivity field are known, the Gaussian distribution parameters, i.e. μ and σ, can be obtained. For a normal distribution, 99.7 % of the probability mass lies within three standard deviation from the mean:

$$\sigma = \frac{1}{6}[\log(K_{max}) - \log(K_{min})] \tag{5-2}$$

$$\mu = \frac{1}{2}[\log(K_{max}) + \log(K_{min})] \tag{5-3}$$

For the concrete domain, K_{max} and K_{min} values of 10^{-6} m/s and 10^{-11} m/s have been used, respectively. The latter value corresponds to an intact state of the concrete barrier. For the waste domain, the minimum value has been replaced by 10^{-7} m/s. An internal *Random* function in Comsol has been used to generate a normal distribution. The histograms of log values for both hydrualic conductivities of concrete and waste domains are shown in Figure 5-32. In Comsol, the normal random distibution of conductivity field is generated in a default $[0.1] \times [0.1]$ spatial domain which then will be extrapolated and mapped to the exact computational domain. The resulting 2D distribution of hydraulic conductivity values in all of the domains, i.e. rock, concrete, and waste, is shown in Figure 5-33 ($\log_{10}$(K(m/s)). It may observed that the Gaussian distribution leads to a hydraulic conductivity field in which the most connected paths are close to the mean value.

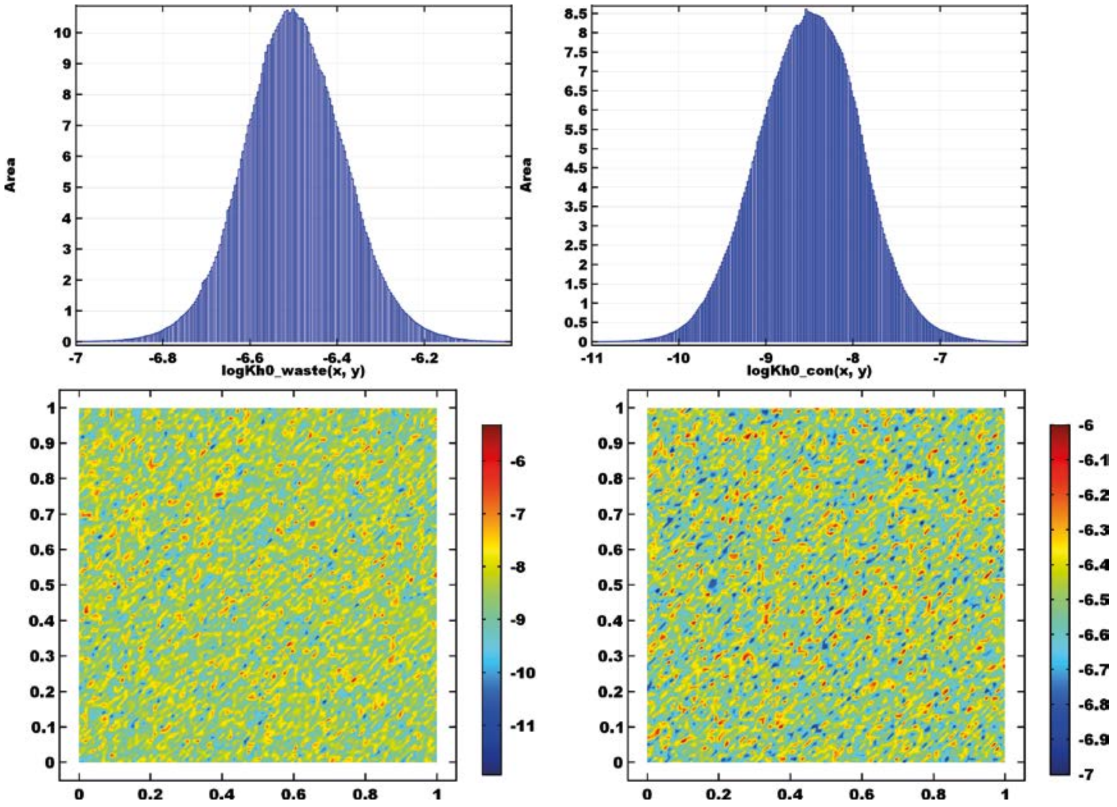

Figure 5-32. *Log values of hydraulic conductivities (m/s) in concrete (left) and waste (right) domains: histograms (top) and 2D distribution (bottom).*

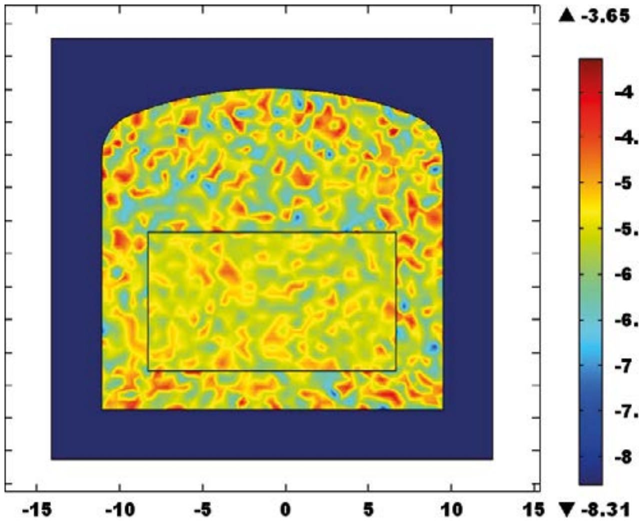

Figure 5-33. *Heterogeneous spatial distribution of hydraulic conductivities, $\log_{10}(K, m/s)$, in the modelled domain using a multivariate Gaussian random model. The hydraulic conductivity of the rock is constant.*

The simulation of heterogeneous initial state is referred to Case II in Table 3-1. Coupling between physical and chemical processes has been considered using the full chemistry setup. Open boundary conditions are considered for solute transport, and therefore the results can be directly compared with those of Case IV. Results are compared with Case IV after 78 500 years in Figure 5-34 to Figure 5-37. Figure 5-34 shows the Darcy velocity field and streamlines. Formation of preferential pathways for flow and transport are clearly visible. These pathways are a result of the heterogeneous conductivity field and lead to an heterogeneous dissolution process in the concrete backfill. Portlandite and C-S-H (jennite-like) dissolution is shown in Figure 5-35 and Figure 5-36, respectively. The pH remains largely unaffected (Figure 5-37). Overall, it may be observed that the effect of using this Gaussian heteregeneous hydraulic conductivity field is not significant when compared to the equivalent homogeneous case (Case IV).

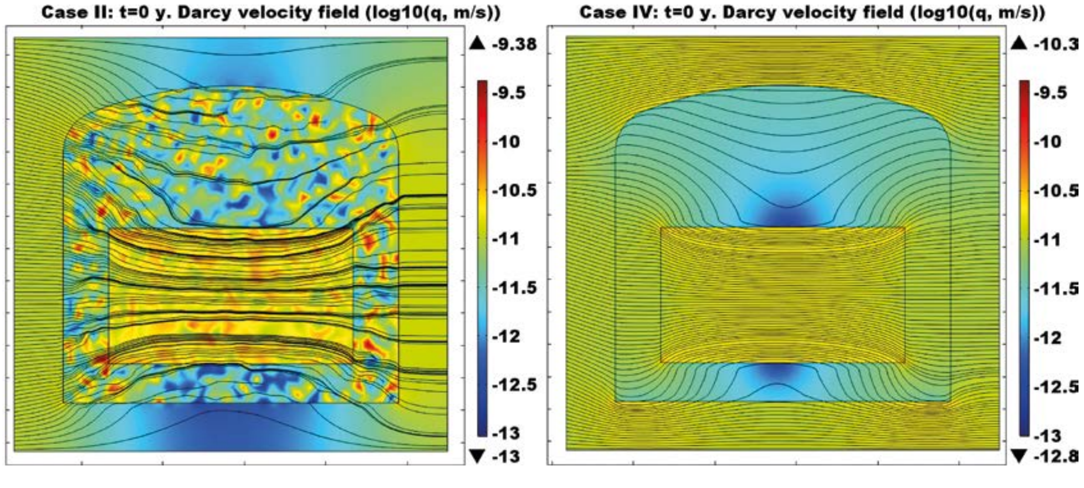

Figure 5-34. *Darcy velocity field, as $\log_{10}(q, m/s)$, and streamlines at time 0 year for heterogeneous Case II and homogeneous Case IV.*

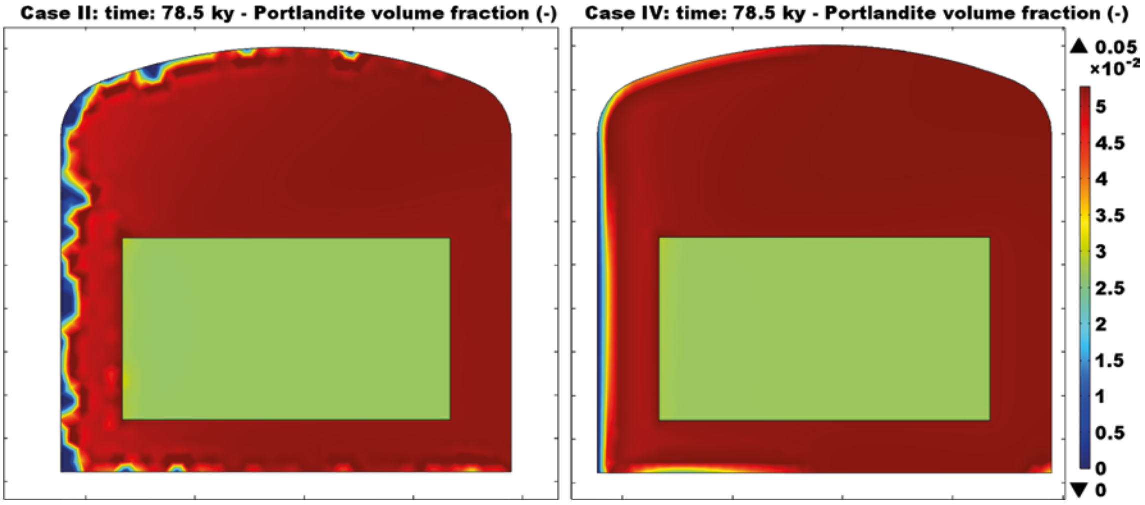

Figure 5-35. Spatial distribution of portlandite volume fraction (–) after 78 500 years for heterogeneous Case II and homogeneous Case IV.

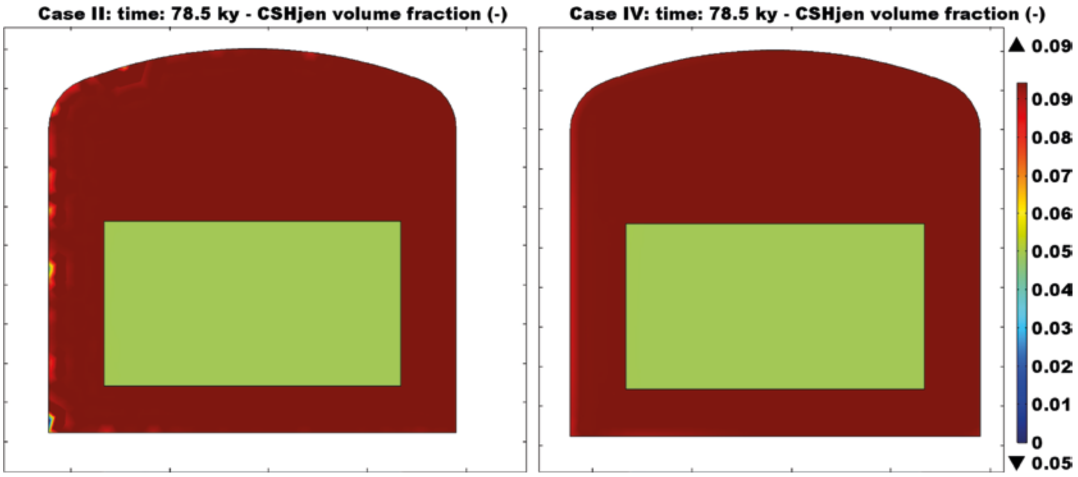

Figure 5-36. Spatial distribution of CSHjen volume fraction after 78 500 years for heterogeneous Case II and homogeneous Case IV.

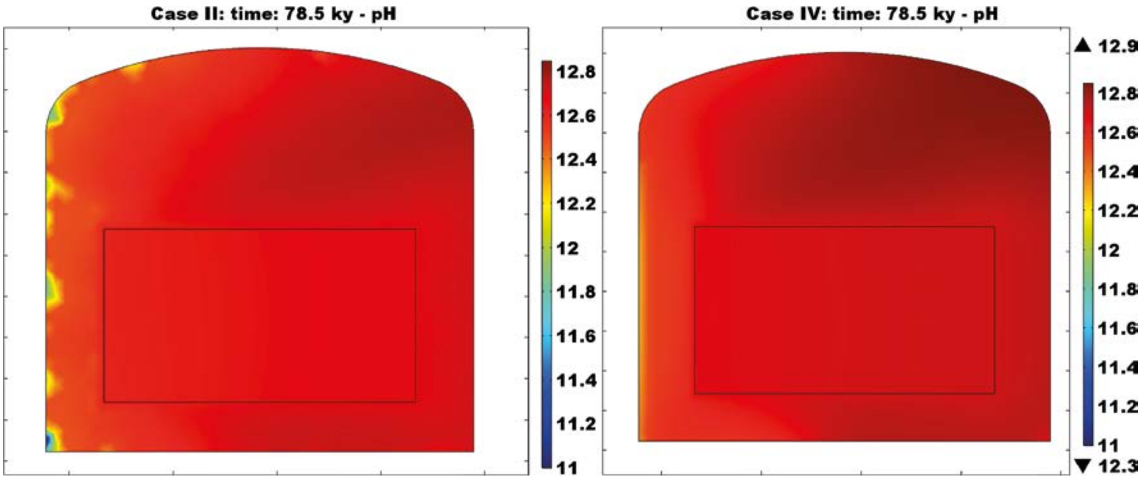

Figure 5-37. Spatial distribution of pH after 78 500 years for heterogeneous Case II and homogeneous Case IV.

5.3.3.2. SGSIM Model (Case III)

One shortcoming of the multivariate Gaussian model presented above is that it generates a field where extreme values are less connected and tend to form clusters rather than inteconnected flowpaths or channels. The resulting effective hydraulic conductivity in Gaussian fields could be approximated by a geometric average value, even for high variance domains. As observed, the net effect on fluid flow and solute transport is therefore limited.

In order to generate a connected field with high hydraulic connectivity (*K*) values, the method of Knudby and Carrera (2005) has been followed. This method is based on the transformation of a multi-Gaussian field in five steps:

1) First, the software SGeMS (Stanford Geostatistical Modeling Software) has been used to generate a conductivity field using its sequential Gaussian simulation subroutine, named *SGSIM* (Remy 2004). A total of five realizations of $Y = \log_{10}(K)$ fields have been generated, each realization consisting of 20 fields. The dimension of each field has been set to 100 × 100 grid cells. The selected field along with its associated histogram is shown in Figure 5-38.
2) Using a normal score transformation (*nscore* algorithm, see Remy 2004) a modified field has been generated with zero-mean and unit-variance Gaussian distribution.
3) By calculating the absolute value of the multi-Gaussian field, the extreme values have been shifted to high values and values close to the mean become low values.
4) The fields have then been converted back using *nscore* algorithm, which results in fields with connected low-K zones and disconnected high-K values.
5) By reflecting high values around the mean, the high values have been transformed to low values and vice versa.

The outcome of the above-mentioned transformations is a field with connected high-K zones and disconnected low-K zones. The final conductivity field is illustrated in Figure 5-39. This field has been imported into the Comsol model through an interpolation function, as shown in Figure 5-40 and Figure 5-41.

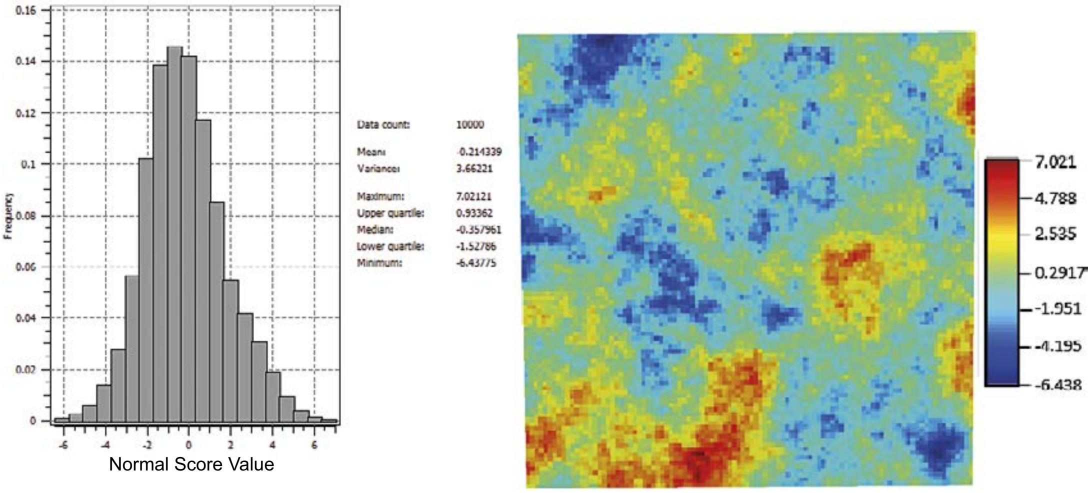

***Figure 5-38.** Original histogram (left) and 2D hydraulic conductivity field ($\log_{10}(K,m/s)$) generated by SGeMS software (right) in a domain of 100 × 100 grid cells.*

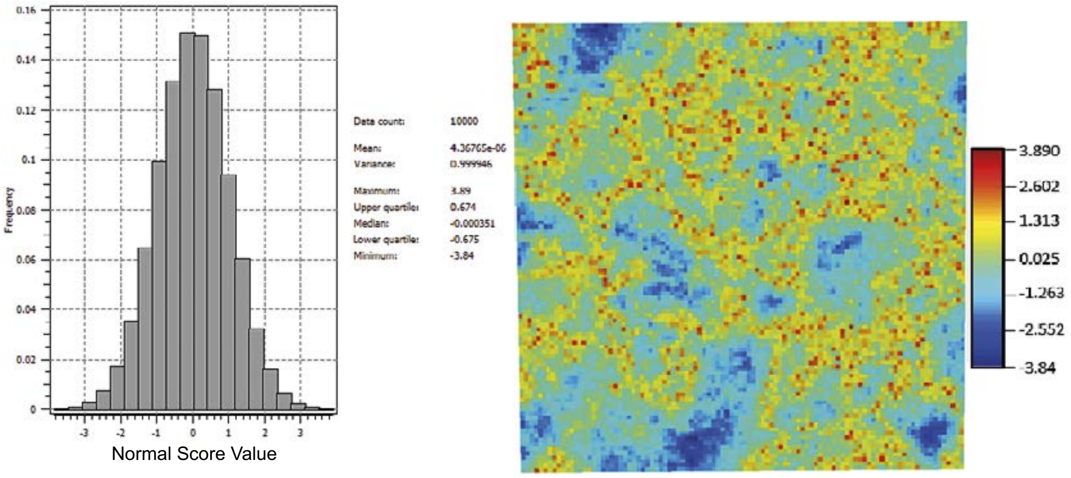

Figure 5-39. *Final histogram generated after series of transformations (left) and associated 2D hydraulic conductivity field (log$_{10}$(K, m/s)) in a domain of 100×100 grid cells.*

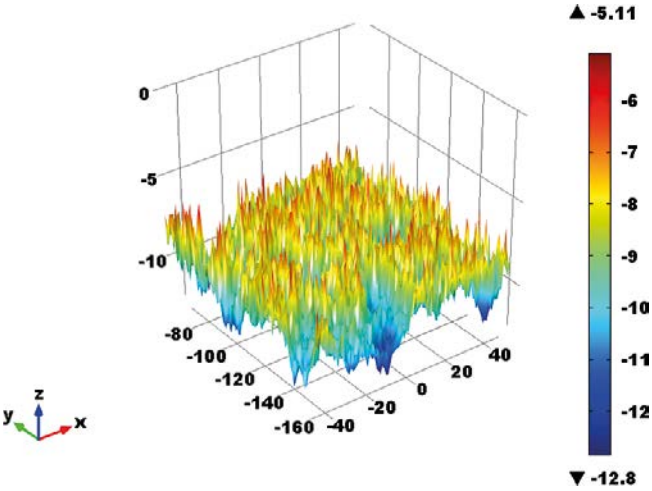

Figure 5-40. *3D representation of the high-K connected field in Comsol (z axis), presented as log$_{10}$(K,m/s). Dimension of the x and y axes are in metres (m).*

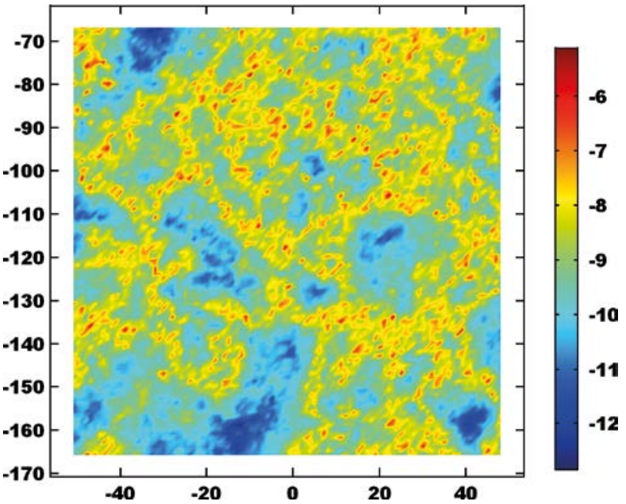

Figure 5-41. *2D representation of the high-K connected field in Comsol, presented as log$_{10}$(K,m/s). Dimensions of the axes in metres (m).*

The simulation that considers this heterogeneous hydraulic conductivity field is referred to as Case III in Table 3-1. A constant hydraulic head gradient is imposed as boundary condition for groundwater flow. For solute transport fixed concentrations are imposed, instead of the open boundary condition for Case II, to maximize the degradation process. The full chemistry setup has been assumed.

Results of the Darcy velocity field at time 0 are shown in Figure 5-42. The connected flow paths can be clearly observed, with streamlines concentrated along high velocity zones. Preferential pathways are more clearly identified compared to the Gaussian distribution case (Figure 5-34).

Figure 5-43 presents the results of portlandite, CSH_{jen}, and CSH_{tob2} after 50 000 and 78 500 years. The effect of the heterogeneity on the degradation of concrete is clearly visible in this figure. After 78 500 years, portlandite dissolution has proceeded through the full thickness of the concrete backfill wall along the high Darcy velocity path.

The results in terms of pH and porosity are depicted in Figure 5-44. Again, the effect of the heterogeneity leads to a lower pH and a higher porosity in the zones where the high hydraulic conductivity field is well connected. Finally, Figure 5-45 presents the mineral volume fractions and resulting porosity after 100 000 years in a 1D profile traversing the preferential portlandite dissolution front. It may be observed that not only the porosity increases in the concrete backfill, but also in the waste domain.

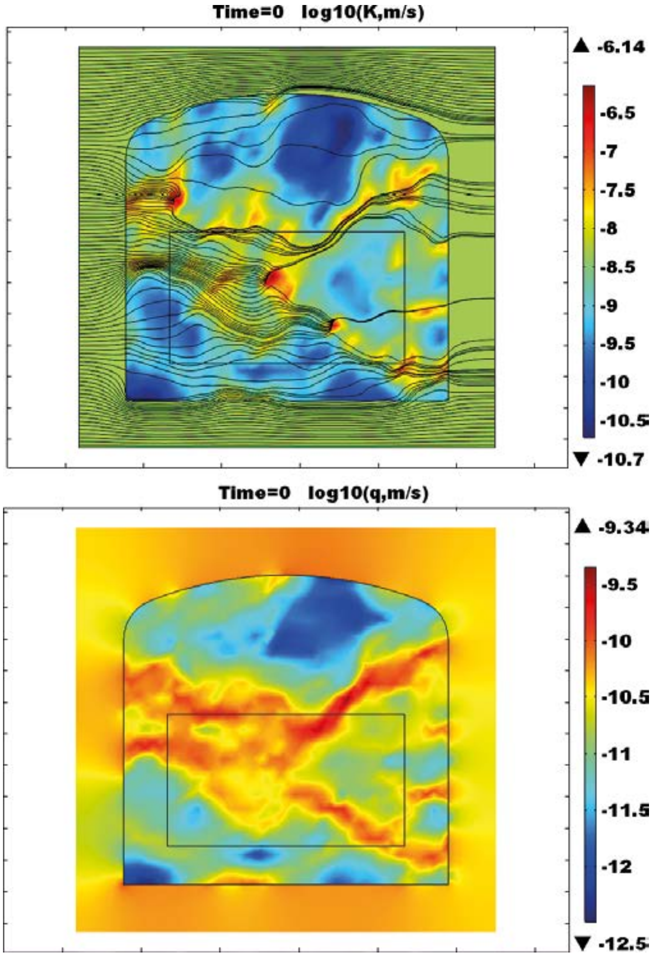

***Figure 5-42.** Streamlines and heterogeneous hydraulic conductivity field, as $\log_{10}$(K,m/s), at the initial state in a high-K connected field (top). Resulting Darcy velocity field, as $\log_{10}$(q,m/s) (bottom).*

Compared to Case II, where open boundary conditions are used for solute transport, Case III leads to a relatively more symmetrical degradation, see the discussion in Section 5.3.2.4. Portlandite dissolution and C-S-H degradation is still much more important across the inflow (left) side, but these processes also take place on the outflow side to a significant extent. The effect of the heterogeneity of the hydraulic conductivity field is only observed on the inflow side due to the fact that advective transport dominates. On the outflow side, degradation occurs mainly due to back diffusion, with a homogeneous diffusion coefficient field (according to Equation 3-4 and 3-5). This can be observed in Figure 5-46, where the 2D distribution of the Darcy flow is shown at the start and at the end of the simulation time (i.e. 100 000 years). As a result of concrete degradation, an increase in the magnitude of the flow can also be observed in certain zones of the concrete backfill.

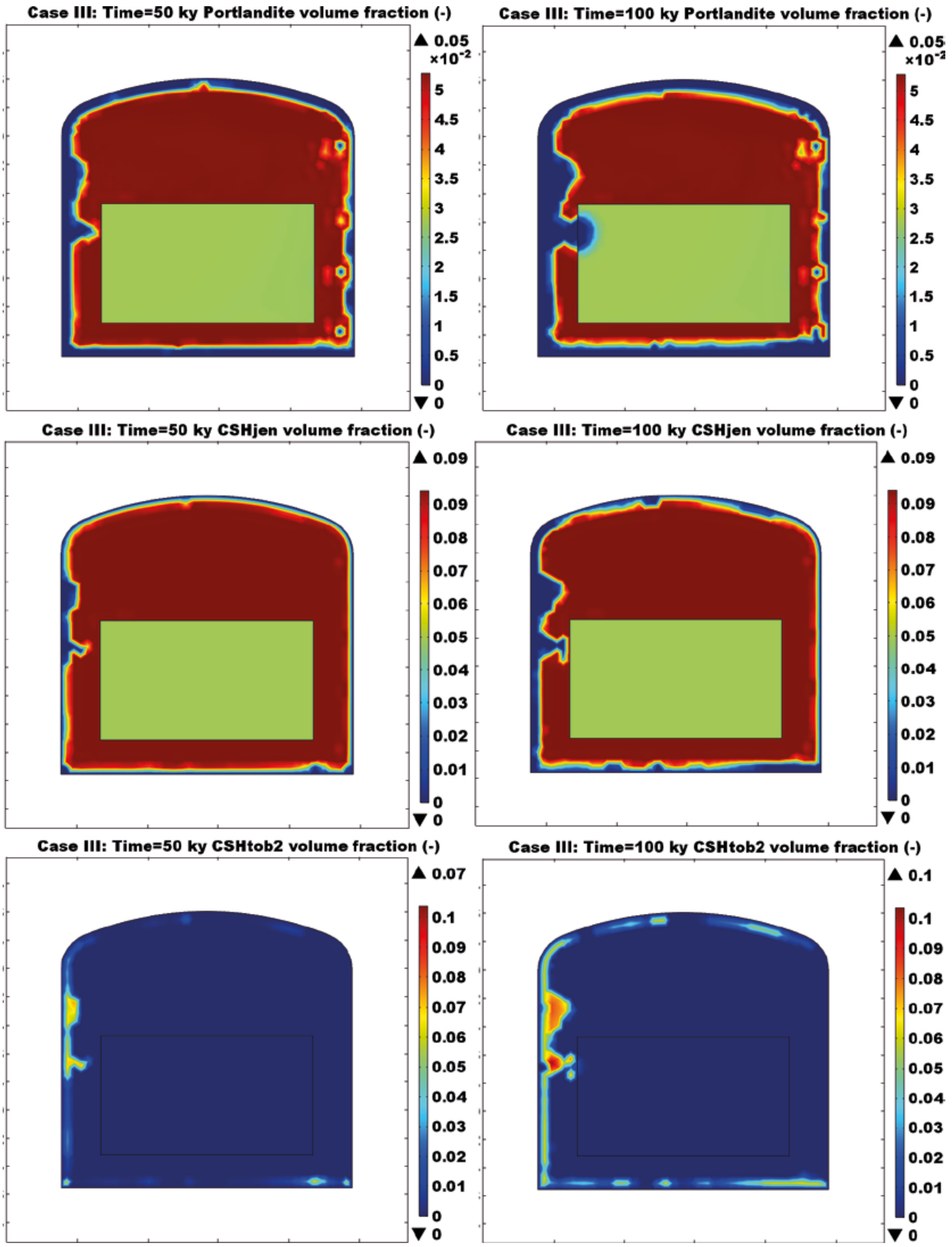

Figure 5-43. *2D spatial distribution of portlandite, CSHjen, and CSHtob2 volume fractions (–) after 50 000 (left column) and 100 000 (right column) years.*

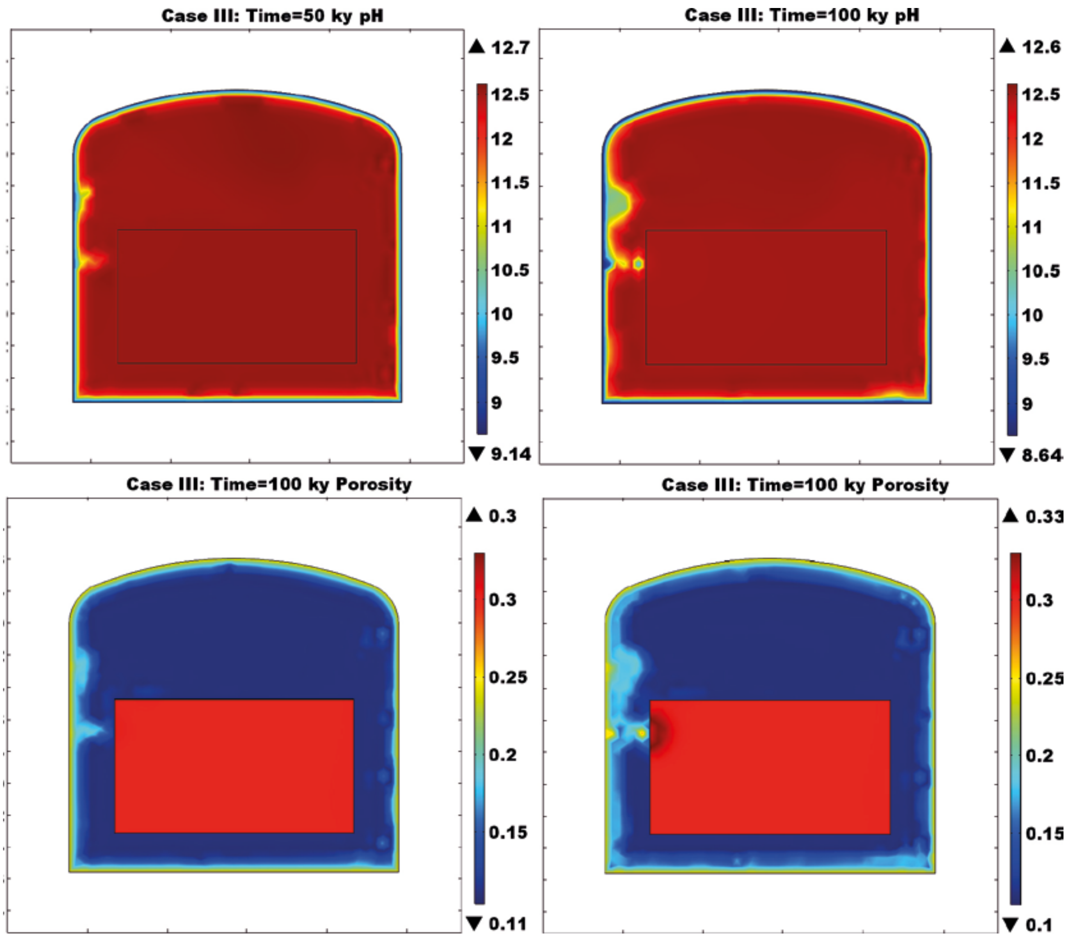

Figure 5-44. *2D spatial distribution of pH (top), and porosity (bottom) after 50 000 (left column) and 100 000 (right column) years.*

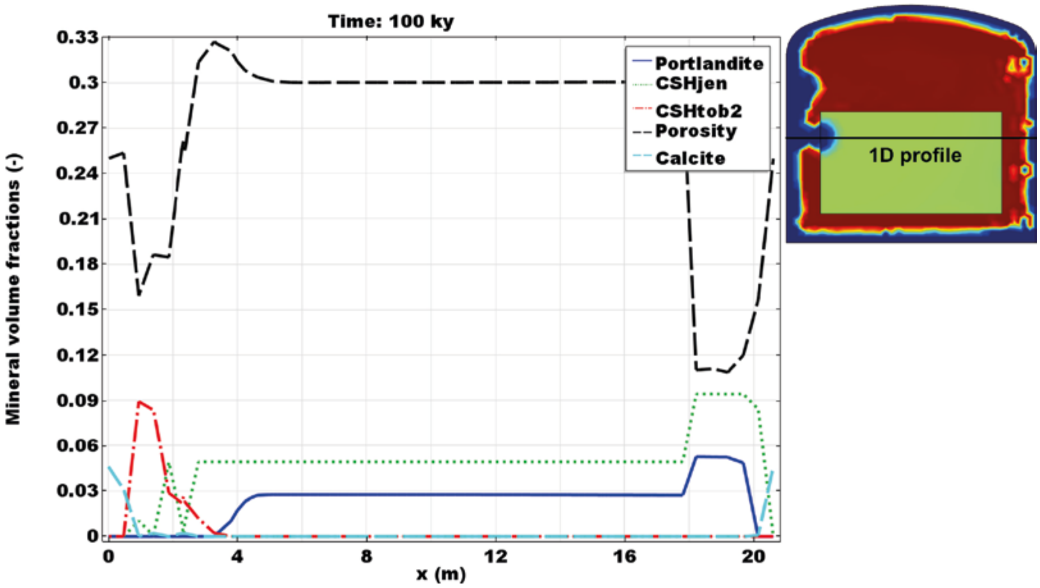

Figure 5-45. *Mineral volume fractions (–) and porosity at the 1D profile shown in the figure after 100 000 years.*

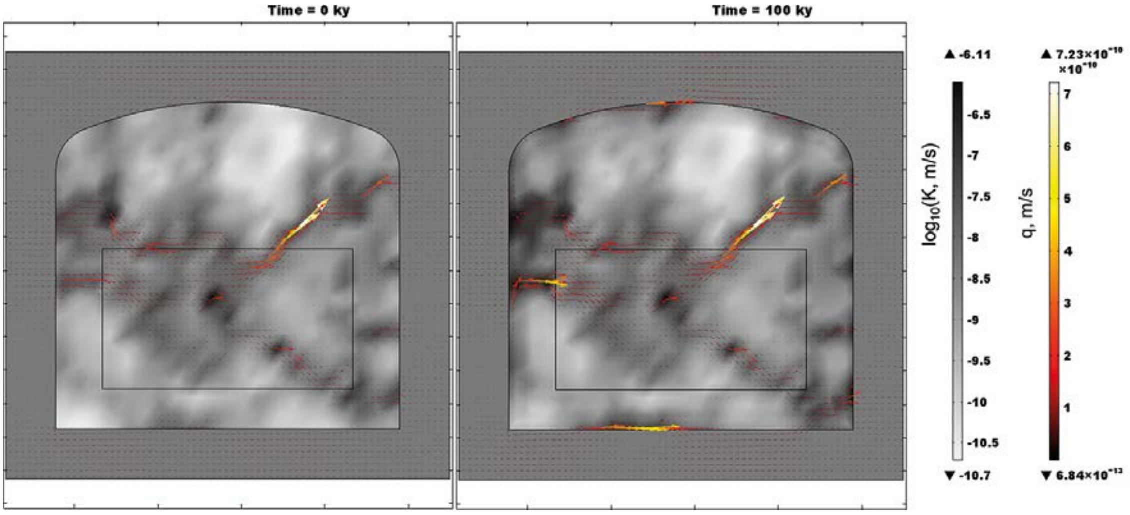

Figure 5-46. *Initial (left) and final (right) 2D spatial distribution of hydraulic conductivity (log$_{10}$(K, m/s)) and Darcy flow (arrow lines proportional to flow and coloured by flow magnitude).*

5.4 Summary of sensitivity cases

A 2D reactive transport model of the degradation of concrete in the BHK vault of the future SFL repository has been implemented using iCP (Nardi et al. 2014). In total, a set of eleven different simulation cases have been performed to examine several modelling assumptions. These are related to physical and chemical properties of the cementitious materials, groundwater flow, and boundary conditions.

The results obtained of the different simulation cases indicate that the concrete barriers are not significantly degraded even after 100 000 years of interaction with groundwater. An exception is the heterogeneous case (Case III), for which a localized zone of portlandite dissolution is observed across the full wall thickness. The reasons behind the long-term performance predicted by the model are the following:

1. Groundwater flow into the BHK vault is limited (Section 5.2.3, Abarca et al. 2016). Darcy velocities in the concrete backfill are on the order of 1×10^{-11} m/s, with fluid velocities slightly lower than 3 mm/y. This gives advective travel times through the cross-section of the vault greater than 5 000 years.
2. The initial effective diffusion coefficient of the concrete backfill is very low (Table 5-1), limiting the extent of groundwater-concrete interaction.
3. Related to the previous statements, the volume of concrete in the BHK vault is very large compared to the amount of water entering the vault. A substantial amount of aggressive species is needed in the model in order to chemically degrade the structure to a significant extent. Given the large advective travel times and the low diffusion coefficients, the resulting chemical interaction is limited.

Case I has been selected as a base case scenario with a model setup that is thought to be representative of the BHK vault conceptual model. The base case considers (Table 3-1): a Darcy flow model with a constant inlet flow boundary condition, along with a solute transport model with fixed concentration boundary condition. It furthermore considers the full chemistry setup (Table 5-4 and Table 5-6). The model domains are assumed to have uniformly distributed physical properties, such as hydraulic conductivity. Feedback between chemical and physical processes is considered by coupling porosity and hydraulic conductivity using the Kozeny-Carman relation. Modifications of these assumptions have produced a set of sensitivity case. A summary of these cases is presented in Table 3-1.

Homogeneous vs. heterogeneous hydraulic conductivity. The effect of spatial heterogeneity of the hydraulic conductivity of concrete has been investigated with two additional simulations by imposing (1) Gaussian and (2) SGSIM models. The Gaussian distribution (Case II) leads to a hydraulic conductivity field with clustered regions of high conductivity values. The outcome is a limited degree of preferential flow pathways. As a result, the degradation of the concrete barriers does not differ significantly from the case with homogeneous properties Case IV). On the other hand, the SGSIM model (Case III) leads to a hydraulic conductivity field with a significantly higher connectivity of high values. This results in a more pronounced concrete degradation as compared to the homogeneous case (Case I). Preferential flow paths and non-uniform reactive fronts are clearly distinguishable in this case.

Effect of boundary conditions. The base case (Case I) considers fixed concentration boundary conditions. This case is representative of a degradation process mainly driven by diffusion and in which out-diffusion from the vault towards groundwater does not affect the composition of the latter. The reason why this condition has been assumed in the base case is the low groundwater flow rates expected in the BHK vault (Abarca et al. 2016). Results using this boundary condition show a relatively symmetric degradation front, which indicates a diffusive controlled system. The case in which this condition is changed to an open boundary condition leads to a significantly reduced degree of concrete degradation (Case IV), with a more asymmetric extent. This has been demonstrated in more detail using the simplified chemistry setup, for both coupled and uncoupled situations (Section 5.3.2.4).

In addition, the effect of different boundary conditions for groundwater flow, i.e. constant inlet flow (Case IV) vs. hydraulic head (Case VIII), has also been tested. The results show that their impact is negligible.

Simplified vs. full chemical setup. The results obtained using a simplified (Case V and Case IX) or a full (Case I and Case IV) concrete chemistry setup (Table 5-7 and Table 5-6, respectively) have been compared. Both sets of cases yield a similar evolution of the pH and porosity in the concrete backfill. The results also show that the full chemistry setup increases the average transport simulation time substantially compared to the simplified setup. The simulation time for the chemistry step is approximately similar in both cases. Furthermore, the comparison between the evolution of physical properties such as hydraulic conductivity, effective diffusion coefficient and porosity of full and simplified chemistry scenarios demonstrates a similar trend. This suggests that simplified chemistry can be selected as the representative chemical composition of waste and concrete domains for the 3D simulations, where computational efficiency is critical.

Coupled vs. uncoupled porosity evolution. A comparison of the coupled and uncoupled scenarios regarding feedback of chemistry on porosity has been performed (Sections 5.3.2.2 and 5.3.2.4). The results show that considering the coupling leads to an enhancement of flow and solute transport. The reason is that the porosity increase leads to an increase of the hydraulic conductivity and the effective diffusion coefficient. However, applying the modified Kozeny-Carman formulation had only a marginal effect on the results compared to the original Kozeny-Carman relation.

Groundwater composition. Finally, the glacial melting water has been tentatively used as alternative boundary water, as in Pękala et al. (2015). Compared with the results of meteoric groundwater, the effect on concrete degradation processes is shown to be limited.

From the results, it may be concluded that Case IX can be used for the 3D simulations of the BHK vault. This case has a similar setup to the base case (Case I), except that in Case IX a simplified chemistry setup has been assumed.

6 3D reactive transport models of the BHK vault

6.1 Description of the 3D compartment- and vault-scale models

The BHK vault will host six waste compartments, as shown in Figure 6-1. In this section, three-dimensional (3D) reactive transport models of a single compartment and of the entire BHK vault are presented and compared to the results presented in Section 5. A 3D representation of the BHK concrete vault has been extracted from the model presented in Abarca et al. (2016), as shown in Figure 6-1. It was concluded from the 2D simulations presented in Section 5 that Case IX (see Table 3-1) can be used as a representative scenario for the 3D models shown here.

One important difference comparing model setup for 3D and 2D geometries concerns the treatment of the Darcy velocities across the repository. In the 2D models, an average value of approximately 1×10^{-11} m/s was used. This value was obtained by averaging the velocities from the 3D hydrogeological model of Abarca et al. (2016). The 2D simulation Case IX considered a constant inlet flow boundary condition for groundwater flow. In the 3D case, the pressure field from Abarca et al. (2016) was directly imposed as boundary condition for the compartment and the vault-scale models. The velocity field is calculated and updated as a function of the constant pressure field and the evolving hydraulic properties of concrete and waste domains.

Another difference is that the modelled domain of the 3D models is restricted in this case to the concrete backfill and the waste compartment (Figure 6-2). In the 2D models (Section 5), part of the host rock domain was included in the model exclusively for groundwater flow calculations. However, in the 3D models, the host rock has not been considered, in order to restrict cpu time.

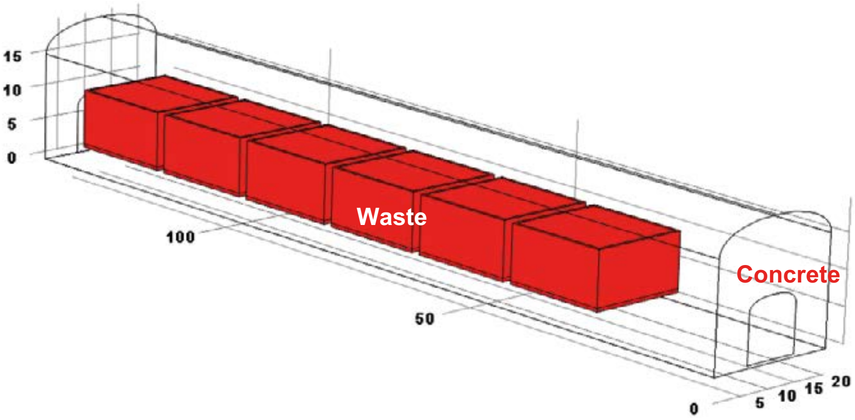

Figure 6-1. *3D BHK vault includes two domains: concrete and waste. Dimensions are in metres (m).*

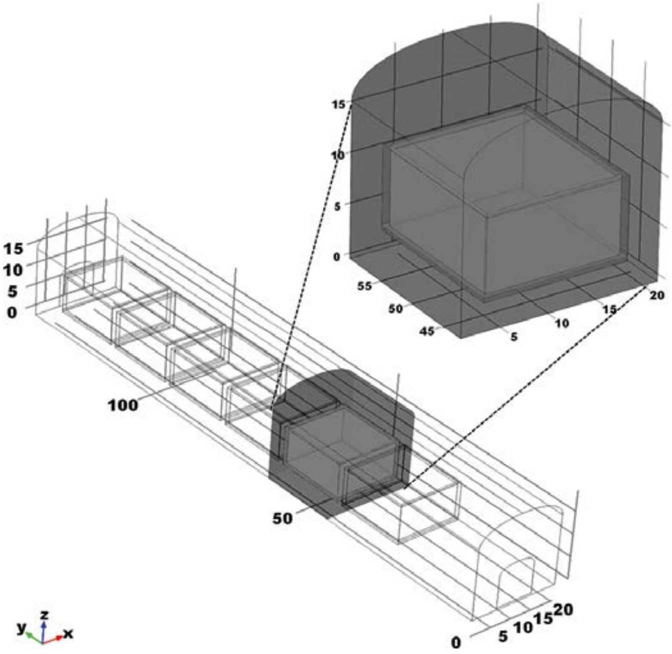

__Figure 6-2.__ 3D BHK vault geometry, showing the compartment-scale model, including two domains: concrete (dark grey) and waste (light grey). Dimensions are in metres (m).

The initial Darcy velocity field in the vault is shown in Figure 6-3. A comparison of this velocity field with the results by Abarca et al. (2016) is presented in Table 6-1 in terms of average values for the entire BHK vault. It may be observed that the values differ slightly between the two models. This is in part due to the different spatial discretization used in the two models (the model presented here is almost 6 times more refined, see Table 6-1) and also due to the interpolation of the pressure field in the boundary of the vault-scale reactive transport model. However, for the purpose of this study these velocity fields are considered as sufficiently similar. The important aspects are that (1) velocities are generally higher than the value of 1×10^{-11} m/s used in the 2D simulations, and (2) the velocity field shows a heterogeneous distribution across the concrete backfill.

The velocities in all the six waste compartments are very similar (the volume average in each waste compartment is 8.61×10^{-11} m/s ± 0.38×10^{-11} m/s). The second BHK compartment (starting from y = 0) was selected, for the concrete degradation modelling.

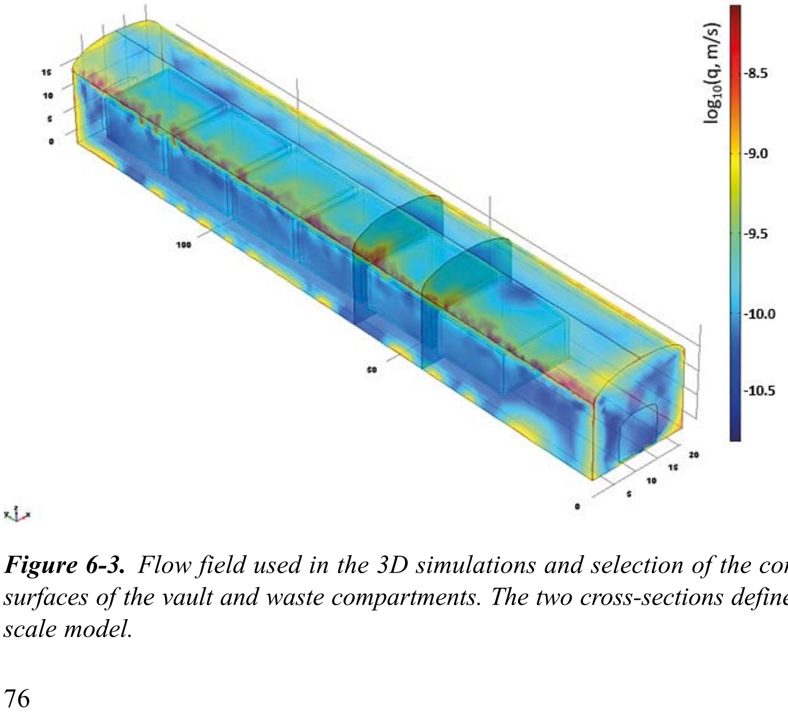

__Figure 6-3.__ Flow field used in the 3D simulations and selection of the compartment: $\log_{10}(q, m/s)$ in the surfaces of the vault and waste compartments. The two cross-sections define the limits of the compartment-scale model.

Table 6-1. Darcy velocities (q) in the BHK vault: values derived from Abarca et al. (2016) and initial values calculated in this work from the pressure field. Volume averages are calculated in the whole vault. Surface average corresponds to the plane x = 0 (yz-plane).

	Abarca et al. (2016)	This work
Volume average q_x (m/s)	3.32×10^{-11}	3.48×10^{-11}
Volume average q (m/s)	5.11×10^{-11}	3.82×10^{-11}
Surface average q (m/s)	3.75×10^{-11}	9.68×10^{-11}
Number of elements	130 847	773 161

For the setup of the 3D models, all of the assumptions related to the composition of concrete and waste domains are identical to the 2D model Case IX with a simplified chemistry setup (see Section 5.1). The concrete and waste domains are composed of different volume fractions of the same concrete composition. Initial porewater composition of concrete is presented in Table 5-5 while the mineralogical phase assemblages of the concrete and waste domains are presented in Table 5-7. Portlandite, C-S-H gels (jennite-like and tobermorite-like), calcite, ettringite, and gypsum are allowed to precipitate and dissolve upon degradation.

Material properties required for the flow and transport simulations are summarized in Table 5-1. Case IX explicitly considers the coupling between the flow and transport calculations and the chemical reactions. Porosity evolves with time as a function of dissolution and precipitation reactions. Following the porosity changes, the hydraulic conductivity, K (m/s), and effective diffusion coefficient, D_e (m^2/s), are also modified. The relation between porosity and hydraulic conductivity is given by the Kozeny-Carman equation (Carman 1937). A fixed concentration boundary condition corresponding to old meteoric groundwater (Table 5-2) is used for solute transport.

The only difference between the compartment and vault-scale models is the geometry of the simulation domain.

6.2 Setup of the numerical models

6.2.1 Finite element meshes

The compartment-scale model domain has been discretized into 184 561 tetrahedral elements. Figure 6-4 illustrates the mesh and the finite element size, which varies between 0.44 (in blue) to 1.44 m (in red). The vault-scale modelled domain has been discretized into 773 161 tetrahedral elements. Figure 6-5 illustrates the mesh and the finite element size, which varies between 0.26 (in blue) to 5.24 m (in red).

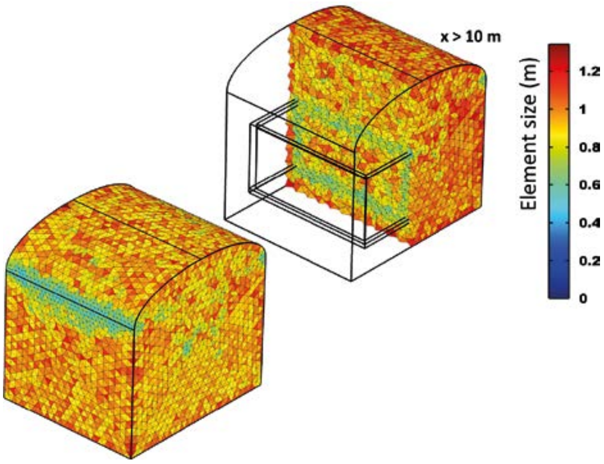

Figure 6-4. *Finite element mesh used in the 3D compartment-scale iCP simulations. Dimensions are expressed in metres. Colours represent the finite element size: 0.44 (in blue) to 1.44 m (in red).*

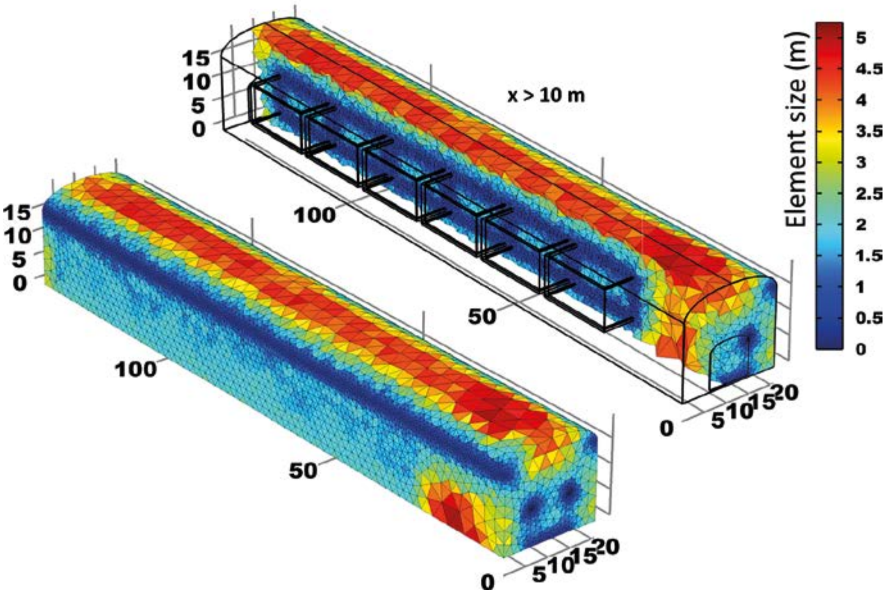

Figure 6-5. Finite element mesh used in the 3D vault-scale iCP simulations. Dimensions are expressed in metres. Colours represent the finite element size: 0.26 (in blue) to 5.24 m (in red).

6.2.2 Temporal discretization

Following the reasoning described in Section 4.2.2, imposing the Courant stability criterion for the vault-scale model suggests maximum time step sizes for operator splitting on the order of tens to hundreds of years for the concrete domain (and up to 4 000 years). For the waste domain, this range is between 14.8 and 228 years. The Von Neumann stability criterion prescribes a larger time step sizes in the whole domain, with a minimum of 12.7 years and up to 90 000 years.

For the compartment-scale model the Courant criterion indicates a maximum time step of 0.15 years only in very narrow zones of higher velocity near the boundary, with values typically much higher than 10 years and locally reaching 11 838 years. In turn, the Von Neumann criterion indicates a smallest maximum time step of 9.25 years again located near the high velocity boundaries, and a maximum of 7 724 years (Figure 6-6).

In order to better compare the results of the 2D model and the 3D compartment-scale model, the same time stepping scheme has been adopted. Time steps ranging between 2 and 9 years have been selected for communication between the multiphysics solver (Comsol) and chemical (Phreeqc) solver. The total simulation time considered in this case is 50 000 years, which is deemed to be sufficient for comparing with the 2D simulations.

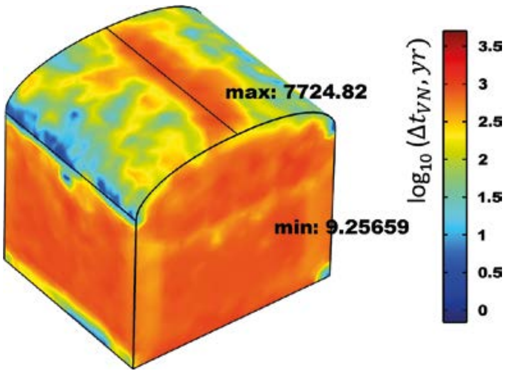

Figure 6-6. Largest and smallest maximum time steps in the compartment-scale model based on the Von Neumann stability criteria (time scale shows $\log_{10}$ values of time step in years).

For the vault-scale model, a slightly coarser time stepping scheme has been adopted, with a constant time step size of 10 years throughout the simulated period of 8 500 years. The main reason behind this choice is to optimize the computational resources. In this case, the total simulation time has been limited to 8 500 years mainly due to the availability of computational resources. However, this simulation time is considered sufficient for the purpose of proving the feasibility and benefits of implementing such a model.

6.2.3 Initial and boundary conditions

The total pressure field from the groundwater flow model of Abarca et al. (2016) has been used as boundary condition along the external surfaces of the concrete domain. This is applicable to the entire boundary of the modelled domains for the compartment-scale as well as the vault-scale models. The main reason to impose pressure values at the boundary instead of the velocity field is to be able to simulate an increase of the velocity of the inflowing water at the boundary as a result of the degradation.

For this purpose, an interpolation function, *BHK_pressure(x,y,z)*, had been defined in the COMSOL input file as shown in Figure 6-7, dependent on the spatial coordinates (*x, y, z*). The same interpolation function has been used to initialize the pressure values over the computational domain. The resulting velocity field over the boundary of the concrete backfill is shown in Figure 6-3.

Dirichlet-type fixed concentration boundary conditions have been imposed over the entire boundary of the concrete domain for solute transport. This is applicable to the entire boundary of the modelled domains for the compartment-scale as well as the vault-scale models. As a result, diffusion of the surrounding water, with a composition described in Table 5-2, will be an active process, in addition to advective transport.

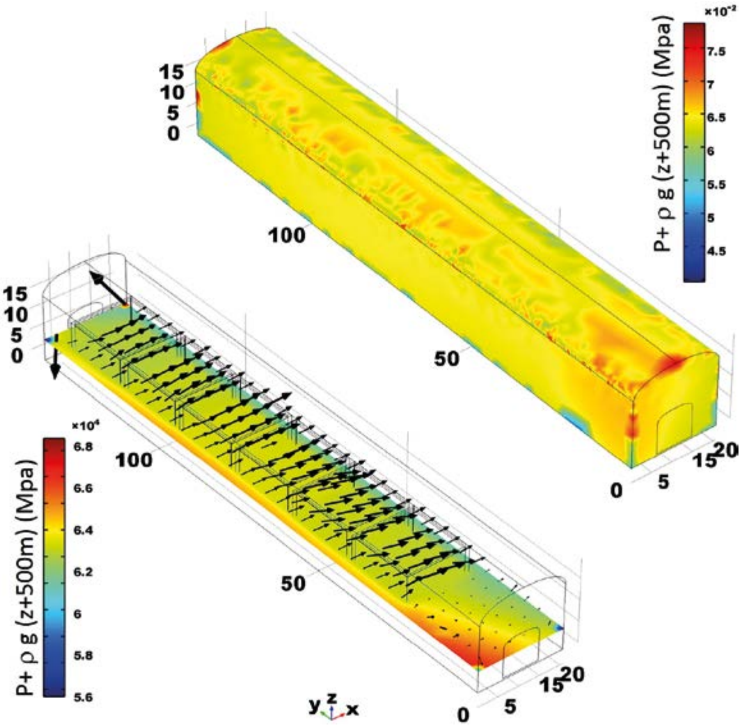

Figure 6-7. *(Left) Arrow flow lines (proportional to flow magnitude) in xy-plane, coloured by P + ρg(z+500 m), and (right) imposed fluid flow boundary conditions: P + ρg(z+500 m) expressed in MPa.*

6.3 Results for compartment-scale model

In this section, the results of the 3D compartment-scale model are presented and compared to the 2D model results of simulation Case IX. The results are illustrated either as 3D distribution plots at given times, multiple slices of the 3D domain, or in a 1D profile. The latter has been defined along a horizontal line crossing through the centre of the waste domain (mid-height and mid-width), as shown in Figure 6-8.

In addition, the heterogeneity of concrete degradation as a result of the uneven velocity distribution is illustrated in an yz-plane of the compartment with x = 0.50 m, as shown in Figure 6-9.

6.3.1 Velocity field

Five xz-planes perpendicular to the vault axis have been selected along the compartment to illustrate the Darcy velocity distribution in different cross-sections. The initial Darcy velocity field is presented in Figure 6-10 and Figure 6-11 (left). However, the velocity field depends on the hydraulic conductivity of the barriers, which in turn is a function of chemical degradation and ultimately of porosity. The velocity field after 50 000 years of interaction with groundwater is therefore different from the initial distribution, as depicted in Figure 6-11 (right). It is clear that velocities have increased significantly near the external boundary of the concrete backfill as a result of degradation. As explained above, the velocity field of the 2D simulations has been calculated in a different way, leading to lower values. Figure 6-12 shows the initial (left) Darcy velocity distribution and after 50 000 years (right) for the 2D model. The values are significantly lower than the 3D simulation and only small changes are predicted after 50 000 years of degradation.

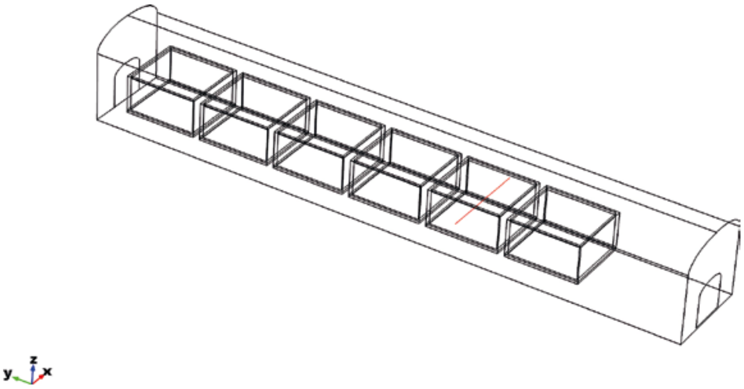

Figure 6-8. *Detail of the 1D profile used to show the results of concrete degradation at different times.*

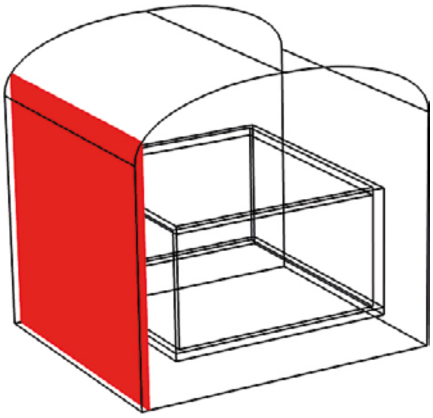

Figure 6-9. *Detail of the 2D yz-plane at x = 0.50 m which has been used to show the results of concrete degradation on a surface of the concrete backfill.*

As a result of the higher velocity field, the Péclet number in the 3D compartment model for the initial state, calculated with Equation (4-1), indicates that in this case advection is relatively more important than in the 2D simulation cases. Typical values of the Péclet number in the concrete backfill range between 5 and 120.

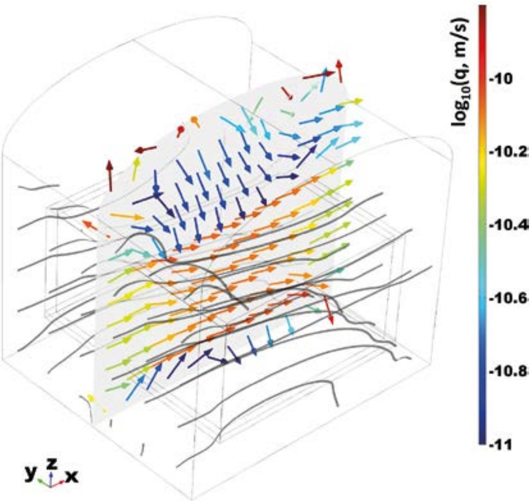

Figure 6-10. *Streamlines in the compartment and arrow flow lines in the mid xz-plane coloured by log$_{10}$(q, m/s) at time 0 showing the direction of the flow.*

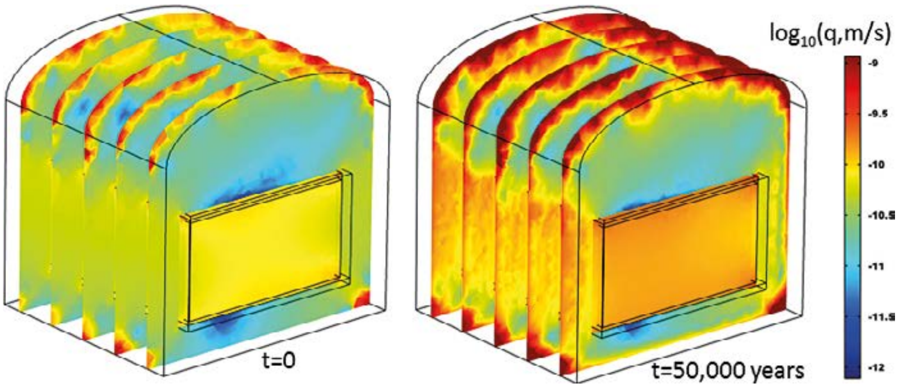

Figure 6-11. *Comparison between the initial (i.e. at time 0, left) and final (50 000 years, right) Darcy velocity fields of the 3D reactive transport simulation. Results are presented as log$_{10}$(q, m/s).*

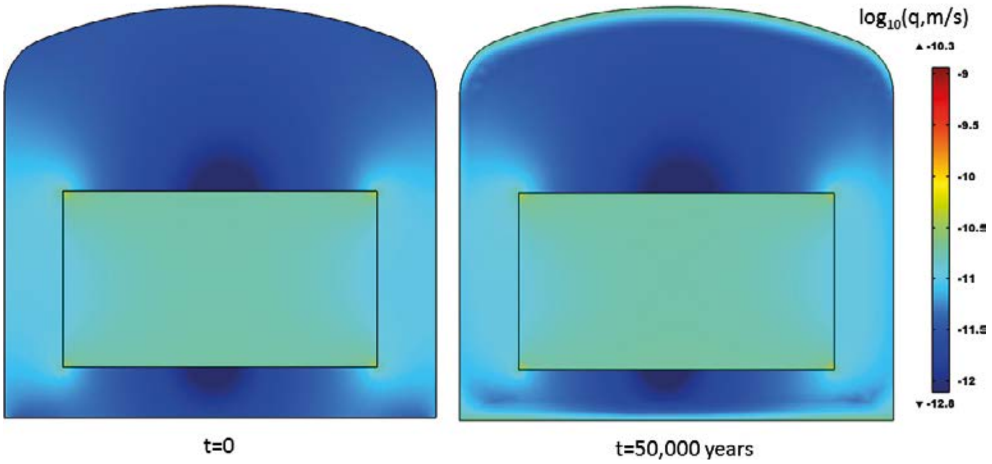

Figure 6-12. *Comparison between the initial (i.e. at time 0, left) and after 50 000 years (right) Darcy velocity fields of the 2D reactive transport simulation Case IX. Results are presented as log$_{10}$(q, m/s).*

Degradation of the concrete backfill does not only affect the magnitude of the velocity field, but also the direction, especially in the vicinity of the concrete external boundary. As an example, Figure 6-13 presents the results in the concrete outer boundary, at a yz-plane at x = 0, of the angle between the x-component of the Darcy velocity (i.e. perpendicular to the plane) and the resultant Darcy velocity vector. A value of $\alpha = 0°$ corresponds to a flow condition in which the resultant flow vector is perpendicular to the plane, while at $\alpha = 90°$ resultant flow vector is equal to the tangential component. Areas with values of $\alpha > 90$, represent a flow condition in which outward horizontal flow component occurs. It is observed that initially (left) the flow is mostly perpendicular to the surface and is directed from the rock to the concrete structure (blue region), except on the top and bottom of the domain. However, after 50 000 years, a significant tangential component of the flow is predicted as a result of concrete degradation. Indeed, chemical degradation leads to an increased conductivity of the external concrete layers. This high hydraulic conductivity at the boundary of the concrete backfill induces a deviation of the original flow, similar to a hydraulic cage effect. Outflowing water from the concrete backfill with a direction perpendicular to the yz-plane is also observed (red region).

6.3.2 Concrete degradation

The heterogeneous velocity field shown in the previous section leads to non-uniform concrete degradation fronts in the modelled domain. Figure 6-14 to Figure 6-23 present the results of concrete degradation in terms of portlandite and jennite-like C-S-H dissolution and calcite and tobermorite-like C-S-H precipitation for three different times (1 000, 36 000, and 50 000 years). In addition, these figures also compare the results of the 3D compartment-scale and the corresponding 2D simulation Case IX. As may be observed, portlandite undergoes complete dissolution at the concrete/rock interface. Whereas in the 2D case the dissolution front is very smooth, the 3D results show a significant degree of heterogeneity mainly due to the velocity field (Figure 6-11). Higher velocities in the 3D case also lead to an increased degree of overall degradation, with a degradation front advancing deeper into the concrete barrier. Portlandite dissolution triggers subsequent chemical reactions in a similar spatially-heterogeneous manner. CSH_{jen} dissolves following portlandite dissolution and CSH_{tob2}, calcite and ettringite precipitate as secondary minerals. Ettringite precipitation is minor and can be neglected (in the range of 1×10^{-4} mol/l_{medium}). In spite of extensive dissolution of jennite-like C-S-H gel in the concrete domain, concrete mineral phases in the waste compartment remain virtually unaffected. Portlandite-controlled pH values are observed, stabilizing at a value around 12, and then start to decrease following its dissolution. Figure 6-24 and Figure 6-25 show the comparison of pH and porosity between the 3D compartment model and the 2D model Case IX after 50 000 years. It may be observed that the heterogeneity in portlandite dissolution and C-S-H degradation impacts the pH of the pore solution, with values lower than 12.

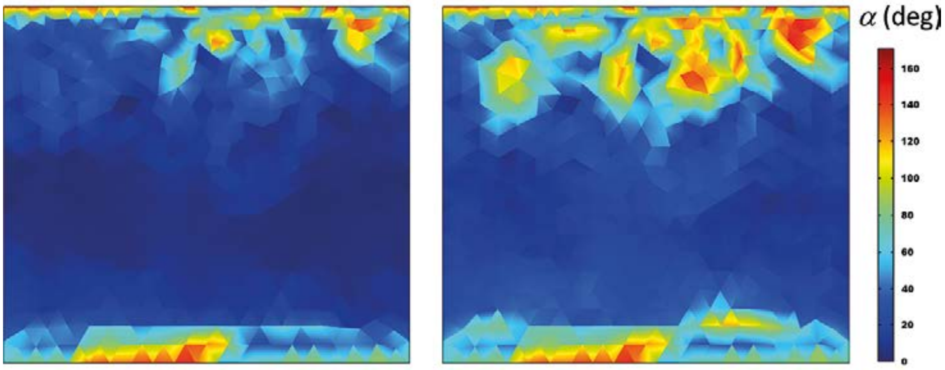

t= 0 years

t= 50,000 years

Figure 6-13. *Angle (degrees) between the x-component of the Darcy velocity and the resultant Darcy velocity vector in the yz-plane x = 0 (concrete external boundary), calculated as* $\alpha = cos^{-1}(q_x \cdot q^{-1})$*. Comparison between the initial (0 years) and final values (50 000 years).*

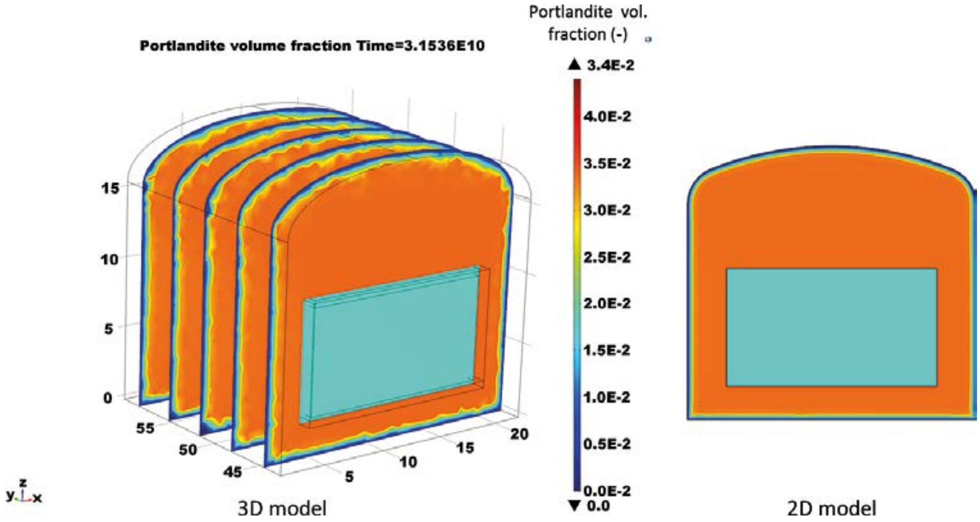

***Figure 6-14.** Portlandite volume fraction (–) after 1 000 years: comparison of the results of the 3D compartment-scale model (left) and the 2D simulation Case IX (right).*

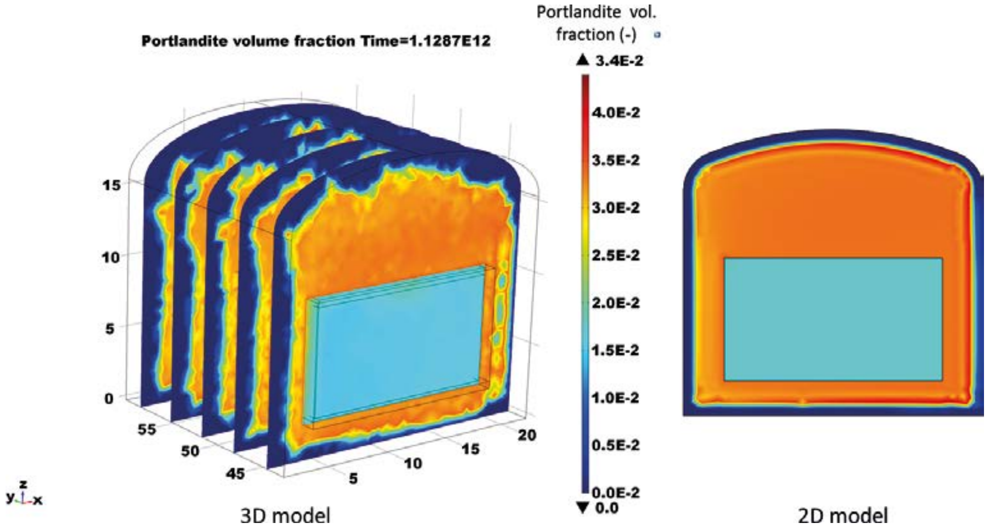

***Figure 6-15.** Portlandite volume fraction (–) after 36 000 years: comparison of the results of the 3D compartment-scale model (left) and the 2D simulation Case IX (right).*

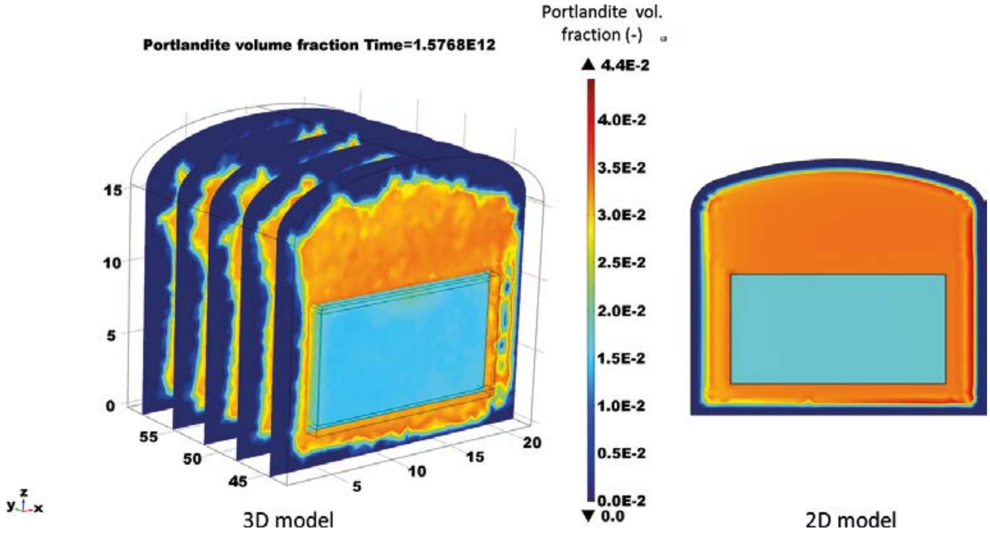

***Figure 6-16.** Portlandite volume fraction (–) after 50 000 years: comparison of the results of the 3D compartment-scale model (left) and the 2D simulation Case IX (right).*

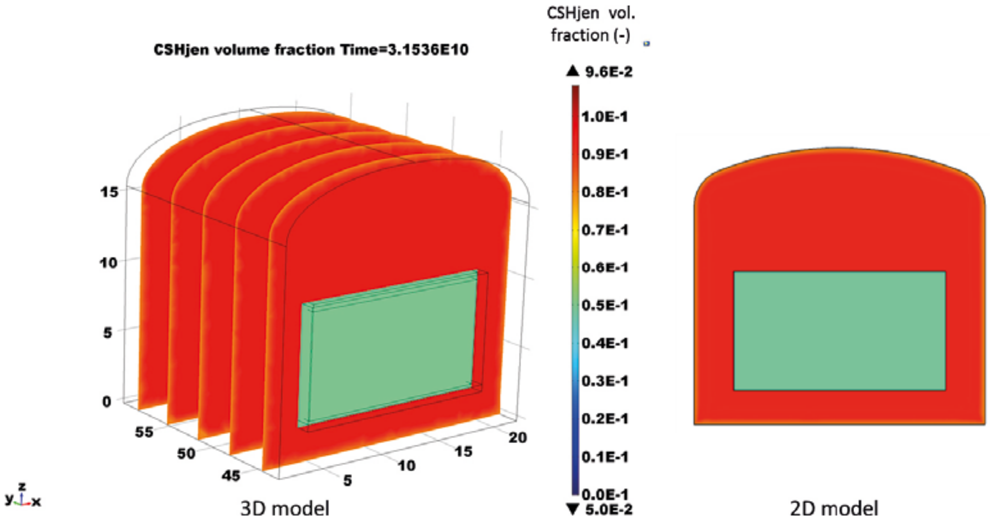

Figure 6-17. *Jennite-like C-S-H (CSHjen) volume fraction (–) after 1 000 years: comparison of the results of the 3D compartment-scale model (left) and the 2D simulation Case IX (right).*

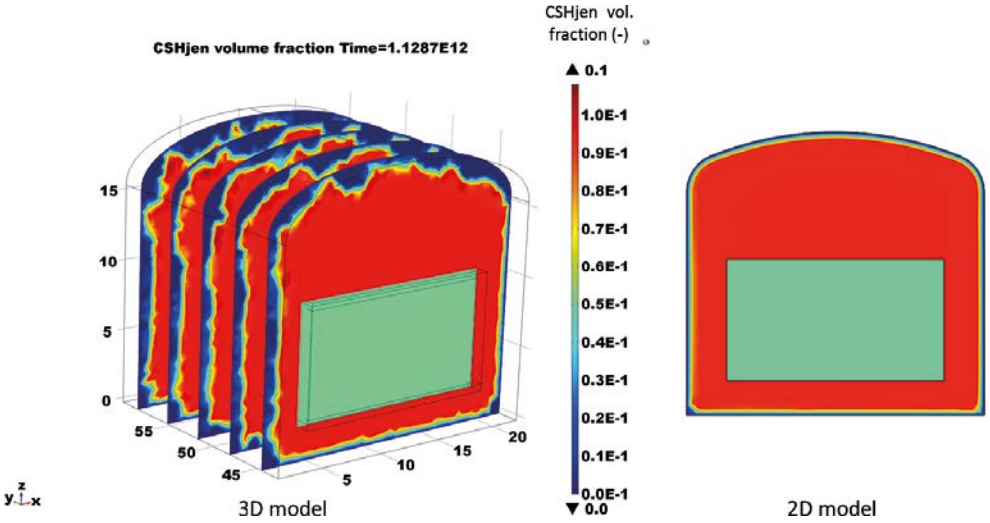

Figure 6-18. *Jennite-like C-S-H (CSHjen) volume fraction (–) after 36 000 years: comparison of the results of the 3D compartment-scale model (left) and the 2D simulation Case IX (right).*

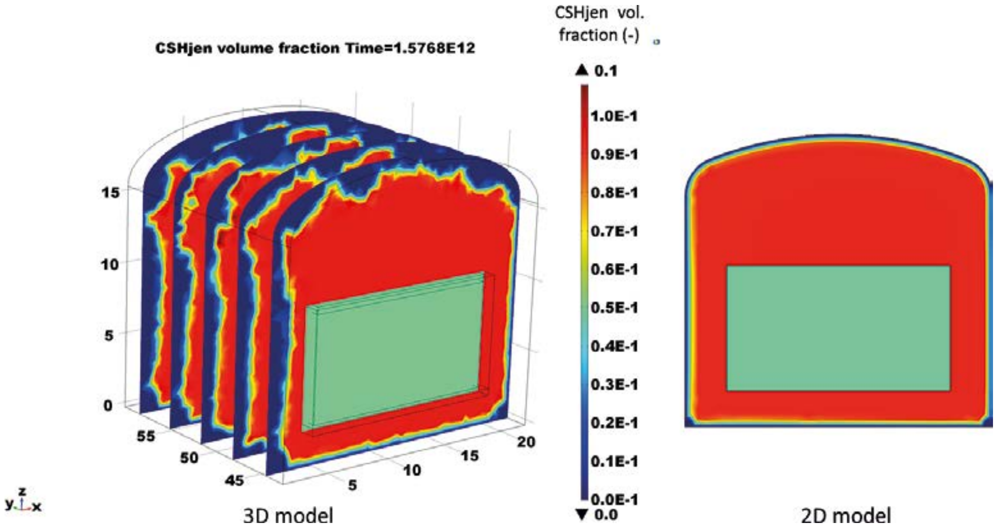

Figure 6-19. *Jennite-like C-S-H (CSHjen) volume fraction (–) after 50 000 years: comparison of the results of the 3D compartment-scale model (left) and the 2D simulation Case IX (right).*

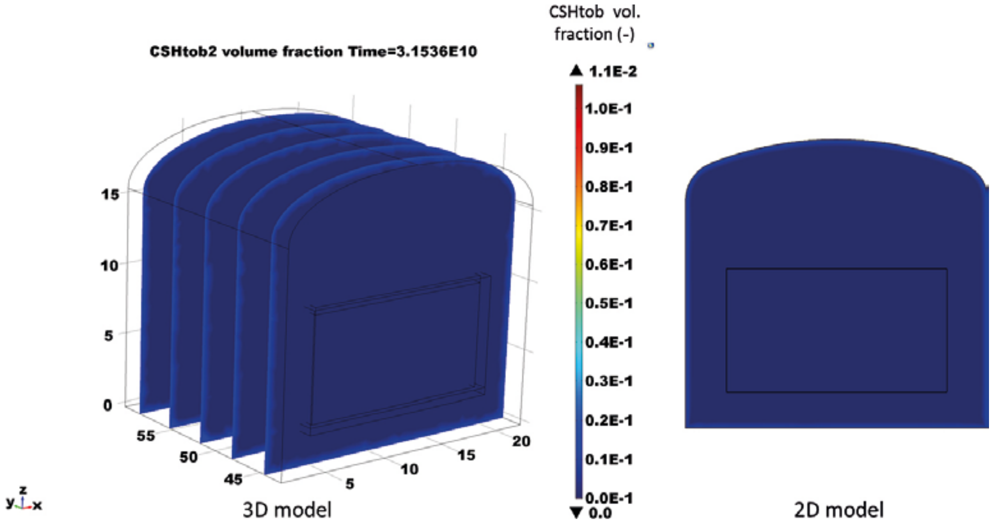

Figure 6-20. *Tobermorite-like C-S-H (CSHtob) volume fraction (–) after 1 000 years: comparison of the results of the 3D compartment-scale model (left) and the 2D simulation Case IX (right).*

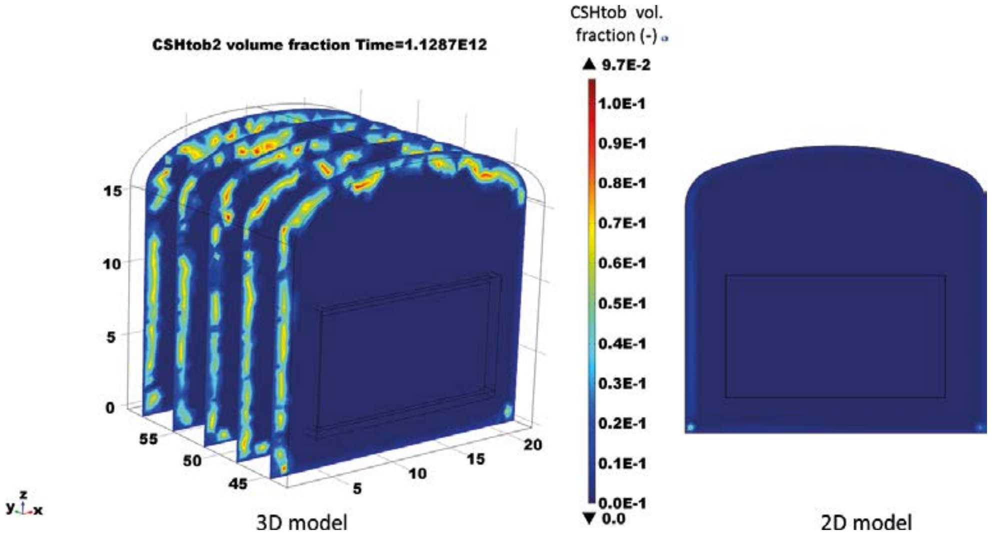

Figure 6-21. *Tobermorite-like C-S-H (CSHtob) volume fraction (–) after 36 000 years: comparison of the results of the 3D compartment-scale model (left) and the 2D simulation Case IX (right).*

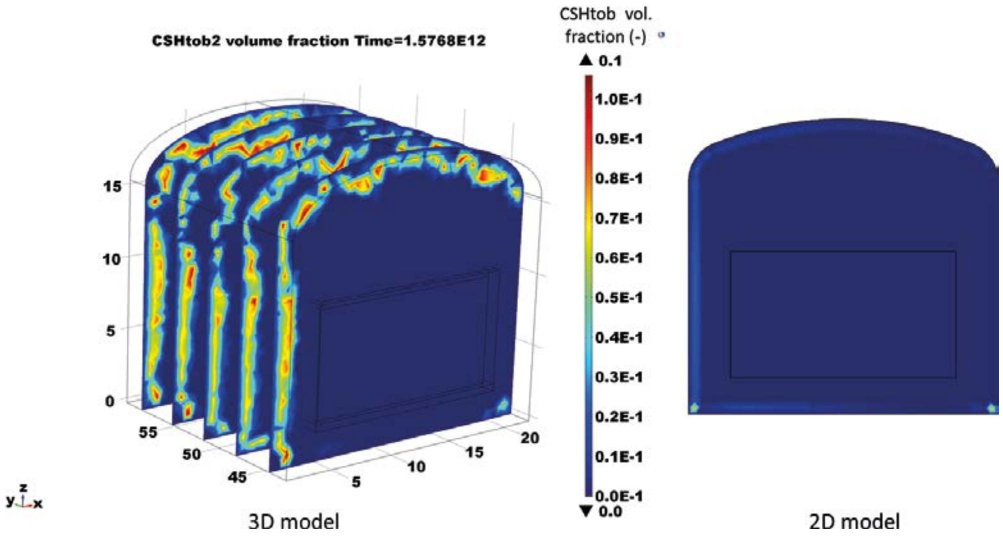

Figure 6-22. *Tobermorite-like C-S-H (CSHtob) volume fraction (–) after 50 000 years: comparison of the results of the 3D compartment-scale model (left) and the 2D simulation Case IX (right).*

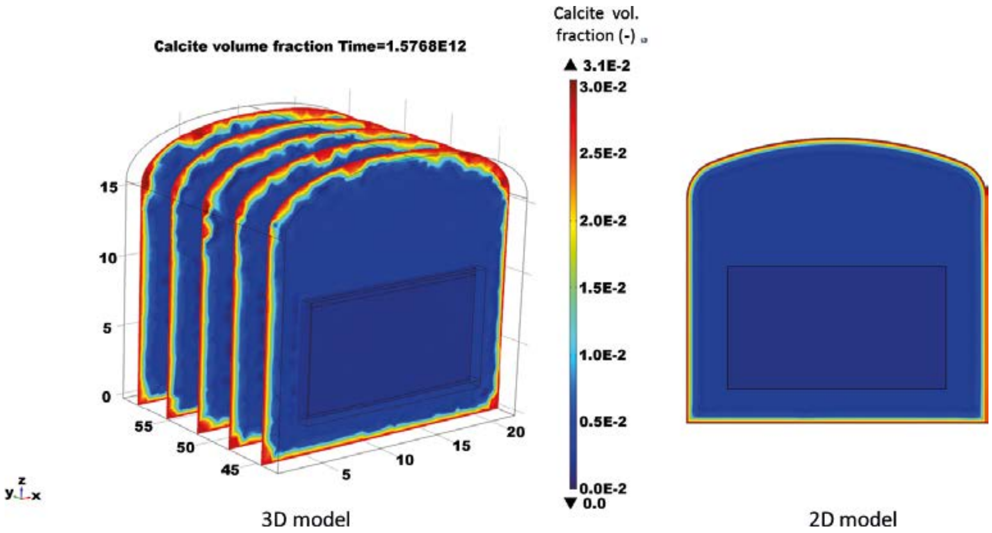

Figure 6-23. Calcite volume fraction (–) after 50 000 years: comparison of the results of the 3D compartment-scale model (left) and the 2D simulation Case IX (right).

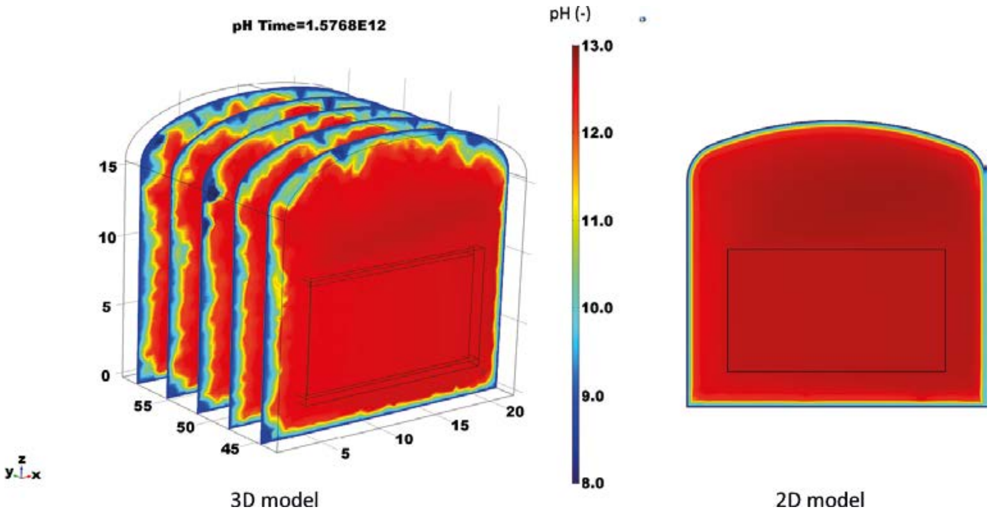

Figure 6-24. pH distribution after 50 000 years: comparison of the results of the 3D compartment-scale model (left) and the 2D simulation Case IX (right).

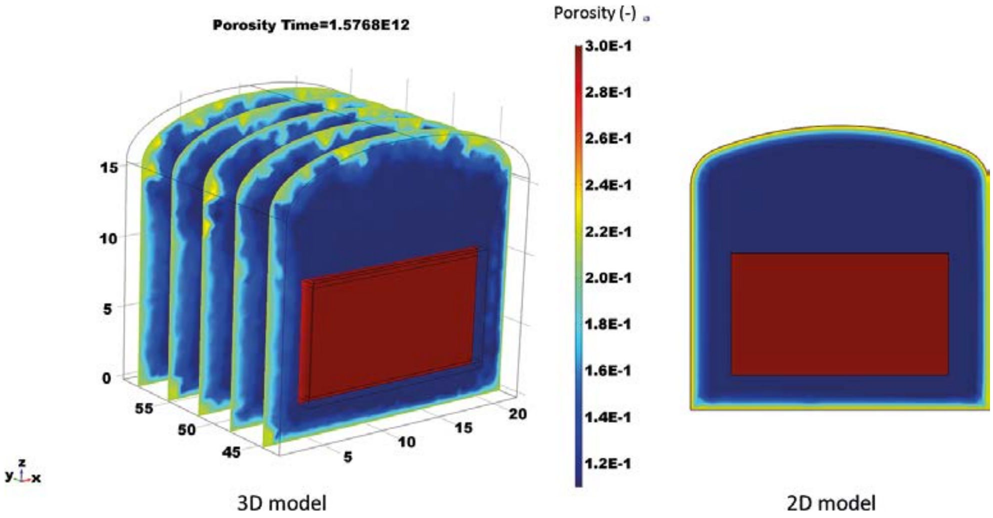

Figure 6-25. Porosity (–) after 50 000 years: comparison of the results of the 3D compartment-scale model (left) and the 2D simulation Case IX (right).

A more quantitative comparison between the 2D and the 3D concrete degradation models is presented in Figure 6-26 in terms of overall portlandite dissolution over time in the modelled domain (divided into concrete and waste domains). Results are presented in relative values (referred to the initial portlandite concentration in each modelled domain). It may be observed how portlandite is gradually dissolved and leached out of the system, with a higher rate in the 3D simulation case. This is due to the higher velocities, especially near the concrete outer boundary. After 50 000 years, around 43.5 % of the portlandite volume fraction has been leached out, which is almost twice the amount leached in the 2D model. Two distinct stages of portlandite dissolution can be observed. The first one has a very short duration and a high rate of portlandite dissolution. The second stage of degradation has a much lower dissolution rate. The first stage can be attributed to two factors: (1) the initially higher velocities near the boundary of the concrete backfill, which favour a faster degradation than the central part; and (2) a boundary effect caused by the fixed concentration boundary condition which leads to a faster dissolution at the boundary elements. Once portlandite is completely dissolved in these regions, dissolution continues in the rest of the domain, at a lower rate due to the lower velocities and to the reduced impact of the boundary conditions.

The heterogeneous degradation of concrete in the 3D compartment-scale model is also illustrated in Figure 6-27, where the portlandite concentration is presented at different times in a plane 50 cm away from the concrete/rock interface. After 200 years of interaction with groundwater, the degree of heterogeneity is still small. However, after 4 000 years the heterogeneity is significant. At the top of the plane, complete dissolution of portlandite is observed (in blue), which is due to the high velocity zones at the top of the compartment (Figure 6-11). This is followed by a zone of less degradation (in red), where the high velocity effects are not dominant. In fact, this zone with reduced portlandite dissolution coincides with the zone where water is outflowing from the concrete backfill towards the rock (Figure 6-13). In the middle zone of the plane, degradation is more extensive as a result of higher velocities. High velocities in this region are a consequence of the effect of the high permeability waste domain, as shown in Figure 6-11. In a similar way, the evolution of porosity over the same yz-plane is shown in Figure 6-28. Porosity increases in a heterogeneous fashion as a result of the dissolution of cement hydrates, especially near the concrete surface. The precipitation of calcite does not compensate the decrease in volume of the solid phases.

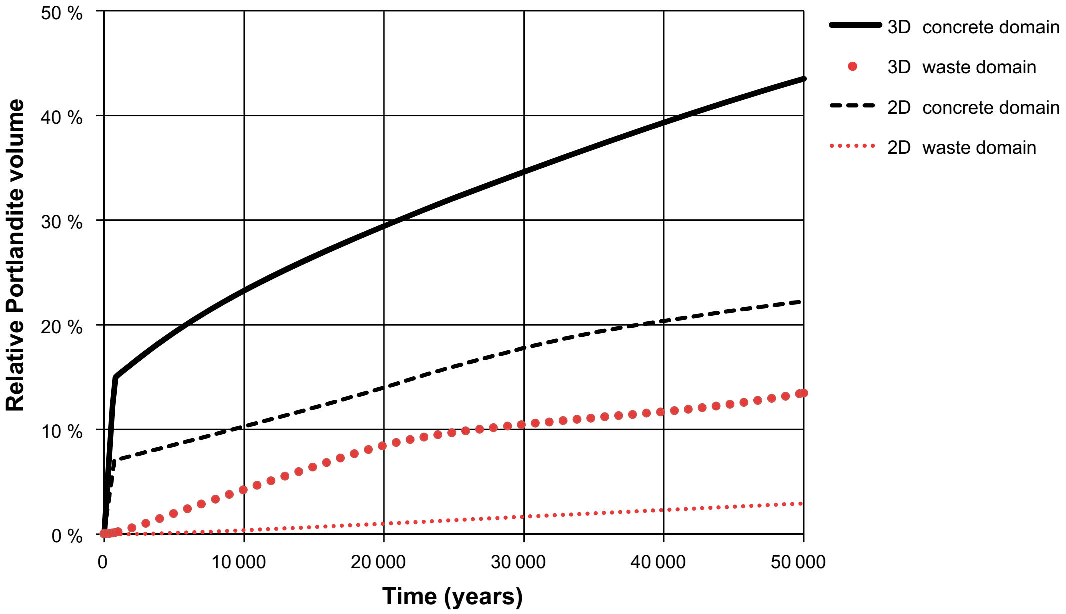

Figure 6-26. Evolution of the total portlandite volume relative to the initial amount in the concrete domain and the waste domain: comparison between the 3D model and the 2D model simulation Case IX. After 50 000 years, 43.5 % of the total portlandite in the concrete domain of the 3D model has been leached.

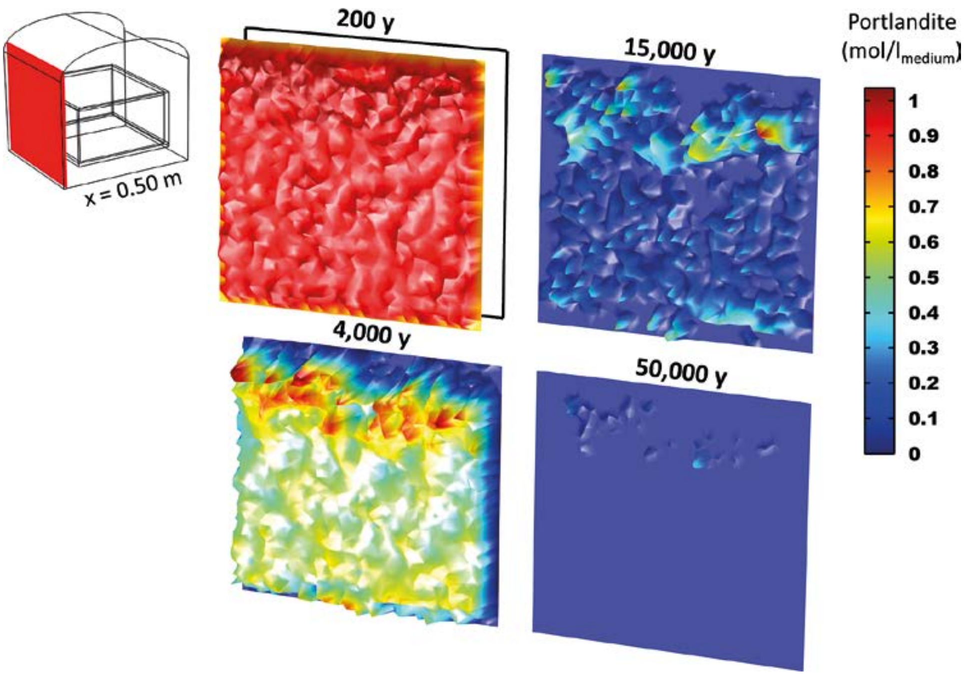

Figure 6-27. *Evolution of portlandite concentration (mol/l$_{medium}$) in the observation yz-plane (x = 0.50 m) at different times (200, 4 000, 15 000, and 50 000 years) for the 3D compartment-scale model.*

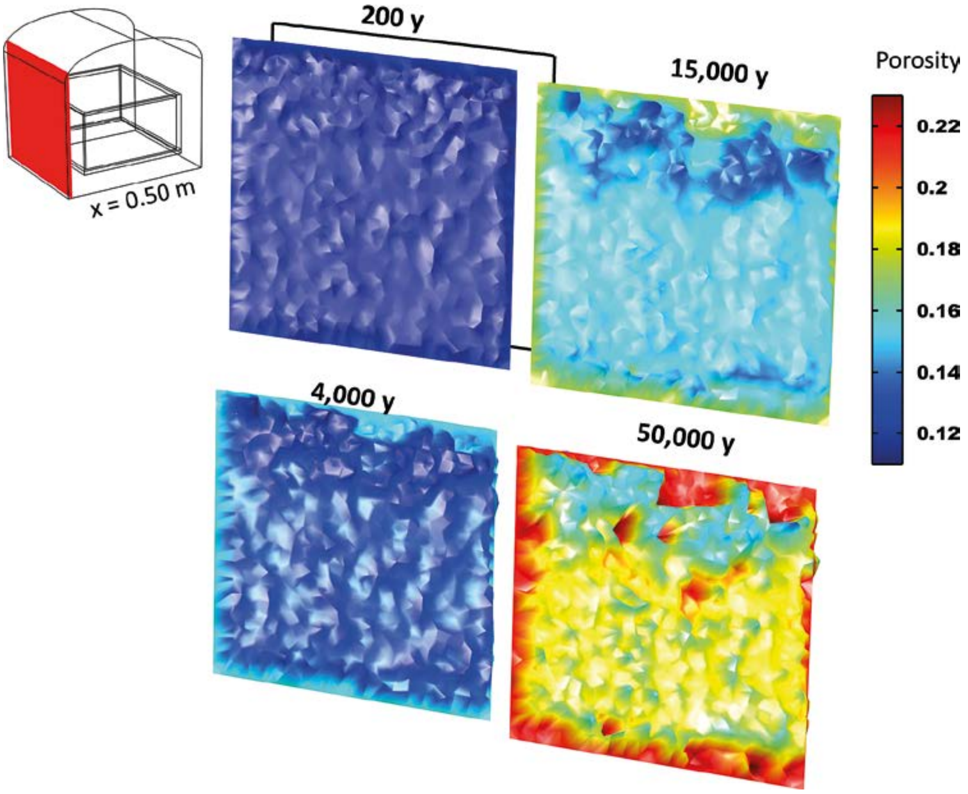

Figure 6-28. *Evolution of porosity (–) in the observation yz-plane (x = 0.50 m) at different times (200, 4 000, 15 000, and 50 000 years) for the 3D compartment-scale model.*

Figure 6-29 presents the degradation state of the concrete backfill after 50 000 years in terms of portlandite concentration. The surface presented (in grey) corresponds to the limit between a zero portlandite concentration (outside the surface) and higher values (inside the surface). The surface has an irregular shape, which is largely due to the effects of the velocity field, also presented in the figure. High velocity zones are related to complete depletion of portlandite.

Finally, a comparison of the results of the 3D and the 2D models in a 1D profile is presented in Figure 6-30 in terms of portlandite concentration, pH, and porosity after 50 000 years of degradation. The selected 1D profiles traverse the concrete and waste domains at mid-height and mid-width of the waste compartment (see Figure 5-7 and Figure 6-8 for the detail of the selected 1D profile in the 2D and 3D models, respectively). It may be clearly observed that the 3D model leads to a faster dissolution of portlandite compared to the 2D model, which is accompanied by a more significant increase in porosity and slightly lower pH values. The reason behind these differences is mainly related to the different velocity fields between the 2D and 3D simulations. Figure 6-11 clearly shows that already at time zero the Darcy velocity in some parts of the concrete rock interface is much higher than the average velocity. On the other hand, the 2D velocity distribution is much more uniform, as shown in Figure 5-5.

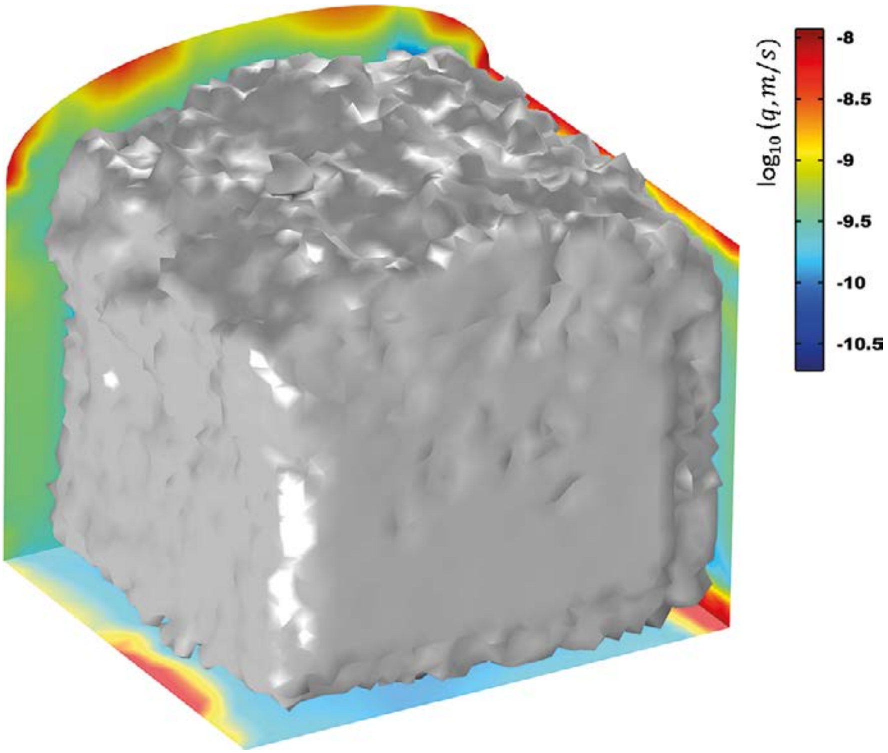

Figure 6-29. *Iso-surface (in grey) of constant zero portlandite volume fraction in the 3D compartment model after 50 000 years. Darcy velocity in the external surface of the concrete backfill presented as* $\log_{10}(q, m/s)$.

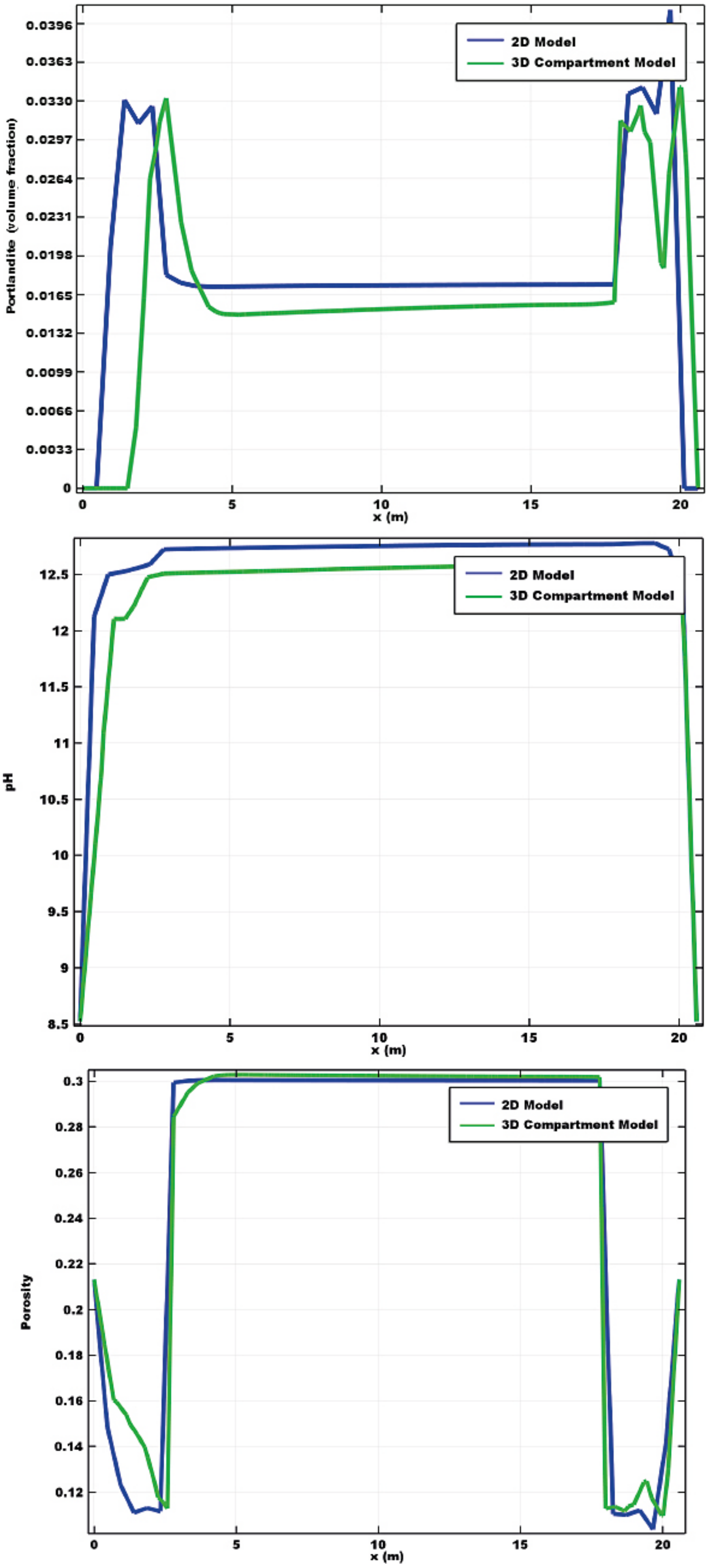

Figure 6-30. *Portlandite volume fraction (–), pH, and porosity (–) in the observation 1D profile (Figure 6-8) for the 3D compartment-scale model and comparison with the 1D profile (Figure 5-7) of the 2D simulation Case IX after 50 000 years.*

6.4 Results of vault-scale model

6.4.1 Velocity field

Four planes are selected along the BHK vault to illustrate Darcy velocity distribution in different cross-sections. Planes 1 to 3 cross through both concrete backfill and waste domains while plane number 4 contains only concrete. Flow arrows proportional to logarithmic values of Darcy velocities are shown in Figure 6-31. It is seen that at cross-section 4, which traverses only the concrete backfill, the velocity vectors are tangential to the plane, showing low values inside the concrete backfill, i.e. away from the concrete-rock interface. It is also observed that the velocity values are higher near the external boundary of the cross-section. Planes 1 to 3, which traverse the more permeable waste domains, show larger velocity values with significant 3D effects (significant axial velocity component) over the interior surface.

6.4.2 Concrete degradation

Degradation of the concrete in the entire BHK vault after 8 500 years is depicted in Figure 6-32 through Figure 6-35. Three cross-sectional xz-planes along the axis of the vault are shown, together with one horizontal xy-plane and one vertical yz-plane. Figure 6-32 shows that the concentration of portlandite is completely dissolved near the boundary of the concrete backfill. Heterogeneity effects are not significant after 8 500 years. The pH is presented in Figure 6-33, showing values near 12.10 in the regions of completely dissolved portlandite. It may also be observed that initial pH values of the porewater (around 13.1) have decreased to values around 12.8. Therefore, after 8 500 years, the alkalis have not yet been completely leached out from the BHK vault. Figure 6-34 depicts the porosity, which inversely correlates well with portlandite dissolution, showing values of up to 0.17, 50 % higher than the initial value of 0.11.

Finally, Figure 6-35 presents the iso-surface of zero portlandite concentration, which shows the incipient state of degradation after 8 500 years. The total volume of dissolved portlandite in the vault-scale model after 8 500 years is 23.6 % of the initial amount, slightly higher than the corresponding compartment-scale model value of 22.1 % after the same period of time.

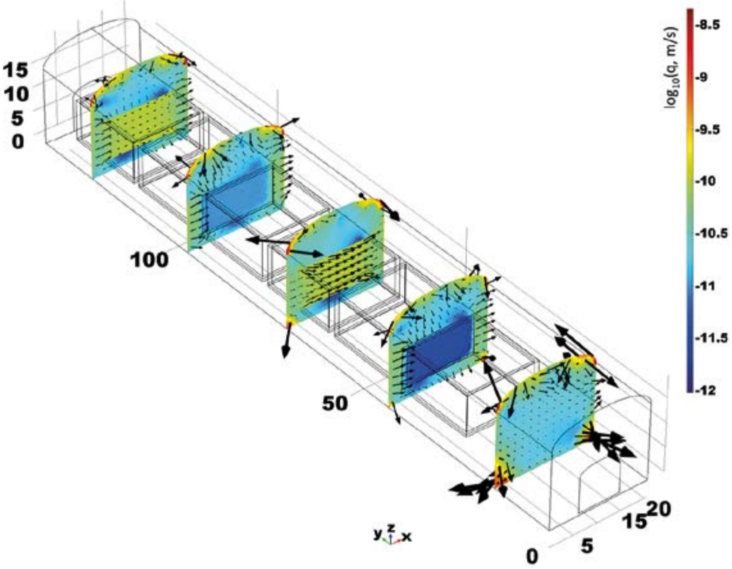

Figure 6-31. *Results of the 3D vault-scale model in 5 xz-planes (coloured by Darcy velocities in log scale): flow arrows proportional to logarithmic values of Darcy velocities in four xz-planes along the vault axis.*

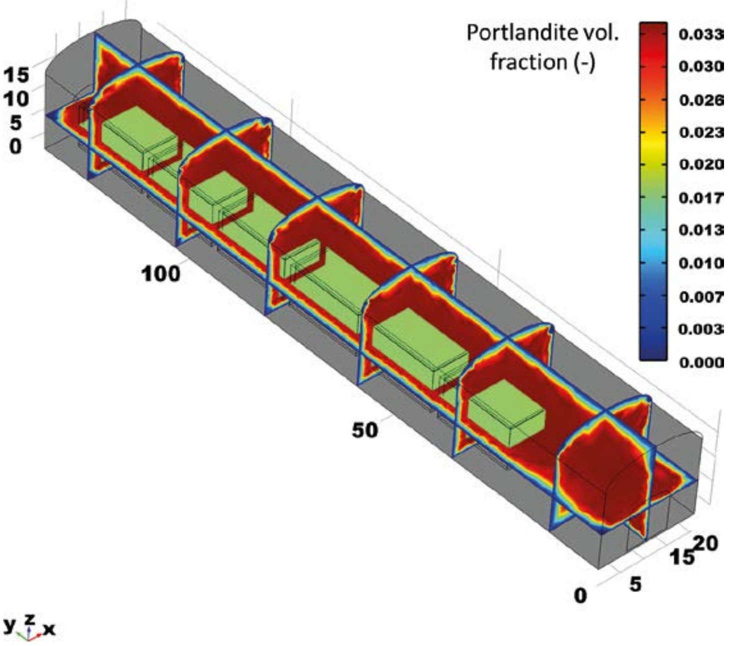

__Figure 6-32.__ Portlandite volume fraction (–) in x, y, and z slices of the 3D vault-scale domain after 8 500 years. Dimensions are in metres.

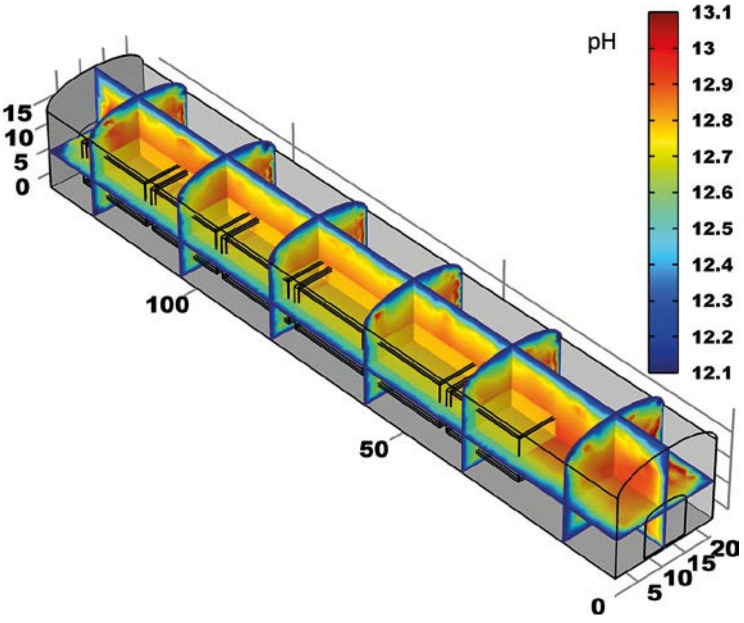

__Figure 6-33.__ pH values in x, y, and z slices of the 3D vault-scale domain after 8 500 years. Dimensions are in metres.

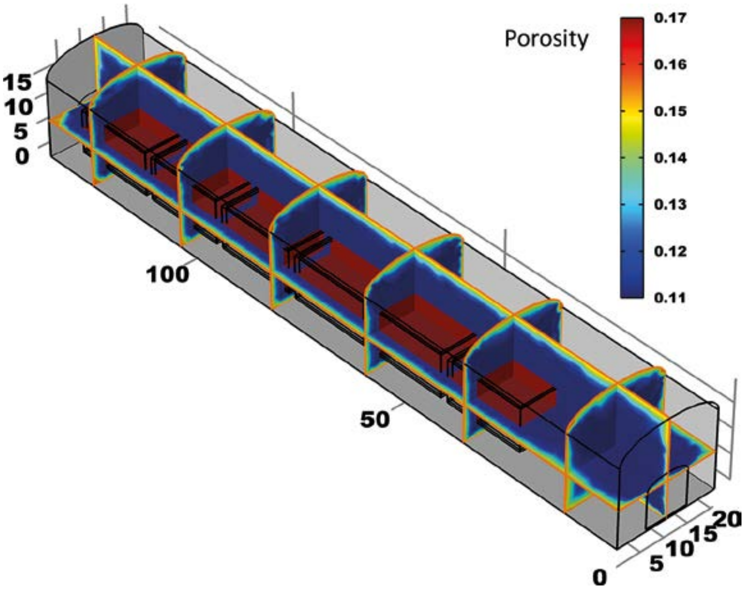

Figure 6-34. *Porosity values in x, y, and z slices of the 3D vault-scale domain after 8 500 years. Dimensions are in metres. Note that porosity of the waste domains is 0.30.*

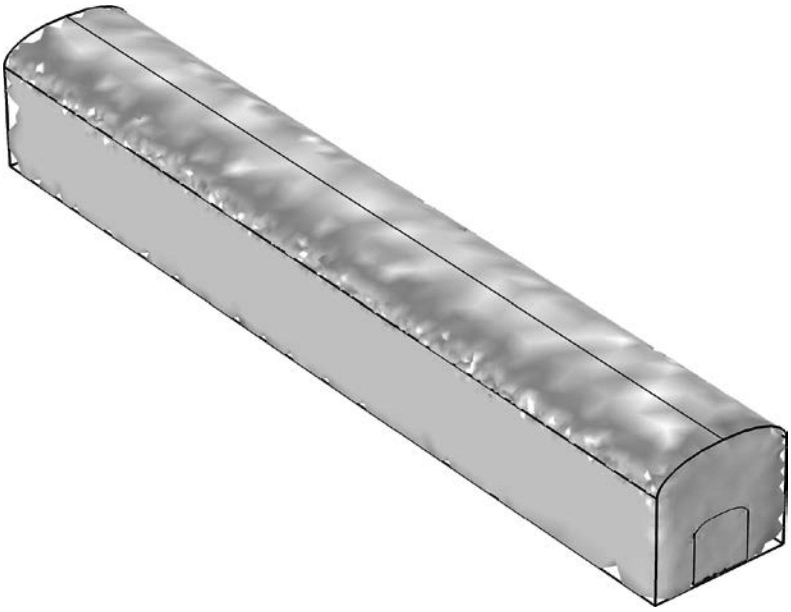

Figure 6-35. *Iso-surface of zero portlandite volume fraction in the 3D vault-scale domain after 8 500 years.*

6.5 Computational resources

Reactive transport simulations of 3D BHK vault-scale and compartment-scale models imply computationally-demanding calculations in terms of required number of processors for multi-thread purposes, memory space, and CPU time. The management strategy of the computational resources depends on the number of degrees of freedom (DOF) of the simulation. In the iCP modelling framework, the number of DOF is defined as a function of the number of:

- Nodes of the finite element mesh.
- Dependant variables (chemical elements).
- Coupled variables, e.g. porosity.
- Selected output.

The underlying finite element mesh used for flow and solute transport calculations, as well as the number of chemical elements (total concentrations) determine the number of DOF in Comsol Multiphysics. Furthermore, in iCP, additional information such as solid phase concentrations, saturation indices, and other user specified quantities can be written in the results file. This is set as "selected Output" in the input file. The larger the number of variables to be retrieved, the larger the number of DOF. Transient 3D simulations have 4/3 times more DOF compared to transient 2D calculations, for a given number of nodes. This is due to 3 spatial and 1 temporal independent variables for the 3D case, instead of 2 spatial and 1 temporal for 2D. As a general rule considering that the same finite element mesh is used for flow and solute transport, the number of DOF for each solver is obtained as:

$$No._{DOF} = No._{mesh\ nodes} \cdot (No._{chemical\ elements} + No._{coupled\ variables} + No._{selected\ output\ variables}) \cdot 4$$

This is directly related to the increased number of DOF when switching from 2D simulations to 3D. As the DOF increases the amount of memory that has to be allocated must be increased proportionally. The most common hurdle that occurs during the simulations is "out of memory" error message, which is denoted by:

"java.lang.OutOfMemoryError: Java heap space"

When iCP is launched, *java virtual machine* (JVM) takes control of running java applications and enhances communication with the physical machine, e.g. CPU, RAM, etc. At the JVM start-up, part of the physical memory is allocated for java execution requirements (Figure 6-36). Memory management is performed by JVM and it allocates new objects in the reserved memory space called *heap* while removing the old and unused objects through its *garbage collector*.

There are two main regions in java memory: heap and stack. Permanent generation is separate from java heap space and is allocated for permanent objects such as class definitions.

Heap size is initiated by specific JVM options, named *–Xms* and *–Xmx*, which set the starting and maximum size of the heap, repectively. Java stack space is used for thread execution, i.e. each thread in java contains its own stack which can be specified by JVM variable *–Xss*. Java stack space is used to store local variables while heap is used to store java objects. The error message related to full stack space is: "java.lang.StackOverFlowError". The theoritical maximum memory heap space in 32-bit and 64-bit machines are 2^{32} (4G) and 2^{64}, respectively.

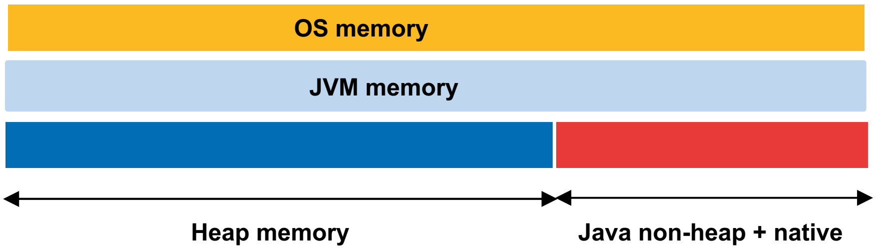

Figure 6-36. *Schematic representation of the management of memory resources. OS: Operating System; JVM: java virtual machine.*

The CPU time needed for the complete simulation time of the 3D models is the following:

- Compartment-scale model: ~15 days for 50 000 years of simulation (i.e. an average of 3 minutes per time step) in a computer with 12 processors of 3.3 GHz and 64 Gb of RAM
- Vault-scale model: ~19 days for 8 500 years of simulation (i.e. an average of 32 minutes per time step) in an in-house workstation of 2 CPU of 2.3 GHz Xeon Haswell E5-2650 V3, 25 Mb cache and 9.6 GT/s and a total of 40 processors, 128 Gb memory DDR4/2133 Mhz ECC Reg.
- These CPU times are respectively 17 times and 104 times higher than the time needed to solve the 2D simulation Case IX for 50 000 and 8 500 years, respectively.

6.6 Concluding remarks

Two 3D reactive transport models of degrading concrete in the BHK vault have been implemented using iCP (Nardi et al. 2014). One model describes concrete degradation of a single compartment of the vault, while the other includes the entire vault geometry. The setup of the models follows that of Case IX of the 2D model presented in Section 5. Coupling between physical and chemical processes has been explicitly taken into account. In particular, hydraulic conductivities and diffusion coefficients have been updated as a function of dissolution/precipitation processes, ultimately modifying the physical porosity of the system.

The feasibility of implementing and solving large-scale 3D reactive transport models of concrete degradation using iCP has been successfully proven. The 3D compartment-scale model has been solved for 50 000 years of simulation time in a finite element mesh of 184 561 elements, while the vault-scale model used a finite element mesh of 777 161 elements and was solved for 8 500 years. The CPU time needed for these simulations has been significantly higher than the time needed for the 2D cases solved on a mesh of 5 168 elements (2 891 elements in reactive domains). Calculation times for the 3D models have been 17 and 104 times greater for the compartment- and vault-scale models, respectively.

Concrete degradation in the 3D models follows a similar sequence and is governed by the same processes. Comparison of the 3D compartment-scale model with the 2D model and the 3D vault-scale model indicates a faster degradation in the 3D models. These different rates of degradation are due to the different velocity fields used in the 2D and 3D simulations. While in the 2D cases an average velocity of 1×10^{-11} m/s was derived from the work by Abarca et al. (2016), in the 3D simulations heterogeneous velocity fields were calculated directly in the model using the pressure field imported from the same work (Abarca et al. 2016). As a result, relatively higher velocities were used in the 3D simulations, ultimately leading to an increased degradation rate and almost doubling the amount of dissolved portlandite of the 2D model. This underlines the difficulty of selecting a representative velocity value for 1D (Pękala et al. 2015) or 2D reactive transport simulations (Section 5). The use of 3D models makes it easier to implement more realistic velocity fields, which have a significant impact on the degradation kinetics. This is one of the main benefits of performing a 3D simulation of the BHK vault with respect to the 2D model of a typical cross-section. In this regard, sensitivity cases using the 2D models presented in Section 5 with different values of the Darcy velocity could be used to overcome this drawback of the 2D simulations.

The results obtained with the 3D models show that in the particular case of the BHK vault, little impact of the reactive transport processes can be expected in the axial direction. This is not very surprising if one considers that the axial dimension is much larger than the cross-sectional dimensions, and that groundwater flow in the different compartments is very similar and has generally small axial components.

7 Summary and conclusions

In this study, reactive transport models of concrete degradation have been implemented in iCP. The goal has been to investigate the long-term chemically-driven degradation of concrete under in-situ conditions for the proposed repository concept for SFL.

First, a benchmark study has been conducted between the reactive transport codes PHAST and iCP. A 2D reactive transport model of the 2BMA vault of the SFR repository extension has been used to this end. The comparison shows that concrete degradation processes can be modelled in an equivalent manner using both codes. However, iCP is well suited to include additional coupled processes in the simulation, such as the feedback between porosity and physical properties, or even mechanical processes. More details are presented in Section 4.4.

Degradation of concrete in the SFL repository has first been studied using a 2D reactive transport model of a cross-section of the BHK vault. Several simulation cases considering different assumptions and simplifications have been carried out. In summary, the main concrete degradation process is driven by leaching of calcium which leads to gradual dissolution of the main the cement hydrates. The rate of this degradation process is shown to be low even after 100 000 years in all the simulation cases considered. This is due to the relatively small flow of water into the repository, together with a low initial diffusion coefficient of the concrete backfill. More details are presented in Section 5.4.

Concrete degradation has also been simulated using 3D reactive transport models at the compartment-scale and at the entire vault-scale. The feasibility of performing large-scale reactive transport simulations over a 3D domain has been successfully proven. To this end, proper management of computational resources has been crucial. Overall, the results compare relatively well with the respective 2D model (Case IX). However, due to higher and heterogeneous Darcy velocities in the 3D models compared to the 2D case, faster chemical degradation is predicted. After 50 000 years, portlandite dissolution is faster in the compartment-scale model, by a factor of two, compared to the corresponding 2D model. The compartment- and vault-scale models lead to similar conclusions. Given the small differences in the velocity fields of the different compartments, degradation of concrete is predicted to occur in a similar way using both 3D models. More details are presented in Section 6.6.

The conclusions of this study are based on predictions of several simulations made with a reactive transport model encompassing chemical reactions, groundwater flow, and solute transport. The effect of chemically-driven concrete degradation on the mechanical stability of the repository has therefore not been assessed. This could be an important aspect to be included in future work, especially in the cases where an initially heterogeneous state of the concrete backfill is assumed. In such a case, a severe degradation of the entire volume of the concrete backfill walls could potentially lead to mechanical instabilities.

References

SKB's (Svensk Kärnbränslehantering AB) publications can be found at www.skb.com/publications. SKBdoc documents will be submitted upon request to document@skb.se.

Abarca E, Idiart A, de Vries L M, Silva O, Molinero J, von Schenck H, 2013. Flow modelling on the repository scale for the safety assessment SR-PSU. SKB TR-13-08, Svensk Kärnbränslehantering AB.

Abarca E, Sampietro D, Miret M, von Schenck H, 2016. Initial modelling of the near-field hydrogeology. Exploring the influence of host rock characteristics and barrier properties. Report for the safety evaluation SE-SFL. SKB R-16-02, Svensk Kärnbränslehantering AB.

Carman P, 1937. Fluid flow through a granular bed. Transactions of the Institution of Chemical Engineers 15, 150–167.

Elfwing M, Evins L Z, Gontier M, Grahm P, Mårtensson P, Tunbrant S, 2013. SFL concept study. Main report. SKB TR-13-14, Svensk Kärnbränslehantering AB.

Gimeno M J, Auqué L F, Gómez J B, Salas J, Molinero J, 2010. Hydrogeochemical evolution of the Laxemar Site. SKB R-10-60, Svensk Kärnbränslehantering AB.

Grahm P, Luterkort D, Mårtensson P, Nilsson F, Nyblad B, Oxfall M, Stojanovic B, 2013. SFL Concept study. Technical design and evaluation of potential repository concepts for long-lived low and intermediate level waste. SKB R-13-24, Svensk Kärnbränslehantering AB.

Höglund L O, 2014. The impact of concrete degradation on the BMA barrier functions. SKB R-13-40, Svensk Kärnbränslehantering AB.

Jacques D, 2009. Benchmarking of the cement model and detrimental chemical reactions including temperature dependent parameters. Project near surface disposal of category A waste at Dessel. NIROND-TR 2008–30 E, ONDRAF/NIRAS, Belgium.

Knudby C, Carrera J, 2005. On the relationship between indicators of geostatistical, flow and transport connectivity. Advances in Water Resources 28, 405–421.

Lagerblad B, Trägårdh J, 1994. Conceptual model for concrete long time degradation in a deep nuclear waste repository. SKB TR 95-21, Svensk Kärnbränslehantering AB.

Lothenbach B, Matschei T, Möschner G, Glasser F P, 2008. Thermodynamic modelling of the effect of temperature on the hydration and porosity of Portland cement. Cement and Concrete Research 38, 1–18.

Nardi A, Idiart A, Trinchero P, de Vries L M, Molinero J, 2014. Interface COMSOL-PHREEQC (iCP), an efficient numerical framework for the solution of coupled multiphysics and geochemistry. Computers & Geosciences 69, 10–21.

Parkhurst D L, Kipp K L, Charlton S R, 2010. PHAST version 2: a program for simulating ground-water flow, solute transport, and multicomponent geochemical reactions. Techniques and Methods 6–A35, U.S. Geological Survey, Denver, Colorado.

Pękala M, Olmeda J, Grivé M, Bruno J, 2015. Assessment of redox state and its impact on the solubility and speciation of selected radionuclides in the SFL repository. Final report. Amphos 21. SKBdoc 1533627 ver 1.0, Svensk Kärnbränslehantering AB.

Remy N, 2004. S-GeMS: The Stanford Geostatistical Modeling Software: a tool for new algorithms development. Geostatistics Banff 2004, Vol. 14 of the series Quantitative Geology and Geostatistics, 865–871. Available at: http://sgems.sourceforge.net/

Simpson M J, Clement T P, 2003. Comparison of finite difference and finite element solutions to the variably saturated flow equation. Journal of Hydrology 270, 49–64.

SKB, 2015. Safety analysis for SFR Long-term safety. Main report for the safety assessment SR-PSU. Revised edition. SKB TR-14-01, Svensk kärnbränslehantering AB.

van Genuchten M T, 1982. A comparison of numerical solutions of the one-dimensional unsaturated–saturated flow and mass transport equations. Advances in Water Resources 5, 47–55.

Appendix A

Saturation indices for groundwaters

Saturation indices of the minerals for the groundwater composition used for the 2BMA benchmark simulations are given in the table below, together with the equilibrium constant of the mineral (log K) and its chemical formula.

Mineral	Saturation indexes	log K	Chemical formula
$(CaO)_3CaCl_2{:}15H_2O$	–129.11	71.25	(CaO)3CaCl2:15H2O
AFm	–33.36	–29.43	Ca4Al2SO4(OH)12:6H2O
Brucite	–5.41	16.79	Mg(OH)2
C_3AH_6(C)	–33.5	–22.54	Ca3Al2(OH)12
Calcite	0.02	–8.47	CaCO3
$CaOCaCl_2{:}2H_2O$	–50.86	25.49	CaOCaCl2:2H2O
CH	–11.15	22.9	Ca(OH)2
$CSH_{0.8}$	–5.7	11.08	Ca0.8SiO2.8:H2O
$CSH_{1.1}$	–7.82	16.72	Ca1.1SiO3.1:H2O
$CSH_{1.8}$	–15.57	32.7	Ca1.8SiO3.8:H2O
Ettr_GCA	–31.38	–44.9	Ca6Al2(SO4)3(OH)12:26H2O
Fried$_{0.86}$Al$_{5.14}$OH	–36.56	–24.45	Ca4Al0.86Cl2(OH)8.58
Fried$_{0.88}$Al$_{5.12}$OH	–37.08	–24	Ca4Al0.88Cl2(OH)8.64
Fried$_{1.04}$Al$_{4.96}$OH	–38.05	–23.61	Ca4Al1.04Cl2(OH)9.12
Fried$_{1.34}$Al$_{4.66}$OH	–38.99	–23.77	Ca4Al1.34Cl2(OH)10.02
Fried$_{1.42}$Al$_{4.58}$OH	–39.18	–23.88	Ca4Al1.42Cl2(OH)10.26
Fried$_{1.96}$Al$_{4.04}$OH	–39.78	–25.24	Ca4Al1.96Cl2(OH)11.88
Friedelsalt	–38.08	–27.09	Ca4Al2Cl2(OH)12
Gypsum_Cem	–2.15	–4.6	CaSO4:2H2O
Hemicarboaluminate	–29.71	–22.44	Ca3Al2O6.5C0.5(OH):11.5H2O
Monocarboaluminate	–33	–31.5	(CaO)3Al2O3CaCO3:11H2O
SiO_2gel(am)	–1.17	–2.85	SiO2
Syngenite	–10.82	–7.48	CaK2(SO4)2:H2O
Thaumasite	–13.44	–49.36	(CaSiO3)2(CaSO4)2(CaCO3)2(H2O)30

In turn, saturation indices for meteoric groundwater composition used in the BHK vault simulations are given in the table below, together with the equilibrium constant of the mineral (log K) and its chemical formula.

Mineral	**Saturation indexes**	**log K**	**Chemical formula**
$Al(OH)_3$am	–1.02	0.24	Al(OH)3
Anhydrite	–2.71	–4.36	CaSO4
Brucite	–3.56	16.84	Mg(OH)2
C_2AH_8	–16.35	–13.56	Ca2Al2(OH)10:3H2O
C_4AH_{13}	–32.85	–25.4	Ca4Al2(OH)14:6H2O
CAH_{10}	–8.24	–7.49	CaAl2(OH)8:6H2O
Calcite	0.12	1.85	CaCO3
CSHjen	–10.15	–13.16	(CaO)1.666667(SiO2)(H2O)2.1
CSHtob$_1$	–8.41	–19.2	(CaO)2(SiO2)2.4(H2O)3.2
CSHtob$_2$	–3.5	–8	(CaO)0.83333(SiO2)(H2O)1.3333
Ettringite	–20.43	–44.84	Ca6Al2(SO4)3(OH)12:26H2O
Gypsum	–2.48	–4.58	CaSO4:2H2O
Hemicarboaluminate	–26.22	–29.12	Ca4Al2(CO3)0.5(OH)13:5.5H2O
HydrogarnetOH	–23.24	–20.84	Ca3Al2(OH)12
HydrogarnetSi	–13.97	–29.87	Ca3Al2(SiO4)0.8(OH)8.8
HydrotalciteC	–3.5	–51.14	Mg4Al2(OH)12CO3:3H2O
HydrotalciteOH	–4.43	–56.02	Mg4Al2(OH)14:3H2O
Monocarboaluminate	–20.98	–31.46	Ca4Al2(CO3)(OH)12:5H2O
Monosulfoaluminate	–21.91	–29.24	Ca4Al2(SO4)(OH)12:6H2O
Portlandite	–8.98	22.81	Ca(OH)2
SiO_2am	–1.17	1.48	SiO2
Stratlingite	–9.9	–19.7	Ca2Al2SiO2(OH)10:3H2O
Syngenite	–11.8	–7.2	K2Ca(SO4)2H2O
Thaumasite	–9.22	–49.36	(CaSiO3)2(CaSO4)2(CaCO3)2(H2O)30
Tricarboaluminate	–22.69	–46.48	Ca6Al2(CO3)3(OH)12:26H2O

Appendix B

Finite differences vs. finite elements

Discrepancies between PHAST and iCP Darcy velocities arise from the difference between the numerical methods that are applied. PHAST has been developed based on finite difference method while iCP uses Comsol for solving flow and transport which is based on the finite element method.

Both Dirichlet and Neumann boundary conditions are imposed for simulating the Darcy flow field. Dirichlet nodes occur when a prescribed hydraulic head is set at the right boundary of the domain. Along the left boundary, Neumann nodes occur where normal flux of groundwater is imposed. The Dirichlet boundary conditions are implemented identically in both methods. However, this is not the case for the implementation of Neumann boundary conditions. At the left boundary node where flux is known, Neumann boundary condition is incorporated into a finite difference algorithm by writing the discrete form of the Darcy law. To treat Neumann boundary condition accurately with a higher discretization order, ghost points are introduced outside the domain next to the boundary.

In finite elements, however, specified Neumann boundary condition is incorporated directly into the flux vector, which results from Galerkin method and integration by parts of the transient Darcy equation at the element level. The approach is summarized below. The transient Darcy equation in 2D is written as:

$$S_s \frac{\partial h}{\partial t} = \frac{\partial}{\partial x}\left(K \frac{\partial h}{\partial x}\right) + \frac{\partial}{\partial y}\left(K \frac{\partial h}{\partial y}\right) \qquad \text{(B-1)}$$

At the left boundary, flux of groundwater is imposed:

$$q_x n_x + q_y n_y = -q_s \qquad \text{(B-2)}$$

Using the shape function N_i for interpolation of hydraulic head inside a finite element and Galerkin method, the original Darcy equation can be written as given below:

$$\int_V \left(\frac{\partial q_x}{\partial x} + \frac{\partial q_y}{\partial x} + S_s \frac{\partial h}{\partial t}\right) N_i dV = 0 \qquad \text{(B-3)}$$

Applying the divergence theorem on the first two terms results in:

$$\int_V S_s \frac{\partial h}{\partial t} N_i dV - \int_V \left[\frac{\partial N_i}{\partial x} \; \frac{\partial N_i}{\partial y}\right] \{q\} dV = -\int_S \{q\}^T \{n\} N_i dS \qquad \text{(B-4)}$$

$$\{q\}^T = \{q_x \; q_y\} \qquad \{n\}^T = \{n_x \; n_y\} \qquad \text{(B-5)}$$

where {n} is the outer normal vector to the left boundary. The Neumann boundary condition is replaced by the term on the right hand side of the equation above.

Therefore, finite difference and finite element methods result in different expressions at Neumann boundary nodes. In fact, comparisons of finite element and finite difference solutions in 2D flow equations have previously demonstrated that both methods mainly differ in how they spatially average variable material properties and how they treat Neumann boundary conditions (van Genuchten 1982, Simpson and Clement 2003). This difference can be eliminated with high resolution discretization in a 1D problem. However, the finite difference solution for a given discretization can introduce a numerical error in 2D problems.

Appendix C

Selected results from R-13-40

Some of the results of the Large20a (simulation of 2BMA concrete degradation) as taken from the report of Höglund (2014) are presented in the following figures, for visual comparison with the results presented in Section 4.

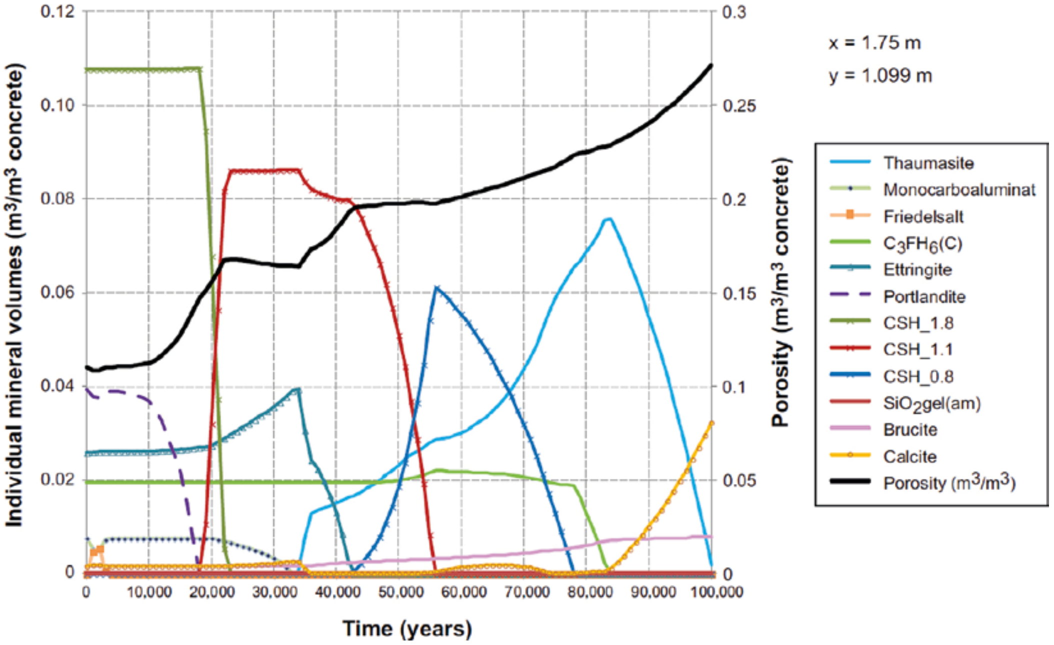

Figure C-1. PHAST results for case Large20a (from Höglund 2014): Temporal evolution of mineral phases at observation point GH (x = 1.75, y = 1.85).

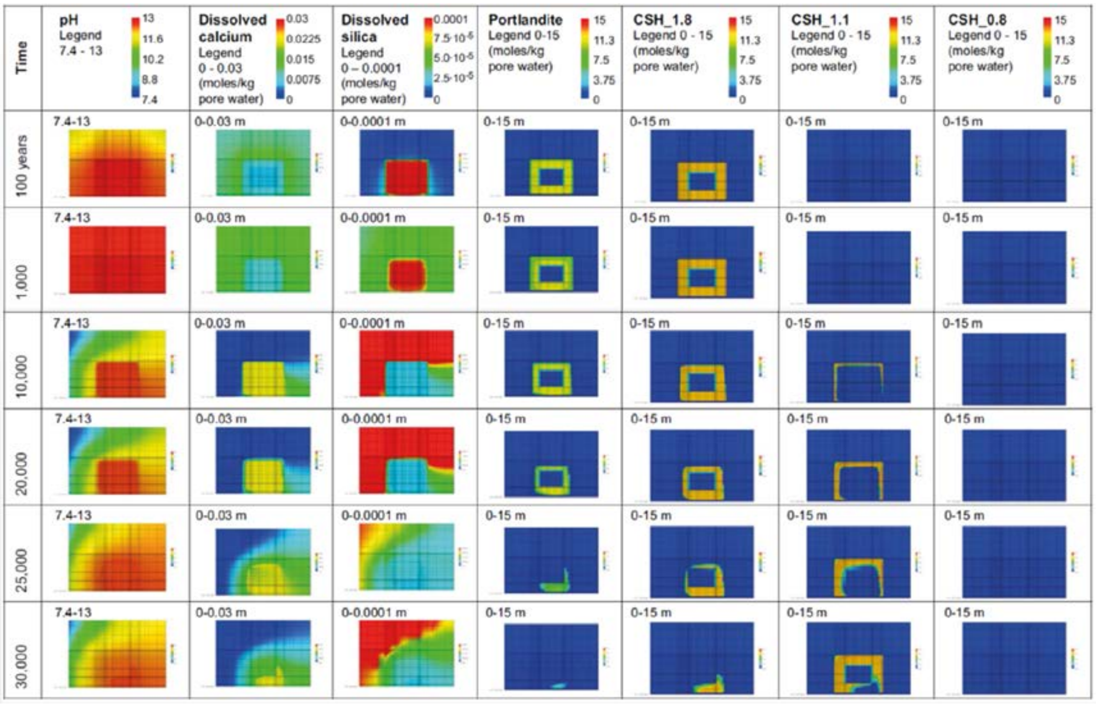

Figure C-2. PHAST results for case Large20a (from Höglund 2014) in the modelled domain at different times: Distribution of some mineral phases (portlandite and C-S-H phases), pH, and calcium and silica in aqueous solution.

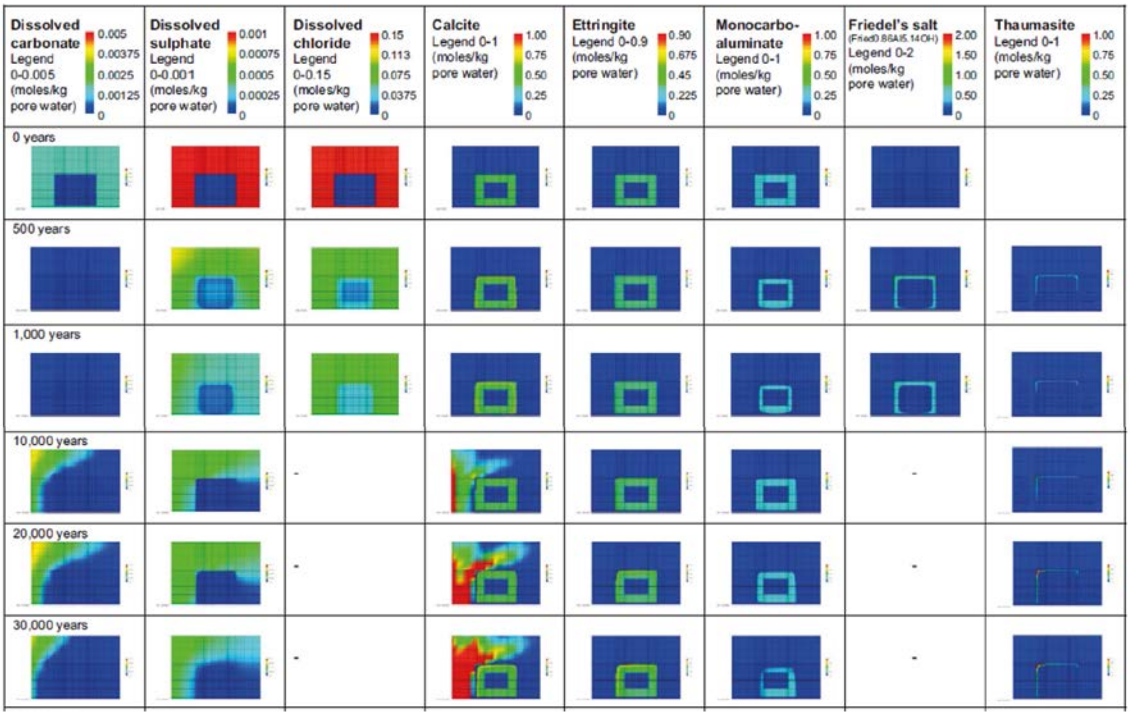

Figure C-3. *PHAST results for case Large20a (from Höglund 2014) in the modelled domain at different times: Distribution of some mineral phases (calcite, ettringite, monocarboaluminate, Friedel's salt, and thaumasite), and carbonate, sulphate, and chloride in aqueous solution.*

Appendix D

1D reactive transport benchmark

This section presents the setup and results of an additional benchmark in 1D using PHAST and iCP. The objective is to increase the confidence in the use of iCP to solve similar reactive transport problems as PHAST. The model considers a 1D representation of the concrete wall of the 2BMA, i.e. a 0.5 m thick concrete wall. The chemical setup is exactly the same as that used for concrete in the 2D benchmark (Section 4), i.e. concrete composition given in Table 4-6 and MintqCem thermodynamic database. The incoming groundwater composition is also the same as the 2D benchmark, and is given in Table 3-3.

In order to simplify the 1D benchmark, the hydraulic boundary conditions and the material properties (diffusivity and permeability) are considered as constant throughout the simulation.

A horizontal groundwater flow is considered entering from the left, with a Darcy flux of 5.0×10^{-11} m/s. For solute transport, an open boundary condition is set on the left boundary while the right boundary is set as outflow.

The 50 cm thick concrete wall is discretized into 25 cells/finite elements with a size of 2 cm in both PHAST and iCP. The material properties considered in the simulations correspond to the concrete values in Table 4-1 between 100 and 10 000 years, with a porosity of 0.11. In both calculations, a hydrodynamic dispersivity of 1×10^{-11} m has been assumed, as in the 2D benchmark. The spatial discretization and material properties yield maximum theoretical time step sizes of 1.4 and 63.4 years according to Courant and Von Neumann criterions, respectively (Table D-1). In order to comply with both criteria, a time step size for the operator splitting of 1 year has been considered in PHAST and iCP. A total simulation time of 17 500 years has been considered in both cases. After this degradation time, complete dissolution of portlandite is predicted over a thickness of 30 cm. Furthermore, C-S-H gel is significantly leached, with dissolution of CSH-1.8 and then of CSH-1.1, giving rise to CSH-0.8 formation. Once an incipient precipitation of CSH-0.8 was predicted in both cases, the simulations were stopped and the results compared.

Table D-1. Maximum theoretical time-step according to Von Neumann (Equation 1) and Courant (Equation 2) criterions for the given spatial discretization and material properties.

Criterion	Maximum time step (years)
Courant	1.4
Von Neumann	63.4

The PHAST and iCP simulations have been set using exactly the same spatial and temporal discretization, using the same material properties, and initial and boundary conditions for flow and chemical composition.

The same numerical setup is used for time and space differencing between the PHAST 1D case presented here and the PHAST 2D simulations in Section 4. For space differencing, upstream-in-space is used, while for time, a backward-in-time (i.e. fully implicit) scheme is used. This choice minimizes the risk of numerical oscillations, which may lead to erroneous balances. These oscillations may result in negative concentrations, which would be balanced by excess positive concentrations in PHAST (for more details, see Parkhurst et al. 2010).

The use of upstream-in-space differencing introduces a spatial numerical dispersion, D_{ns} ($\mathrm{m^2/s}$), which results from the truncation error of the finite-difference approximation. For a 1D case, it can be estimated as:

$$D_{ns} = \frac{v_x \Delta x}{2} = 4.55 \times 10^{-12}\ \mathrm{m^2/s} \qquad \text{D-1}$$

In turn, backward-in-time differencing introduces an additional numerical dispersion resulting from the truncation error of the finite-difference approximation. For a 1D case, it can be estimated as:

$$D_{ns} = \frac{v_x^2 \Delta t}{2} = 3.26 \times 10^{-12}\ \mathrm{m^2/s} \qquad \text{D-2}$$

The numerical dispersion due to time and space discretization is the sum of both, 7.80×10^{-12} m²/s, which is much higher than the assumed longitudinal dispersion, and higher than the effective diffusion coefficient (5.0×10^{-12} m²/s).

To compare the effect of numerical dispersion introduced in PHAST (Equations D-1 and D-2) and in iCP, the results of a conservative tracer are shown in Figure 8-1 for both cases. Chloride (Cl) is used as a tracer, since no Cl-bearing minerals are initially present nor they precipitate during the simulation. The results are presented in terms of the breakthrough curve at x = 0.5 m (right boundary of concrete wall). It may be observed that the results compare well, although PHAST introduces a slightly higher numerical dispersion than iCP.

The profiles of the mineralogical phase assemblages of the PHAST and iCP simulations are presented and compared in Figure 8-2, after 17 500 years. Overall, a generally good agreement is obtained. Portlandite is a relatively soluble phase in cement and is the first solid to dissolve. In this figure, portlandite dissolution is shown to occur relatively faster in PHAST, which could be due to the increased dispersivity of the system in PHAST. On the other hand, degradation of C-S-H phases is slightly faster in iCP, while calcite, brucite, and thaumasite precipitation is slightly more important in iCP.

The chemical system is complex and therefore small differences in solute transport, for example due to different numerical dispersivities, could lead to appreciable discrepancies in the results. This is specially the case in systems where the number of pore water replacements is large. In this example, given the water velocity and the size of the domain, the pore water in the concrete wall is replaced around 500 times at the end of the simulation (17 500 years).

It may be concluded that the degradation of concrete can be modelled in a similar way using both PHAST and iCP, provided the same chemical and flow and transport setup is used in both cases.

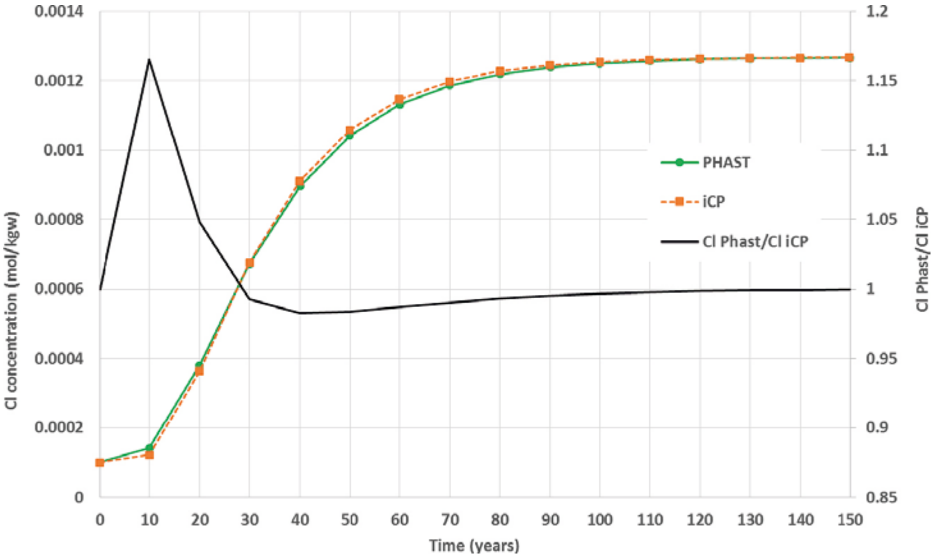

***Figure D-1.** Comparison of results of PHAST and iCP for a conservative tracer (Cl) in the 1D benchmark: breakthrough curve at x = 0.5 m.*

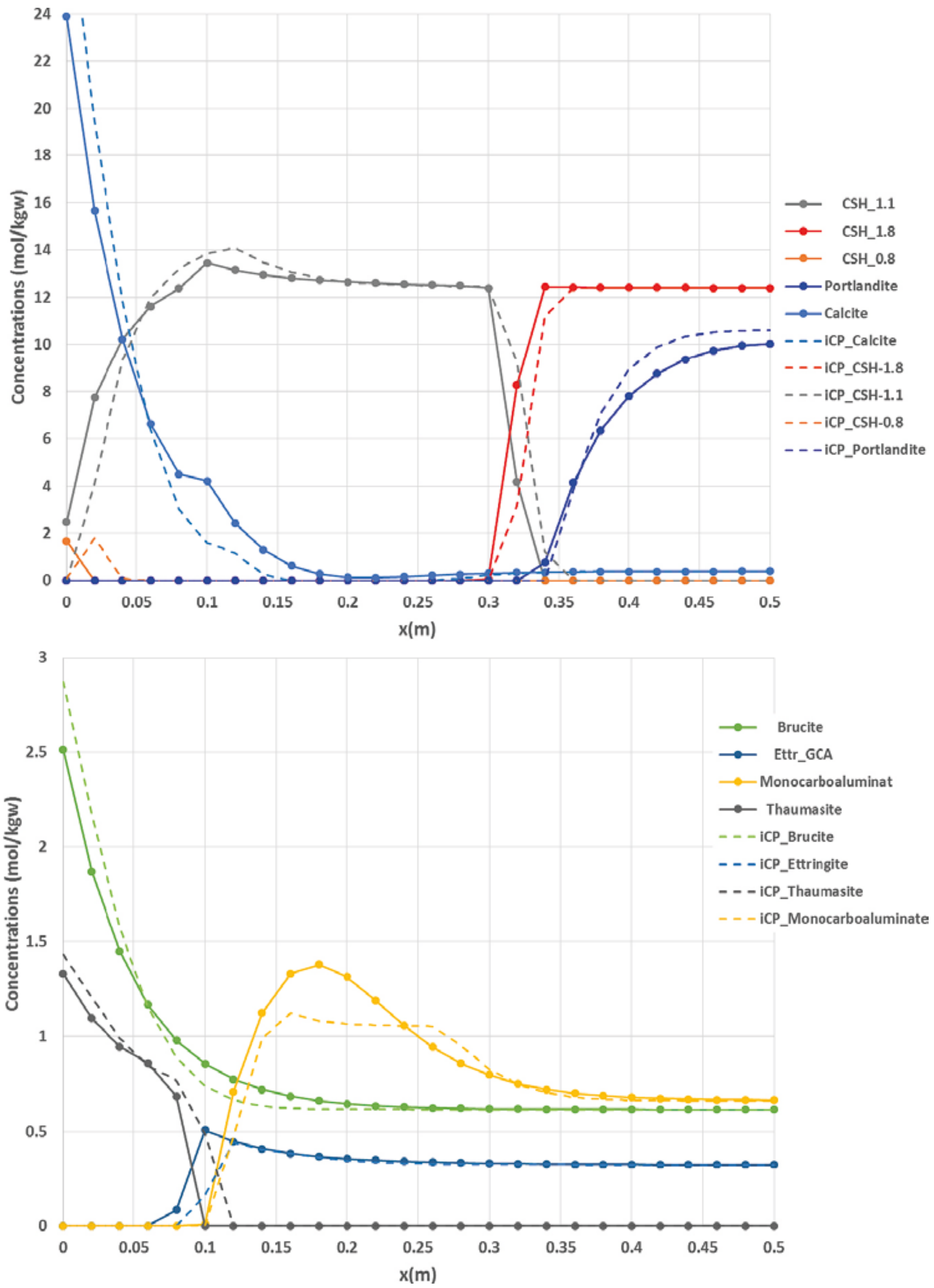

Figure D-2. *Comparison of results of PHAST and iCP for reactive minerals.*

Arkitektkopia AB, Bromma, 2019

SKB is responsible for managing spent nuclear fuel and radioactive waste produced by the Swedish nuclear power plants such that man and the environment are protected in the near and distant future.

skb.se